

**VAPOR-LIQUID EQUILIBRIUM CALCULATIONS WITH A NEW STEP POTENTIAL
MODEL AND EBULLIOMETRIC MEASUREMENTS**

By

Abu Mokhtarul Hassan

A DISSERTATION

**Submitted to
Michigan State University
in partial fulfillment of the requirements
for the degree of**

DOCTOR OF PHILOSOPHY

Chemical Engineering

2011

ABSTRACT

VAPOR-LIQUID EQUILIBRIUM CALCULATIONS WITH A NEW STEP POTENTIAL MODEL AND EBULLIOMETRIC MEASUREMENTS

By

Abu Mokhtarul Hassan

Robust thermodynamic property prediction is vital to the design of chemical process technologies. SPEAD (Step Potential Equilibria and Dynamics) is a rapid method of vapor-liquid equilibrium property calculations using discontinuous molecular dynamics (DMD) simulations in conjunction with thermodynamic perturbation theory (TPT). Though the potential predicts vapor pressures of several compounds reasonably well, the liquid densities seem to be systematically overpredicted. Equilibrium densities provide a vital test for the accuracy and transferability of a potential, since thermodynamic properties are sensitive to small changes in densities.

A new four step potential model called StePPE (Step Potentials for Phase Equilibria) is developed, based on the theory of SPEAD, which reproduces the liquid densities significantly better. The improvement in vapor pressure predictions for the compounds in this study is moderate, but the accuracy is improved for a wider range of reduced temperatures, and is better especially at lower reduced temperatures in comparison to SPEAD. Furthermore, the transferability of parameters is observed to be better than SPEAD for a broader chain length within a homologous series and from one homologous series to another, evidenced by a reduction in the number of adjustable parameters for most of the compounds studied. A guideline for obtaining the first guess of the diameters of the functional groups is developed based on the

van der Waal's volumes of the sites. The optimized site diameters are observed to be close to 97% of the first guess.

To provide vapor pressure data for compounds for which data is limited or unavailable in literature, new ebulliometers are designed, which can accurately measure the boiling temperatures of pure compounds using a small amount of sample. Activating the heated surface with powdered glass and the use of Cottrell type tube were observed to be effective in removing superheat. Condensate hold-up in these ebulliometers is estimated in order to use these ebulliometers for the measurement of bubble points of binary mixtures, without measuring any of the equilibrium compositions.

**Copyright by
ABU MOKHTARUL HASSAN
2011**

To my mother Haidery Begum, who fought against all odds to fulfill one of her very few dreams
of getting me an education

ACKNOWLEDGEMENTS

I thank Allah for any benefit this work can bring to anyone, and seek his forgiveness for the shortcomings in me, from which I have tried to save this work.

Any accomplishment in this work would not have been possible without the support of some talented individuals, and this short acknowledgement is not enough to appreciate their efforts towards completion of this dissertation. I would first of all, like to thank my advisor Dr. Carl Lira, for having the confidence in me to do this work. I still remember the first day when I talked to him about possible projects in his group, when he showed me a beautiful ethyl lactate molecule on his computer screen and asked me if I was interested in simulating properties of molecules using molecular simulations. Though I was quite impressed with the visuals, it wasn't enough to dispel my fear of anything that had to do with programming triple integrals and quadruple summations. I however started working on it somewhat, just to get a 'flavor', and about fifty run-time errors later, I realized I had underestimated Dr. Lira's patience more, than I had underestimated my abilities. I remember the many discussions we had that lasted four hours and several cappuccinos, but in the end they were all worth it. I am thankful to him for his help, not only as a good research supervisor, but also for being a good mentor and friend outside research.

I am thankful to my committee members Dr. Nikolai Priezjev, Dr. Micahel Feig and Dr. Dennis Miller (not in the order of people who asked me the most difficult questions). While Dr. Feig's quantum level questions helped me grasp some of the minutest details in our model, Dr. Priezjev's molecular level questions helped me understand some of the shortcomings of our model and think about improvements. Dr. Miller's uncanny knack of extracting out the smallest

details from a pile of data is almost superhuman. Without the thought provoking comments and questions from these individuals, I wouldn't have had a complete understanding of this work.

My lab mates in Lira/Miller group deserve special thanks for developing a workplace with learning and nurturing environment. Our post docs Dr. Lars Peerebom, Dr. Aspi Kolah and Dr. Ambareesh Murkute have been very helpful in making me learn to be competitive yet collaborative. Venkata Sai has been a good friend with whom I have often shared my ups and downs during my studies. Alvaro Orjuela, Anne Lown, Xi Hong, Arathi Santhankrishnam and Aron Oberg have been very good lab mates. Undergrads Joe Zalokar, Pete Rossman, Dushyant Barpaga, Jonathan Evans and Alex Smith have been a crucial help in both, my experimental and computational endeavors.

I am also thankful to my friends and teachers from undergrad. Tabish Maqbool deserves special words of appreciation for being a constant support throughout my career and a true friend who I could always rely on. I will also always remember my days with Yusuf Ansari and Zaid Bin Khalid who have been best of friends. My undergrad teacher Miss Seemi Rafique is one of the important individuals who helped in my early days when I had been struggling, not really knowing whether I wanted to go for higher studies. Dr. Hamid Ali's constructive criticism is something I will always appreciate.

My days in East Lansing would not have been as enjoyable without some important friends. I have enjoyed and company and learned something from all of them. My earlier roommate Farhan Ahmad's passion for research is unmatched. It's been hard for me to persuade him to talk about anything but research, though I'm somewhat at a loss trying to figure out his penchant, bordering on monomania, for a certain chicken curry, cooked exactly in a certain way with precise amounts of certain ingredients! Rehan Baqri's confidence in talking about subjects

like chemical engineering and world politics, and anything that lies in between amazes me. He's a neuroscientist by the way. Basir Ahmad's simplicity and willingness to help, sometimes by putting himself in trouble, is something really scarce these days. I thank all my other friends in the Islamic Center of East Lansing and our little basketball group in Spartan Village for making my days in East Lansing memorable.

I would also like to acknowledge the help of the staff in the CHEMS office. Joe Ann, Lauren Brown, Jennifer Peterman, Nikole Shook, Donna Fernandez and Kim McClung, have been our hands and feet, and I don't even want to imagine the mayhem the department would be in without them.

Finally, and importantly, I thank my family for their selfless support. Ma and baba, may Allah always take care of you as you took care of me when I was little. Your unflinching faith in me and unconditional support is something I cannot compensate for, no matter what. The sacrifices of my brothers Zafar and Hassan to make me reach where I am today is something I will be indebted to all my life. I will always cherish the boundless love and affection of my sisters Ishrat and Zakia. I cannot imagine going through this journey without the love and support of my dear wife Zahida, who has always stood beside me in sharing my difficulties and celebrating my achievements. I thank Allah for blessing me with this wonderful family.

I cannot count the bounties Allah has bestowed upon me, and the people mentioned here are my greatest blessings. As I embark upon a new journey, I ask Allah for his guidance.

TABLE OF CONTENTS

LIST OF TABLES	xi
LIST OF FIGURES	xiii
1. INTRODUCTION	1
1.1 Research Overview	1
1.2 Objectives and overview of thesis	2
1.3 References.....	7
2. OVERVIEW OF VAPOR-LIQUID EQUILIBRIUM CALCULATION WITH SPEAD METHOD	8
2.1 Introduction.....	8
2.2 DMD simulations for thermodynamic properties.....	10
2.3 SPEAD background.....	11
2.4 References.....	25
3. PREDICTION OF LIQUID DENSITIES AND VAPOR PRESSURES WITH SPEAD: MOTIVATION FOR A NEW STEP POTENTIAL MODEL.....	28
3.1 Summary of results with SPEAD: model parameters and the liquid density errors.....	28
3.2 Improvements: the StePPE model	30
3.3 Summary of comparison of errors with SPEAD and StePPE.....	37
3.4 References.....	40
4. LIQUID DENSITIES AND VAPOR PRESSURES OF PURE COMPOUNDS WITH StePPE MODEL	41
4.1 Site diameter and step potential optimization: summary.....	41
4.2 Discussion of results with StePPE parameters and comparison with other UA models	43
4.3 References.....	70
5. MEASUREMENTS OF VAPOR PRESSURES AND BUBBLE POINTS WITH EBULLIOMETRY	74
5.1 Introduction.....	74
5.2 Ebulliometer designs for pure compounds	75
5.3 Ebulliometer for measuring T-x of a binary liquid.....	79
5.4 References.....	84

6. CONCLUSIONS AND RECOMMENDATIONS FOR FUTURE WORK.....	86
6.1. VLE calculations with StePPE.....	86
6.2 Ebulliometric measurements.....	96
6.3 References.....	99
 APPENDICES	 102
A.1 Angle distribution in butyl propionate.....	102
A.2. Bond lengths	103
A.3. Finding the first guess of site sizes from excluded volumes.....	104
A.4. Liquid density and vapor pressure plots	106
A.5. Tail corrections	117
A.6. Ratio of the number of intramolecular attractive pairs to total attractive pairs	119

LIST OF TABLES

Table 3.1: Summary of errors in vapor pressure and liquid density predictions with SPEAD and StePPE	37
Table 4.1: Summary of optimized parameters for sites used in this study. The sites within parentheses in the first columns are the sites to which the group in that column is bonded, or a special case. For example ‘CH3 (-CH2-/-CH3)’ represents a methyl group, which is bonded to another methyl or methylene group. The ‘>’ or ‘<’ signs mean two sigma bonds and the ‘=’ sign denotes a double bond. For example, the carbonyl carbon, which has two sigma bonds and a double bond is represented by ‘>C=’. θ is the bond angle. The term ‘ σ ’ denotes the site diameter and the term ‘ k ’ in well energies is the Boltzmann constant.	42
Table 4.2: Vapor pressures and liquid densities of n-alkanes with StePPE. P^{sat} , T_r^{min} , and T_r^{max} in this and the subsequent tables mean vapor pressure, minimum reduced temperature and maximum reduced temperature.....	44
Table 4.3: Vapor pressures and liquid densities of branched alkanes with StePPE	48
Table 4.4: Vapor pressures and liquid densities of alkenes with StePPE.....	55
Table 4.5: Vapor pressures and liquid densities of primary alcohols with StePPE.....	57
Table 4.6: Vapor pressure and liquid density deviations of secondary alcohols with StePPE.....	61
Table 4.7: Vapor pressure and liquid density deviations of ethers with StePPE.....	62
Table 4.8: Vapor pressure and liquid density deviations of ketones with StePPE	65
Table 4.9: Deviations in liquid densities and vapor pressures of esters with StePPE	68
Table 6.1: Comparison of errors of secondary alcohols with two different sizes of the methine group	89

Table 6.2: Errors in liquid densities and vapor pressures of n-alkanes with StePPE with tail corrections.....	91
Table 6.3: Comparison of the radius of gyration of n-alkanes with the most likely end-to-end distance in StePPE simulations	96
Table A2.1 Bond lengths used in StePPE model.....	103

LIST OF FIGURES

Figure 1.1: Comparison of methods for performing molecular simulations	3
Figure 2.1: Illustration of bonds and pseudobonds for three adjacent sites in an alkane represented as overlapping spheres. The solid lines a and b represent the covalent bonds between the adjacent sites (1-2, 2-3) and the dashed line c represent the pseudobond between sites 1 and 3 to constrain the angle θ	11
Figure 2.2: Illustration of the multistep potential used in SPEAD. The innermost well represents a covalent bond and the second inner well represents pseudobond to constrain bond angles	12
Figure 2.3: Finding the pseudobond length (given by the dashed lines) for cis/trans interactions in cis/trans butene.....	13
Fig 2.4: SPEAD simulation steps to get the EoS	21
Fig 2.5: Flowsheet of equilibrium pressure and density calculations. Symbol meanings- P_r : Reduced pressure, T_r : Reduced temperature, ω : Compressibility factor, b : Core volume (volume/molecule), η : Packing fraction (V: vapor, L: liquid), f : Fugacity, A : Helmholtz energy departure.....	22
Figure 3.1: Published results of vapor pressure and liquid densities using SPEAD.....	28
Figure 3.2: Density predictions of normal alkanes with Akron SPEAD. The dots are experimental points and the lines are model predictions.....	29
Figure 3.3: Optimized site diameters (ordinate) compared to diameters obtained from van der Waal's volumes (abscissa) in Å; (a) StePPE, based on 20% volume correction per bond, (b) TraPPE, based on 24% volume correction per bond.....	33
Figure 3.4: Core volumes predicted with StePPE plotted against van der Waal's volumes of alkanes. The x-axis denotes the number of C atoms in the alkane chain	34

Figure 3.5: Comparison of A2 using polynomial function as in Akron- SPEAD and exponential function as in MSU-SPEAD for trioxane.....	35
Figure 3.6: Liquid density deviations of selected compounds with SPEAD (filled symbols). Symbols are: diamonds- alkanes, circles- 1-alkenes, triangles- ketones, squares- acetates. The open symbols are with StePPE	38
Figure 4.1: Liquid densities from left to right of (a) n-propane, n-pentane and n-octane, and (b) n-dodecane and n-hexadecane. The symbol meanings are same in (a) and (b)	45
Figure 4.2: Vapor pressures, from right to left, of, <i>n</i> -propane, <i>n</i> -pentane, <i>n</i> -octane, <i>n</i> -dodecane and <i>n</i> -hexadecane. For interpretation of the references to color in this and all other figures, the reader is referred to the electronic version of this dissertation.	46
Figure 4.3: (a) Liquid densities of (left to right) isopentane, neopentane and 2,2-dimethylhexane; (b) saturation pressures of (right to left) isopentane, neopentane and 2,2-dimethylhexane. The legend meanings are same in (a) and (b).....	49
Figure 4.4: Liquid densities (a) and saturation pressures (b) of 3,4-dimethylhexane and 2,5-dimethylhexane. The lines are from correlations in DIPPR, filled symbols are from TraPPE and the open symbols are from StePPE.....	50
Figure 4.5: Experimental liquid densities of C9 isomers and 2,2,3,3- tetramethylbutane. The curves are from equations in DIPPR 801 database.....	51
Figure 4.6: (a) liquid densities (left to right) of propene, 1-butene, 1-pentene and 1-octene; (b) vapor pressures of (right to left), propene, 1-butene, 1-pentene and 1-octene. The symbol meanings are same in (a) and (b)	53
Figure 4.7: liquid densities (a) and vapor pressures (b) of butene isomers. The meanings of the legends are same in (a) and (b).....	54
Figure 4.8: Liquid densities (a) and vapor pressures (b) of (right to left) propanol, 1-pentanol and 1-octanol. In (a) the dotted, solid and dashed lines are for propanol, 1-pentanol and 1-octanol respectively.....	58
Figure 4.9: Liquid densities of selected 1-alcohols with SPEAD and StePPE. Dashed lines are with SPEAD and the solid lines are with StePPE	59

Figure 4.10: Liquid densities of methanol (a) and ethanol (b) with SPEAD and StePPE. The symbol meanings are same in (a) and (b)	59
Figure 4.11: Liquid densities and vapor pressures of 2-butanol (circles) and 2-propanol (squares) with TraPPE and SPEAD. The closed symbols are with TraPPE and the open symbols are from StePPE.....	60
Figure 4.12: (a) liquid densities of (left to right) dimethyl ether, dipropyl ether and di-pentyl ether and di-nonyl ether; vapor pressures of (right to left) dimethyl ether, dipropyl ether and di-pentyl ether and di-nonyl ether	63
Figure 4.13: Liquid densities (a) and vapor pressures (b) of acetone, 2-pentanone and 2-octanone with SPEAD, TraPPE and StePPE. In (a), the filled symbols are from TraPPE and open symbols are from StePPE. In (b), from top to bottom: acetone, 2-pentanone, 2-octanone	66
Figure 5.1: Ebulliometer based on Hoover’s design for vapor pressure measurement	76
Fig 5.2: Cottrell tube ebulliometer. In (a), the entire assembly is shown, (b) shows the Cottrell tube insert with a funnel shaped bottom to catch the vapors, which get carried to the equilibrium chamber with the boiling liquid. The contents get squirted on the temperature probe (not shown) in this chamber. The height of the outside tube is about 6” and the diameter is about 1”.....	77
Figure 5.3: Ebulliometer with Washburn pump	77
Figure 5.4 Stirred round bottom flask ebulliometer for vapor pressure measurements.....	78
Figure 5.5: Measurement of P^{sat} of monoethyl succinate with Cottrell, Hoover and stirred flask ebulliometers	78
Figure 5.6: Measurements of water P^{sat} with Cottrell and Washburn ebulliometers	79
Fig 6.1: Liquid densities of neopentane and 2,2-dimethylhexane with StePPE. The symbols are from DIPPR801 correlations	88

Fig 6.2: Vapor pressure and liquid density deviations with StePPE, using ‘34’ and ‘77’ intramolecular interactions; x-axis denotes the total number of carbon atoms in the ester chain	92
Fig 6.3: Ratio of intramolecular attractive pairs (N_I) to total number of attractive pairs (N_T) with x . The legends denote the total number sites in the molecule	93
Figure 5.4: Vapor pressures of ethers with StePPE with and without correction for partial charges	95
Figure A.1: Distribution of some angles in butyl propionate. The legends denote the three sites that form the angle, and the site within the parentheses is the central angle. The vertical lines denote the equilibrium values (109.5° and 120°)	102
Fig A3.1: Schematic for finding site diameters from given excluded volumes.....	104
Figure A.4. 1: Liquid densities (a) and vapor pressures (b) of n -alkanes	106
Fig A.4.2: Liquid densities of branched alkanes (a); isobutane (b)	107
Fig A.4.3: Vapor pressures of branched alkanes (a); isobutane (b).....	108
Figure A.4.4: Liquid densities (a) and vapor pressures (b) of alkenes	109
Figure A.4.5: Liquid densities (a) and vapor pressures (b) of primary alcohols. The symbol ‘1olCx’ denotes a primary alcohol with ‘x’ carbons in the backbone. For example, 1olC8 in 1-octanol	110
Figure A.4.6: Liquid densities (a) and vapor pressures (b) of secondary alcohols.....	111
Figure A.4.7: Liquid densities (a) and vapor pressures (b) of ethers.....	112
Figure A.4.8: Liquid densities (a) and vapor pressures (b) of ketones	113
Figure A.4.9: Liquid densities (a) and vapor pressures (b) of acetates.....	114

Figure A.4.10: Liquid densities (a) and vapor pressures (b) of methyl esters 115

Figure A.4.11: Liquid densities (a) and vapor pressures (b) of esters higher than acetates 116

CHAPTER I

1. INTRODUCTION

1.1 Research Overview

Phase equilibria plays a critical role in a variety of technical and industrial applications ranging from combustion of fuels inside an engine to process technology development in the chemical industry. From applying adhesives and coatings, to simply melting ice, phase behavior is also at the core of many day-to-day applications. Physical property calculations are at the core of process engineering design because the properties determine the sizes for equipment and utility demands, which in turn govern economic profitability of processes.

This thesis encompasses both, experimental and modeling aspects of fluid properties, primarily focusing on predictions and measurement of vapor pressure. Recent advancements in computational efficiency have enabled the application of advanced molecular simulation techniques to generate phase equilibria of relatively complex systems, using atomistic or united atom (UA) models. Vapor-liquid coexistence properties, which are available from experiments for a variety of systems, can be used to parameterize, or test the accuracy and transferability of the force-fields developed for the different simulation schemes. Liquid density has been the preferred property for force-field optimization and testing, since system thermodynamic properties are highly sensitive to density. Vapor pressure is another key equilibrium property of interest for the study of potentials, which is also critical in industrial applications such as chemical separation[1] and liquid fuel combustion[2]. The prediction of accurate vapor pressures can be leveraged to secondary properties by integration, differentiation, or other correlation. For example, the vapor pressure governs the flash point of a fuel[3] and is related to its surface tension and heat of vaporization[4].

This thesis also presents the development and testing of various ebulliometers. To measure vapor-liquid equilibrium (VLE) experimentally, either static equilibrium cells, or dynamic equilibrium circulation stills are used. The static method is more accurate, but it is slow, and the auxiliary equipment needed makes it expensive[5]. On the other hand, ebulliometry, which is the most widely used dynamic method, is fast, inexpensive, and has been improved over time to give extremely accurate results[6-8]. Ebulliometry works on the principle that at a given temperature, a liquid will boil at its vapor pressure. In this method, rather than measuring the bubble pressure, the bubble temperature of the fluid is measured at a fixed pressure.

In this work, we have used ebulliometry as our method of measuring VLE and have developed an ebulliometer to be used for vapor pressures of pure compounds in a broad pressure range of 30 mbar to atmospheric. The focus is also to develop ebulliometers versatile enough for both, pure compounds and binary mixtures.

1.2 Objectives and overview of thesis

The objective of this work is to develop a tool for engineering predictions of equilibrium properties. A spectrum of simulation methods are available spanning from quantum mechanics to empirical group contribution methods. As shown in Figure 1.1, the level of confidence increases with the level of detail, but the computational costs for quantum mechanical calculations of systems of molecules are rarely justified. On the other hand, group contribution methods for predictions of properties such as vapor pressure typically require estimation of critical properties and then apply a corresponding states model to estimate the properties. Such methods have been shown to lead to large and unpredictable errors. On the other hand, group contribution methods such as UNIFAC use group-based energies and are fairly reliable for predicting activity coefficients in mixtures. For the purposes here, it is desirable to include more detailed molecular

information, but also to compromise on the level of detail to provide a robust predictive method. The existing model called SPEAD (Step Potentials for Equilibria And Dynamics) has been shown to provide rapid accurate estimates for vapor pressure. The method uses realistic simulation of the molecular geometry, but simplifies the pair potentials and the intramolecular vibrations and torsions. The method is also limited because it does not provide an direct accurate prediction of the critical point due to the limitations of the truncated series expansion used to represent the Helmholtz energy. However, the method is accurate enough in the engineering ranges needed for fuel properties that reexamination of the capabilities is justified. The method appears to provide a good balance of realistic simplifications and molecular detail to provide good engineering estimates of vapor pressure and density.

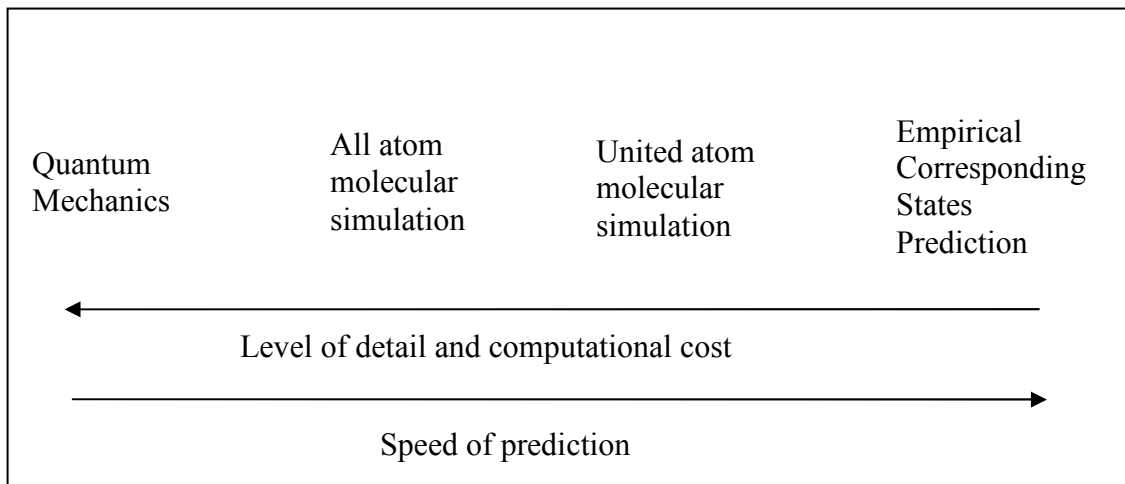


Figure 1.1: Comparison of methods for performing molecular simulations

The purpose of this study is to develop a transferable four step potential model similar SPEAD for accurately predicting the equilibrium densities, which gives the vapor- liquid coexistence curves (VLCC), vapor pressures and heats of vaporization of fluids. This study will address the inadequacies in the SPEAD model and provide a fundamental guideline for site diameter selection based on van der Waal's volumes. All the improvements are aimed at

improving transferability, and wherever possible, reducing the number of parameters. Though the other UA models reproduce the liquid densities well, vapor pressure, which is a relatively important fluid property in the chemical/petrochemical industry, is not reproduced accurately with these models, especially for longer molecules. This model would thus be a much faster alternative compared to traditional UA models for accurate property predictions. The goals of the work are to provide predictions for ketones, esters, ethers, and alcohols which are all potential biofuel molecules. Further, we would like to extend the work to higher molecular weights typical of diesel-type fuels.

In order to complement the model, ebulliometers for accurate vapor pressure measurement would be designed, to provide data for pure compounds as well as binary mixtures, which are currently unavailable in literature. The purpose of the new designs is to eliminate superheat effectively yet keeping the operation simple and inexpensive.

The following chapters discuss the development of the potential model and the ebulliometry apparatus in order to meet the goals stated above. Conclusions and recommendations for future work are provided in the final chapter. The following paragraphs give a brief overview of the chapters in this thesis.

Chapter II evaluates simulation-perturbation technique of SPEAD and shows systematic errors in liquid density predictions. Citing the importance of reproducing the liquid densities accurately, improvements to the model are discussed and then a revised model called StePPE (Step Potentials for Phase Equilibria) is developed in Chapter III. Vapor liquid equilibrium calculations for pure compounds with the new model are discussed in Chapter IV. Comparisons of the results for individual homologous series, wherever possible, are made with the TraPPE, NERD and SPEAD models. Next, the thesis discusses the development of ebulliometers for

vapor pressures measurements of pure compounds and bubble pressures of binary mixtures in Chapter V. Finally, the conclusions and recommendations for future work are presented in Chapter VI. Some of the supporting material is presented in the Appendix at the end.

REFERENCES

1.3 References

1. Prausnitz, J.M.; Lichtenthaler, R.N.; de Azevedo, E.G., "Molecular Thermodynamics of Fluid-Phase Equilibria". 3rd ed. **1999**, Prentice-Hall, Inc.: Upper Saddle, New Jersey.
2. Faeth, G.M., "Evaporation and Combustion of Sprays". *Progress in Energy and Combustion Science*, **1983**, 9, 1-76.
3. Perry, R.H.; Green, D.W., "Perry's Chemical Engineers' Handbook". **1997**.
4. Pollara, L.Z., "Surface Tension and Vapor Pressure". *J. Phys. Chem.*, **1942**, 46, 1163-1167.
5. Hala, E.; Pick, J.; Fried, V.; Vilim, O., "Vapor- Liquid Equilibrium". **1958**, Pergammon Press: New York.
6. Rogalski, M.; Malanowski, S., "Ebullimeters Modified for the Accurate Determination of Vapor-Liquid Equilibrium". *Fluid Phase Equilibria*, **1980**, 5, 97-112.
7. Chernyak, Y.; Clements, J.H., "Vapor Pressure and Liquid Heat Capacity of Alkylene Carbonates". *Journal of Chemical & Engineering Data*, **2004**, 49, 1180-1184.
8. Raal, J.D.; Gadodia, V.; Ramjugernath, D.; Jalari, R., "New Developments in Differential Ebulliometry: Experimental and Theoretical". *Journal of Molecular Liquids*, **2006**, 125, 45 – 57.

CHAPTER II

2. OVERVIEW OF VAPOR-LIQUID EQUILIBRIUM CALCULATION WITH SPEAD METHOD

2.1 Introduction

To obtain phase equilibrium properties of fluids and mixtures, the industry has relied on semi empirical equations of state (EoS) like the Peng-Robinson[1] or SAFT[2], or macroscopic group contribution methods, like UNIFAC[3]. Both methods become increasingly inaccurate with increasing temperatures and pressures as well as with molecular complexity[4-7]. An alternative is to use site-site interaction potentials (considering either an atom or a group of atoms as a “site”), and use molecular simulations for equilibrium thermodynamic properties. Such formalism would include well established bond lengths, angles and torsions in a molecule, thereby incorporating more realistic structural contributions to the properties being calculated. References [4-7] demonstrate the advantages molecular simulation models have over the equations of state or the group contribution methods. The key, however, is the development of a site-site potential model (or a force-field), which is both accurate, and “transferable” from molecule to molecule. That is, the parameters optimized for a particular site-site interaction is usable in any molecule in which that site is present.

Several UA models with 12-6 Lennard-Jones potential, like OPLS[8], TraPPE[9] and NERD[10] have been used successfully for generating vapor-liquid coexistence curves and critical properties. While all of these models reproduce saturation liquid densities and critical temperatures well for the chain lengths for which they were optimized, the vapor pressure estimation lacks accuracy. OPLS, which was optimized to reproduce saturation liquid densities and heats of vaporization of short chain molecules at ambient conditions, overpredicts liquid

densities at elevated temperatures, and underestimates vapor pressures even at ambient conditions,[9, 11] and the errors increase with increasing chain length. TraPPE predicts the liquid densities better than OPLS for relatively longer chains (up to C10), but higher errors have been reported for longer chains[10], where NERD seems to perform better. Vapor pressures are consistently overpredicted with both the models, but the errors are smaller with NERD[12].

All atom (AA) simulations would be more accurate, especially at higher densities, but their CPU times are roughly an order of magnitude higher compared to UA simulation models. A discussion of various all atom simulations for phase behavior for n-alkanes can be found in the study of Chen et al[13]. An intermediate solution is the anisotropic models[14], which are computationally less demanding than the AA simulations.

The SPEAD method is another UA model which can predict vapor pressures and heats of vaporization approximately 50 times faster than conventional full potential molecular simulations[15]. It is a combination of discontinuous molecular dynamics (DMD) simulation and thermodynamic perturbation theory (TPT), which gives an equation of state for VLE calculations. SPEAD estimates vapor pressures of hydrocarbons including alkanes[16], aromatics[17], low molecular weight ethers and primary alcohols[16], and acetates[18] with errors of less than 10% of the experimental values for a reduced temperature range of 0.45 to 1.0. However, as discussed later in this study, a systematic overprediction in liquid densities is observed with increasing chain length. Notwithstanding the inadequacies, for calculations away from the critical point, SPEAD offers a great industrial tool. If the force-field can be improved to estimate liquid densities better, SPEAD would be a more robust alternative to equations of state and group contribution methods on one hand, and a much faster alternative to the other UA models with similar accuracy, on the other.

2.2 DMD simulations for thermodynamic properties

In molecular dynamics (MD) simulations, a system of particles that obey Newton's Laws of motion is created and the configurational energy of the system is given by a defined potential function (also known as a force-field). Based on initial positions and momenta, the trajectory of the particles can be created by integrating the Newton's laws of motion numerically, and by using standard statistical mechanical analysis tools, the required time averaged property of the system can be calculated from the trajectory. The kinetic energy of the particles defines the system temperature, and the forces on the particles are calculated using the force-field. For Lennard-Jones type continuous potential functions, the choice of a suitable time step is important. Also, to avoid 'heating' of the system during the simulation, a suitable numerical "thermostat" has to be employed. An overview of the method can be found in standard simulation textbooks[19, 20].

Obtaining the system trajectory is much simpler in discontinuous MD simulations. The system acts as hard billiard balls which undergo completely elastic collisions. There is no time-step to be chosen since no velocity change occurs until a collision takes place, and since the collisions are completely elastic, the positions and velocities of the particles post collision can be calculated by conservation of energy and momenta considerations. Alder and Wainwright[21] devised a method for calculating the trajectory of square well spheres. In addition to hard collisions, well interactions were considered, and the dependency of velocities and positions on the well depth was obtained. Rappaport[22] extended the study to chains formed by tethering the spheres by using infinite potential wells to represent bonds. For a more in-depth analysis of the continuous and discontinuous MD simulation methods, Maginn and Elliott's review[23] on MD is suggested.

The DMD simulation method in SPEAD develops from Rappaport's treatment of tethered hard sphere polymer chains[24]. The step-potentials are added post simulation using TPT, which allows equilibrium property calculations. The time required is an order of magnitude smaller compared to MD simulations with full potentials, as only hard interactions are accounted for. The following sections discuss the SPEAD theory in a greater detail.

2.3 SPEAD background

SPEAD model combines DMD simulation of a "reference" system with thermodynamic perturbation theory, which incorporates the disperse interactions. The reference fluid is composed of hard-sphere chains, with each hard sphere representing a united atom site. For example, the alkanes would be formed by methyl (CH₃) and methylene (CH₂) sites, with the distance between each site equivalent to C-C bond length in literature. The bonds angles are constrained by using a pseudobond between alternative sites (Fig 2.1). The bonded spheres within a molecule overlap due to the fact that the bond length is smaller than the site diameters. For non-bonded interactions however, the sites act as hard-spheres.

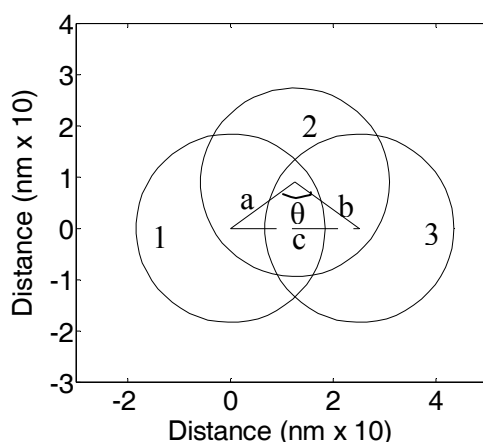


Figure 2.1: Illustration of bonds and pseudobonds for three adjacent sites in an alkane represented as overlapping spheres. The solid lines a and b represent the covalent bonds between the adjacent sites (1-2, 2-3) and the dashed line c represent the pseudobond between sites 1 and 3 to constrain the angle θ

1. SPEAD force- field

Infinite potential wells are used to restrict bond lengths and bond angles within a molecule (Fig 2.2). The innermost infinite well represents a covalent bond, and the second infinite well is used for a pseudobond between first and third neighbors in order to restrict the bond angles. Both the wells are centered corresponding to realistic equilibrium values of bond lengths and angles, and allowed to vary within 5% of those values. For example, for a C-C bond would be represented by a well centered at 0.154nm and a C-C-C bond angle would be depicted by a well centered at a value corresponding to ~ 110 degrees. A third well is used for additional bonds for 1-4 interactions to constrain cis/trans configuration. The center of the well for the cis/trans configuration is obtained from simple geometry (Fig 2.3). The non-bonded interactions during the simulation are repulsive only.

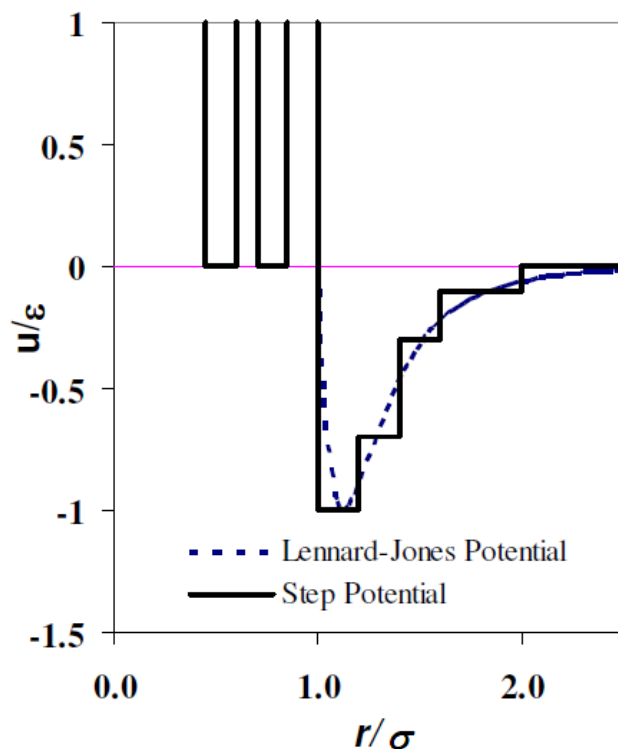


Figure 2.2: Illustration of the multistep potential used in SPEAD. The innermost well represents a covalent bond and the second inner well represents pseudobond to constrain bond angles



Figure 2.3: Finding the pseudobond length (given by the dashed lines) for cis/trans interactions in cis/trans butene

The effect of the non-bonded disperse interactions is added post-simulation as perturbation. A step-wise approximation to the Lennard-Jones model is used, which mimics the r^{-6} behavior of potential expected theoretically (Fig 2.2). Such an approximation can provide properties that are similar to the continuous potential for spheres[25]. While an infinite number of small steps may be the best approximation of the continuous potential, recent efforts focus on optimization of a four-step potential. Following the reference simulation, the inner and outer well depths corresponding to the four steps are adjusted, and the two central wells are interpolated. The four step-wells are located at $r/\sigma = 1.2, 1.5, 1.8, 2.0$, where σ is the site diameter, as shown in Figure 2.2. Hydrogen bonding is represented as an additional perturbation using Wertheim's theory as discussed in the next section.

2. Reference Simulation

The reference system is composed of hard sphere chains with bond lengths and bond angles constrained at literature values as described in the previous section. First the core volume (volume occupied by one molecule, b) is found by simulating a single molecule. For n number of unit cells, $4n$ molecules are then arranged in an *fcc* lattice and the simulation is started. For molecules with more than 20 sites, 256 molecules are used and for smaller molecules, 108

molecules are used for the simulation. The simulation box is further divided into a number of cells for event tracking, such that for a particular site, only the sites in the adjacent cells are considered for an event. The events that are kept track of are bond “collisions”, cell crossings, and site-site collisions. For efficiency, the algorithm for tracking the events is based on Rappaport’s event tree formalism[26, 27]. The system equilibrates for a given number of intermolecular hard collisions, before the production run starts when data is collected. Typically, the number of collisions for equilibration is set to about 500,000. The total number of collisions range from about 6000,000 to 10,000,000, the higher number generally being used for bigger molecules. The actual simulation time ranges between a few hundred to a few thousand picoseconds depending on the size of the molecule and density of the system. Low density (packing factors < 0.01) runs with small molecules take the highest amount of wall time to run. For example, the CPU time using a 64 bit processor for a molecule with ten sites is about two hours at packing fractions of 0.001 and about one hour at a packing fraction of 0.56. During the simulation, there is no fluctuation in the velocities since the attractive interactions are not present to accelerate the particles. The velocities are checked periodically to confirm the temperature remains constant. The simulation is repeated for about 21 dimensionless packing fractions (represented by ‘ η ’ which is equal to $b\rho$, where b is the molecular core volume and ρ is the density corresponding to the reciprocal units of b) ranging from vapor-like to liquid-like densities ($b\rho$ ranging from 0.001 to 0.54). During the simulation, the number counts for pair types in well limits are collected and averaged in order to later apply the TPT, as discussed in the section below. Typically 300 samples are averaged over the course of the run. The parameters for interactions of unlike sites are represented by Lorentz-Berthelot combining rules,

$$\sigma_{ij} = \frac{1}{2}(\sigma_i + \sigma_j) \text{ and } \varepsilon_{ij} = (\varepsilon_i \varepsilon_j)^{\frac{1}{2}}, \text{ where } i \text{ and } j \text{ are different site types. While } \sigma_{ij} \text{ is}$$

used in the reference simulation for the hard-site collisions, \mathcal{E}_{ij} is used during the application of TPT, where the attractive wells are introduced.

Pair types are distinct from pairs in following discussions. For example, consider a system of propane molecules. Using the united atom approach, the propane molecule is represented by two CH₃ groups connected by a CH₂ group. When two propane molecules interact, there are nine site pairs that interact. However, there are only three pair types (CH₃ + CH₃, CH₂ + CH₂, CH₂ + CH₃). When accumulating interactions, the two approaches share many similarities, and can be proven to be equivalent. In the following discussion, sums are written over pair types.

3. Perturbation theory in SPEAD

TPT in SPEAD is based on Barker and Henderson's formalism[28], which builds on the commonly known high temperature series expansion of the configurational partition function developed by Zwanzig[29]. The basic idea is to divide the potential energy of the system of interest into a reference (unperturbed) and a perturbed part, and mathematically express the Helmholtz free energy as a series expansion in inverse temperature. The different terms in the expansion can be found using ensemble averages over the reference system. The derivation is shown below.

From statistical mechanics:

$$A = -kT \ln Q \quad (1)$$

where, k is the Boltzmann constant, A is the extensive Helmholtz energy and Q is the canonical partition function, or the configurational integral. Zwanzig divided the potential energy of the system to an unperturbed part (U_o) and a perturbation contribution (U_P), as:

$$U = U_0 + U_P \quad (2)$$

This facilitates writing the configurational integral in (1) as:

$$Q = Q_0 \left\langle \exp\left(-\frac{U_P}{kT}\right) \right\rangle_o \quad (3)$$

The angular brackets denote an ensemble average and the subscript “*o*” implies an average over the unperturbed system (dropped in following equations for simplicity) and Q_0 denotes the configurational integral of the unperturbed system.

For an ensemble of monatomic molecules with a single square well on each site, Barker and Henderson simplified equation (3) to:

$$Q = Q_0 \exp\left(-\frac{1}{kT} \sum_i \langle N_i \epsilon_i \rangle\right) \left\langle \exp\left[-\frac{1}{kT} \sum_i (N_i - \langle N_i \rangle) \epsilon_i\right] \right\rangle \quad (4)$$

In equation (4), “*i*” denotes a pair type, ϵ_i denotes the potential well depth for pair type *i* and

N_i is the number of pairs of type *i* within the well, as determined by evaluating snapshots of the simulation. Expanding the exponentials in equation (4) and taking the logarithm (see equation (1)), we get:

$$\frac{A}{NkT} = \frac{A_0}{NkT} + \frac{1}{kT} \sum_i \langle N_i \rangle \epsilon_i - \frac{1}{2(kT)^2} \sum_i \sum_j \left(\langle N_i N_j \rangle - \langle N_i \rangle \langle N_j \rangle \epsilon_i \epsilon_j \right) \quad (5)$$

where, A_0 is the Helmholtz energy of the reference system, N is the total number of molecules and *i* and *j* denote pair types. Extending the analysis to four step wells, the Helmholtz free energy departure can be expressed as,

$$\frac{A - A^{ig}}{NkT} = \frac{A_0 - A^{ig}}{NkT} + \frac{1}{NkT} \sum_i \sum_m \langle N_{im} \rangle \varepsilon_{im} - \frac{1}{2N(kT)^2} \sum_i \sum_j \sum_m \sum_n \left(\langle N_{im} N_{jn} \rangle - \langle N_{im} \rangle \langle N_{jn} \rangle \right) \varepsilon_{im} \varepsilon_{jn} \quad (6)$$

In equation (6) the subscript i, j are for pair types, while m, n are for wells, such that $\langle N_{im} \rangle$ would be the average number of pairs of type i in well m . For example, in alkanes, there are three pair types, so i and j would vary from 1 to 3 and m and n would vary from 1 to 4 for the wells. The well energies for unlike sites in a pair type (the CH3-CH2 pair in alkanes) would be given by the Lorenz-Berthelot combining rule, as stated above. An excellent review on the progress of TPT for thermodynamic properties is presented in the review by Zhou and Solana[30].

The second and third terms on the right-hand side of the equation are the commonly known first and second order perturbation contributions to the Helmholtz free energy. When hydrogen bonding is present, an association contribution to the Helmholtz energy is added to (6). The first and second order perturbation sums are abbreviated by A_1 and A_2 (except T dependence is kept explicit), and the hydrogen bonding perturbation is added so that (6) can be written as:

$$\frac{A - A^{ig}}{NkT} = \frac{A_0 - A^{ig}}{NkT} + \frac{A_1}{T} + \frac{A_2}{T^2} + \frac{A^{assoc}}{NkT} \quad (7)$$

The term A_1 represents the average configurational energy of the system due to perturbation, while A_2 represents the fluctuation of that energy around the mean value. The A^{assoc} term is included if hydrogen-bonding sites are present. Care is taken in implementation of

the sums to avoid double-counting in the programming of the sums. From classical thermodynamics:

$$\frac{(A - A^{ig})_{T,V}}{RT} = \int_0^\rho \frac{(Z - 1)d\rho}{\rho} \quad (8)$$

Therefore, the corresponding equation of state ($Z = f(P, V, T)$) can be represented as:

$$Z = 1 + \frac{\rho}{RT} \left[\frac{d}{d\rho} (A - A^{ig})_{T,V} \right] \quad (9)$$

Since $\eta = b\rho$, $\frac{\rho}{d\rho} = \frac{\eta}{d\eta}$. Therefore:

$$Z = 1 + \eta \left(\frac{d(A_0 - A^{ig})}{d\eta} \right) + \eta \frac{dA_1}{d\eta} \left(\frac{1}{T} \right) + \eta \frac{dA_2}{d\eta} \left(\frac{1}{T^2} \right) + Z^{Assoc}$$

(10)

or introducing shorthand variables:

$$Z = Z_0 + Z_1 \left(\frac{1}{T} \right) + Z_2 \left(\frac{1}{T^2} \right) + Z^{Assoc} \quad (11)$$

The term Z_0 in equation (11) denotes the compressibility factor of the unperturbed fluid, which is used to calculate the Helmholtz energy departure of the reference fluid. From (10), one can deduce:

$$Z_0 = 1 + \eta \left(\frac{d(A_0 - A^{ig})}{d\eta} \right) \Rightarrow (Z_0 - 1) \frac{d\eta}{\eta} = d(A_0 - A^{ig}) \quad (12)$$

Therefore the Z_0 terms are collected from the simulations at all the packing fractions and a polynomial function is fit to the values as shown below, which can be used in equation (12) to calculate the Helmholtz energy departure $(A_0 - A^{ig})$ of the reference fluid.

$$Z_0 = \frac{1 + a_1\eta + a_2\eta^2 + a_3\eta^3}{(1 - \eta)^3} \quad (13)$$

To represent hydrogen bonding, Wertheim's theory[31] is used and the contribution of association has to be included in the Helmholtz energy and the equation of state. For a molecule with M different associating sites, the contribution of association to the Helmholtz energy is given by[32]:

$$\frac{A^{assoc}}{NkT} = \sum_i \left[\ln X^i - \frac{X^i}{2} \right] + \frac{1}{2}M \quad (14)$$

where, X^i is the mole fraction of hydrogen bonding sites that are *not* bonded. For one donor and one acceptor site, $M = 2$, so that the above equation can be written as,

$$\frac{A^{assoc}}{NkT} = \ln X^A - \frac{X^A}{2} + \ln X^D - \frac{X^D}{2} + 1 \quad (15)$$

The superscripts A and D denote acceptor and donor in the above equation. Furthermore, since the current implementation of SPEAD does not differentiate between donors and

acceptors, $X^D = X^A$, therefore, equation (15) can be simplified as:

$$\frac{A^{assoc}}{NkT} = 2 \ln(X^A) + (1 - X^A) \quad (16)$$

The corresponding contribution to the compressibility factor can be given by:

$$Z^{assoc} = -(1 - X^A) \left(\frac{1 + \eta - \eta^2 / 2}{(1 - \eta)(1 - \eta / 2)} \right) \quad (17)$$

where, η is the packing fraction, and X^A is calculated by:

$$X^A = \frac{-1 + \sqrt{1 + 4\alpha}}{2\alpha} \quad (18)$$

In the above equation, α , and is given by[33]:

$$\alpha = \rho \Delta^{AD} \quad (19)$$

In equation (19), ρ is the molar density and Δ^{AD} is the “strength” of association as it includes the range and depth of the association square well and is dependent upon the hard-sphere radial distribution function ($g(r)^{hs}$)[2, 33]:

$$\Delta^{AD} = g(r)^{hs} K^{AD} \left(\exp(\varepsilon^{AD} / kT) - 1 \right) \quad (20)$$

In the above equation, K^{AD} is the bond volume, depicted by the width of the square well for association, and ε^{AD} is the bond energy. Using equations (19) and (20) and the Carnahan and Starling’s equation for hard sphere radial distribution function:

$$g(r)^{hs} = \frac{(1 - \eta / 2)}{(1 - \eta)^3} \quad (21)$$

we get:

$$\alpha = \frac{\rho(1 - \eta / 2)}{(1 - \eta)^3} K^{AD} [\exp(\varepsilon^{AD} / kT) - 1] \quad (22)$$

The bond volume is calculated from an empirical correlation:

$$K^{AD} = \kappa \left[1 + \lambda \left(\frac{n_{hb}}{n_t} \right) \right] \quad (23)$$

where n_{hb} is the number of hydrogen-bonding sites in the molecule, n_t is total number of sites, and κ and λ are empirical constants for a given type of hydrogen bonding moiety. The empirical relation (23) causes the perturbation to be smaller in larger molecules.

4. Summary of steps in the SPEAD method

Once the compressibility factor for the reference fluid (Z_0) is calculated from the reference simulation, TPT can be applied to include the contributions from the first and second order perturbation terms as well as association, to complete the calculation of the compressibility factor for the intended fluid. A flowsheet of the steps is shown below.

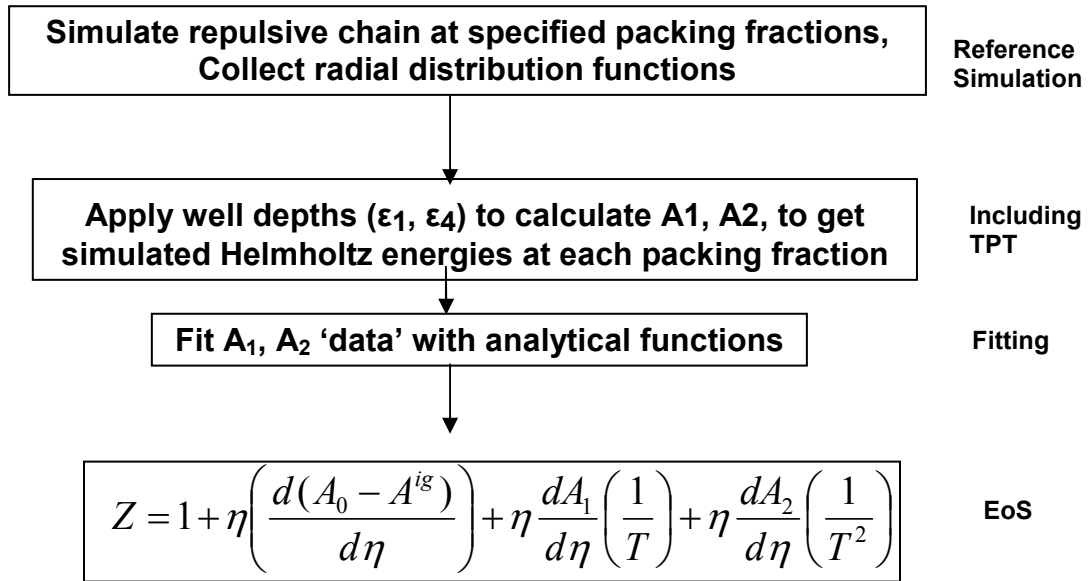


Fig 2.4: SPEAD simulation steps to get the EoS

5. Vapor pressure and orthobaric densities from SPEAD EoS

To perform the vapor pressure calculations, the compressibility factor is used to determine the Gibbs energy departure (a measure of fugacity). Solving for densities that provide equal Gibbs departures for the vapor and liquid phases gives the vapor pressure for the given temperature, and the densities at the saturation pressure correspond to the equilibrium liquid and vapor densities. The temperatures for the vapor pressure and density calculations are obtained from a data file that includes the experimental vapor pressures and liquid densities for the given compound. The algorithm is shown in the flowsheet below.

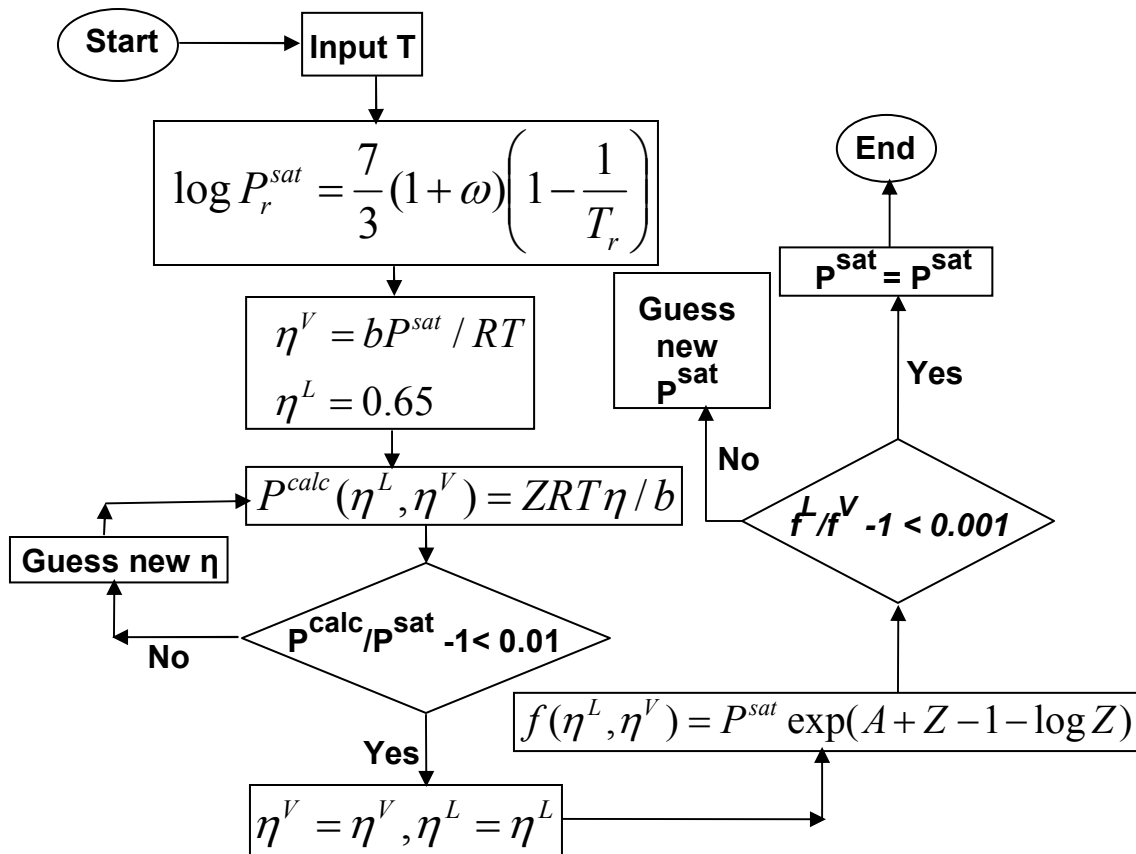


Fig 2.5: Flowsheet of equilibrium pressure and density calculations. Symbol meanings- P_r : Reduced pressure, T_r : Reduced temperature, ω : Compressibility factor, b : Core volume (volume/molecule), η : Packing fraction (V: vapor, L: liquid), f : Fugacity, A : Helmholtz energy departure

To obtain the optimum values of the step wells, vapor pressure and density calculations are performed by changing the well parameters globally of a selected set of compounds (training set) for which experimental data is available. The well-parameters that give the minimum global error for the training set give the optimized values of the well energies. The parameters can then be used for calculating the densities and vapor pressures of an unknown system.

REFERENCES

2.4 References

1. Prausnitz, J.M.; Lichtenthaler, R.N.; de Azevedo, E.G., "Molecular Thermodynamics of Fluid-Phase Equilibria". 3rd ed. **1999**, Prentice-Hall, Inc.: Upper Saddle, New Jersey.
2. Chapman, W.G.; Gubbins, K.E.; Jackson, G.; Radosz, M., "New Reference Equation of State for Associating Liquids". *Industrial & Engineering Chemistry Research*, **1990**, 29, 1709-1721.
3. Fredenslund, A.; Jones, R.L.; Prausnitz, J.M., "Group-Contribution Estimation of Activity Coefficients in Nonideal Liquid Mixtures". *AIChE Journal*, **1975**, 21, 1086-1099.
4. Spyriouni, T.; Economou, I.G.; Theodorou, D.N., "Phase Equilibria of Mixtures Containing Chain Molecules Predicted Through a Novel Simulation Scheme". *Physical Review Letters*, **1998**, 80, 4466-4469.
5. Nath, S.K.; Escobedo, F.A.; de Pablo, J.J.; Patramai, I., "Simulation of Vapor-Liquid Equilibria for Alkane Mixtures". *Industrial & Engineering Chemistry Research* **1998**, 37, 3195-3202.
6. Bureau, N.; Jose, J.; Mokbel, I.; de Hemptinne, J.-C., "Vapour Pressure Measurements and Prediction for Heavy Esters". *Journal of Chemical Thermodynamics*, **2001**, 33, 1485-1498.
7. Asher, W.E.; Pankow, J.F.; Erdakos, G.B.; Seinfeld, J.H., "Estimating the Vapor Pressures of Multi-Functional Oxygen-Containing Organic Compounds Using Group Contribution Methods". *Atmospheric Environment*, **2002**, 36, 1483-1498.
8. Jorgensen, W.L.; Madura, J.D.; Swenson, C.J., "Optimized Intermolecular Potential Functions for Liquid Hydrocarbons". *Journal of the American Chemical Society*, **1984**, 106, 6638-6646.
9. Martin, M.G.; Siepmann, J.I., "Transferable Potentials for Phase Equilibria. 1. United-Atom Description of n-Alkanes". *Journal of Physical Chemistry B*, **1998**, 102, 2569-2577.
10. Nath, S.K.; Escobedo, F.A.; de Pablo, J.J., "On the Simulation of Vapor-Liquid Equilibria for Alkanes". *Journal of Chemical Physics*, **1998**, 108, 9905-9911.

11. Delhommelle, J.; Tschirwitz, C.; Ungerer, P.; Granucci, G.; Millie', P.; Pattou, D.; Fuchs, A.H., *Journal of Physical Chemistry B*, **2000**, 104, 4745-4753.
12. Errington, J.R.; Panagiotopoulos, A.Z., "A New Intermolecular Potential Model for the *n*-Alkane Homologous Series". *Journal of Physical Chemistry*, **1999**, 103, 6314-6322.
13. Chen, B.; Martin, M.G.; Siepmann, J.I., "Thermodynamic Properties of the Williams, OPLS-AA, and MMFF94 All-Atom Force Fields for Normal Alkanes". *The Journal of Physical Chemistry*, **1998**, 102, 2578-2586.
14. Toxvaerd, S., "Molecular Dynamics Calculation of the Equation of State of Alkanes". *Journal of Chemical Physics*, **1990**, 93, 4290-4295.
15. Case, F.; Chaka, A.; Friend, D.G.; Frurip, D.; Golab, J.; Gordon, P.; Johnson, R.; Kolar, P.; Moore, J.; Mountain, R.D.; Olson, J.; Ross, R.; Schiller, M., "The second industrial fluid properties simulation challenge". *Fluid Phase Equilibria*, **2005**, 236, 1-14.
16. Unlu, O.; Gray, N.H.; Gerek, Z.N.; Elliott, J.R., "Transferable step potentials for the straight-chain alkanes, alkenes, alkynes, ethers, and alcohols". *Ind. Eng. Chem. Res.*, **2004**, 43, 1788-1793.
17. Gray, N.H.; Gerek, Z.N.; Elliott, J.R., "Molecular Modeling of Isomer Effects in Naphthenic and Aromatic Hydrocarbons". *Fluid Phase Equilibria*, **2005**, 228, 147-153.
18. Baskaya, F.S.; Gray, N.H.; Gerek, Z.N.; Elliott, J.R., "Transferable Step Potentials for Amines, Amides, Acetates, and Ketones". *Fluid Phase Equilibria*, **2005**, 236 42–52.
19. Frenkel, D.; Smit, B., "Understanding Molecular Simulation". 2nd ed. **1996**, Academic Press: San Diego.
20. Allen, P.; Tildesley, D.J., "Computer Simulation of Liquid". **1987**, Oxford Science Publication: Oxford.
21. Alder, B.J.; Wainwright, T.E., "Studies in Molecular Dynamics. I. General method". *Journal of the American Chemical Physics*, **1959**, 31, 459- 436.
22. Rappaport, D.C., "Molecular Dynamics Simulation of Polymer Chains with Excluded Volume". *Journal of Physics A: Mathematical and General*, **1978**, 11, L213-L217.

23. Maginn, E.J.; Elliott, J.R., "Historical Perspective and Current Outlook for Molecular Dynamics As a Chemical Engineering Tool". *Industrial & Engineering Chemistry Research* **2010**, 49, 3059-3078.
24. Rapaport, D.C., "Molecular Dynamics Study of a Polymer Chain in Solution ". *Journal of Chemical Physics*, **1979**, 71, 3299-3303.
25. Chapela, G.A.; Scriven, L.E.; Davis, H.T., "Molecular Dynamics for Discontinuous Potential. IV. Lennard Jonesium". *J. Chem. Phys.*, **1989**, 91, 4307.
26. Rapaport, D.C., "The Event Scheduling Problem in Molecular Dynamic Simulation". *Journal of Computational Physics*, **1980**, 34, 184-201.
27. Rappaport, D.C., "The Art of Molecular Dynamics Simulation". 2nd ed. **2004**, Cambridge University Press: Cambridge, UK.
28. Barker, J.A.; Henderson, D., "Perturbation Theory and Equation of State for Fluids: The Square-Well Potential". *The Journal of Chemical Physics*, **1967**, 47, 2856-2861.
29. Zwanzig, R.W., "High- Temperature Equation of State by a Perturbation Method. I. Nonpolar Gases". *The Journal Of Chemical Physics*, **1954**, 22, 1420-1426.
30. Zhou, S.; Solana, J.R., "Progress in the Perturbation Approach in Fluid and Fluid-Related Theories". *Chemical Reviews*, **2009**, 109, 2829-2858.
31. Wertheim, M.S., "Fluids with highly directional attractive forces. II. Thermodynamic perturbation theory and integral equations". *J. Stat. Phys.*, **1984**, 35, 35-47.
32. Wertheim, M.S., "Fluids with Highly Directional Attractive Forces. IV. Equilibrium Polymerization". *Jornal of Statistical Physics*, **1986**, 42, 477-492.
33. Elliott, J.R., "Efficient Implementation of Wertheim's Theory for Multicomponent Mixtures of Polysegented Species". *Industrial & Engineering Chemistry Research*, **1996**, 35, 1624-1629.

CHAPTER III

3. PREDICTION OF LIQUID DENSITIES AND VAPOR PRESSURES WITH SPEAD: MOTIVATION FOR A NEW STEP POTENTIAL MODEL

3.1 Summary of results with SPEAD: model parameters and the liquid density errors

The SPEAD force-field is a major improvement in comparison to TraPPE for vapor pressure predictions away from the critical point, especially at lower reduced temperatures[1]. For the classes of compounds shown in Figure 3.1, the average absolute deviations (AAD) in vapor pressure predictions with SPEAD are within 16% of the experimental data.

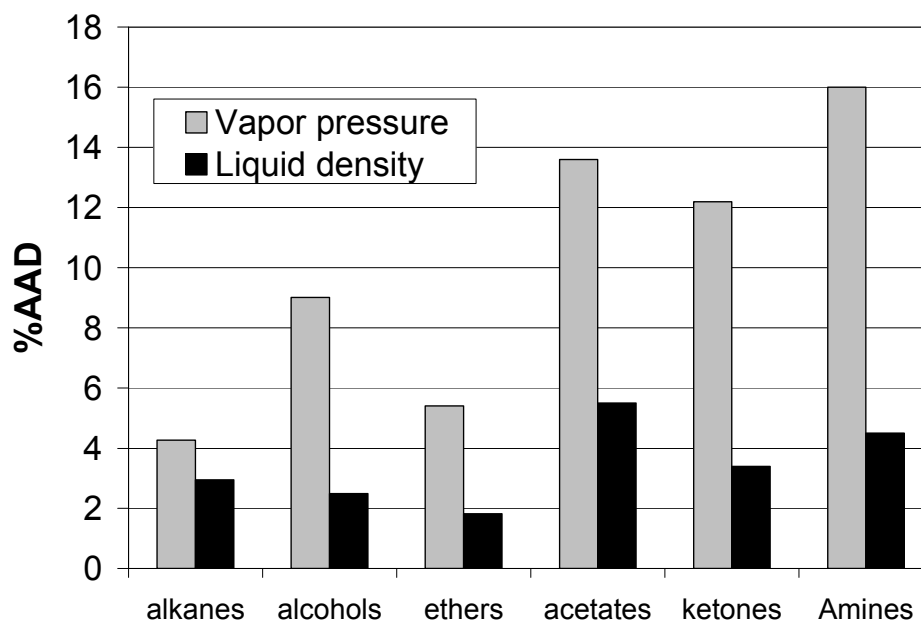


Figure 3.1: Published results of vapor pressure and liquid densities using SPEAD

However, this improvement comes at the expense of accuracy in the liquid density predictions. Except for the ethers, the density deviations of all the other compounds in Figure 3.1 are approximately between 2.5- 6%. It is desirable that the density deviations fall within 1-2% of the experimental values, since small changes in densities can greatly affect other thermodynamic

properties. Figure 3.2 below shows the simulated liquid densities of alkanes with the SPEAD model. With increasing molecular weight, the densities are increasingly overpredicted. A similar trend is observed in the density errors of ketones, acetates, α -olefins, ketones and acetates (Fig 3.6). This trend is not so clear in some of the compounds which have been optimized only for smaller chains, for example, ethers[1]. Intuitively, this could be a result of “overoptimization” of the non-alkane parameters in these compounds, in order to compensate for the errors being carried over from the alkane parameters. These errors in the densities are observed despite the use of extra parameters for some of the functional groups, like alcohols[1], ketones[2] and acetates[2].

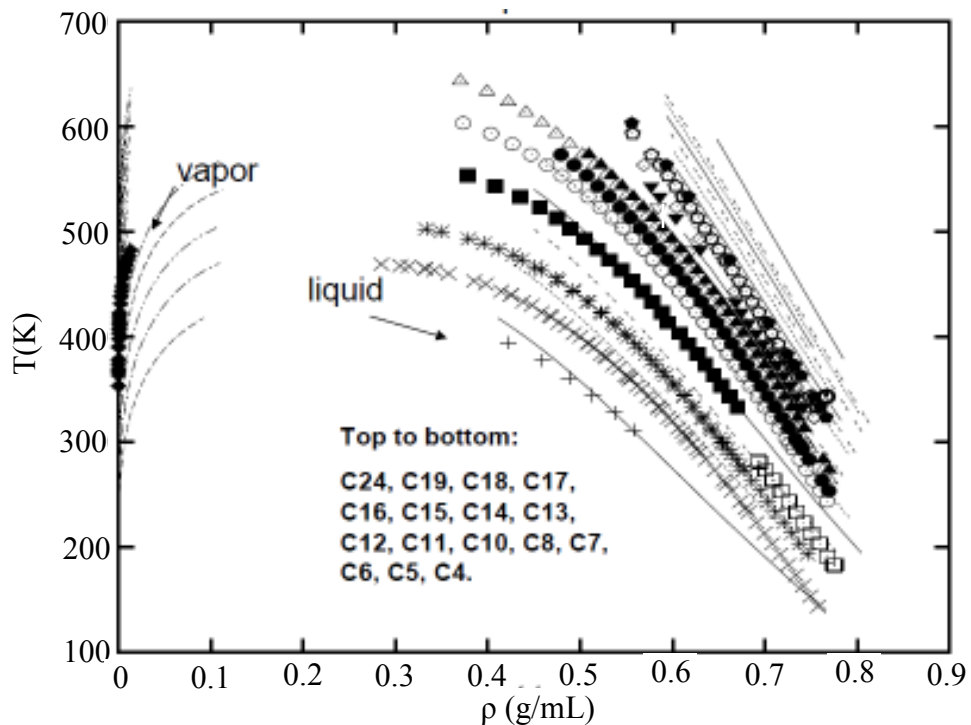


Figure 3.2: Density predictions of normal alkanes with Akron SPEAD. The dots are experimental points and the lines are model predictions

Since thermodynamic properties are sensitive to small changes in densities, it is imperative for any new potential to reproduce densities well. Care also needs to be taken to ensure transferability of the parameters, which can be achieved by including a broader range of molecular weights in order to incorporate the smallest possible contribution from a functional group.

3.2 Improvements: the StePPE model

To remedy the discrepancies in SPEAD discussed above, some of the model parameters, such as site sizes and intramolecular interaction parameters, needed readjustment in order to study their effect on the vapor pressure and density predictions. The site sizes can be changed manually, but to change any other simulation parameter, access to the source code is required. The SPEAD software is a compiled version instead, owned by ChemStations Inc. of Houston, Texas, and the source code is unavailable. Therefore, with the aim of developing a robust step potential model, using DMD and TPT, which could be used as a fast tool in a variety of industrial applications, a new source code was developed. To avoid confusion with the SPEAD model and parameters, we refer to this new model as StePPE, which stands for Step Potentials for Phase Equilibria, though it uses much of the same methodology as SPEAD. As the name suggests, the form of the force-field is the same (see “SPEAD theory” in the introduction part), but some changes were necessary in order to reproduce the liquid densities more accurately, without compromising the speed or accuracy in the vapor pressure predictions observed with the SPEAD model. The changes are discussed in the following sections.

1. Hard-site diameters from excluded volumes

Intuitively, the density errors in alkanes can be addressed by revisiting the hard-site diameters used for the methyl and methylene groups, since the errors in other compounds may be due to poor transferability of the alkane parameters. The site diameters in SPEAD were found by fitting the experimental vapor pressures. In the following paragraphs, we discuss our method of site-size selection using excluded volume considerations.

Hard site diameters can be found by mapping of the explicit atom potentials to UA potentials and then mapping it to a hard site potential, as described by McCoy[3]. A coarser method is to use a combination of the tabulated excluded volumes of the individual atoms in a particular group, and find the diameter of an equivalent sphere. Both methods have been shown to be in close agreement for the diameter of methane[4]. If the volume lost due to overlaps is accounted for correctly, the latter method can work reasonably well for other sites as well.

In our model, we use the core volumes of *groups*, as tabulated by Bondi[5]. Bondi determines the group core volumes by summing the contributions of spheres for the individual atoms. In this work, we find an equivalent sphere to represent the group core volumes as a single united atom group sphere and not spheres for the individual atoms, and we then calculate the united atom site diameter. Volume lost due to overlap by each covalent bond is calculated by simple geometry (see Appendix A.2) and added to the excluded volume of the group. The diameter of an equivalent sphere with this corrected volume gives the first guess of the site diameter. The volume correction would obviously depend on the adjacent sites and bond lengths, which would be tedious to tabulate for every site. Just for the quaternary carbon in branched alkanes, a total of 24 different sizes would have to be tabulated!

We calculated the volume corrections using all possible site combinations in an n-alkane, namely, CH₃-CH₃, CH₂-CH₂ and CH₃-CH₂. Using an analysis based on the bond lengths and

the excluded volumes as described by Bondi[5] and Slonimskii et al[6], we found that the volume lost for each covalent bond in each case was close to 20%. We used that correction for sites in all other functional groups to provide a first guess at the site diameters. For example, the first guess for the diameter of the quaternary carbon was obtained from adding an 80% correction, 20% for each covalent bond. We refer to the diameters calculated by the approximation as σ_{vdw} . Starting from this diameter, we found the optimized diameters to be slightly smaller than σ_{vdw} . Figure 3.3 (a) and (b) show the site sizes based on our analysis and the optimized sizes in StePPE and TraPPE respectively. In both cases, the final optimized site sizes follow the sizes obtained from van der Waal's volumes closely, the sp^3 CH in TraPPE being the only outlier that doesn't follow that trend. The sensitivity of the site diameters on the volume correction increases with the number of covalent bonds. For example, the sp^3 C in the branched alkanes has four covalent bonds, so will be affected most by a change in the volume correction. The methyl group would be least sensitive. The unusually big size of the sp^3 C in TraPPE (6.4 Å) can be explained based on this reasoning.

The site sizes in the UA models in general, are obtained from fitting available experimental thermodynamic data, such as vapor-liquid coexistence properties or critical properties. In the continuous models, sigma and epsilon are optimized simultaneously. Changing either parameter would require the simulation to be run again. In SPEAD, the well parameters are optimized post simulation, but changing the site diameter would require the simulation to be repeated. Therefore, whether it is the computationally more expensive continuous models, or the four step TPT model, a methodology to get a good first guess for the size diameter would be extremely helpful in minimizing the CPU time for optimization.

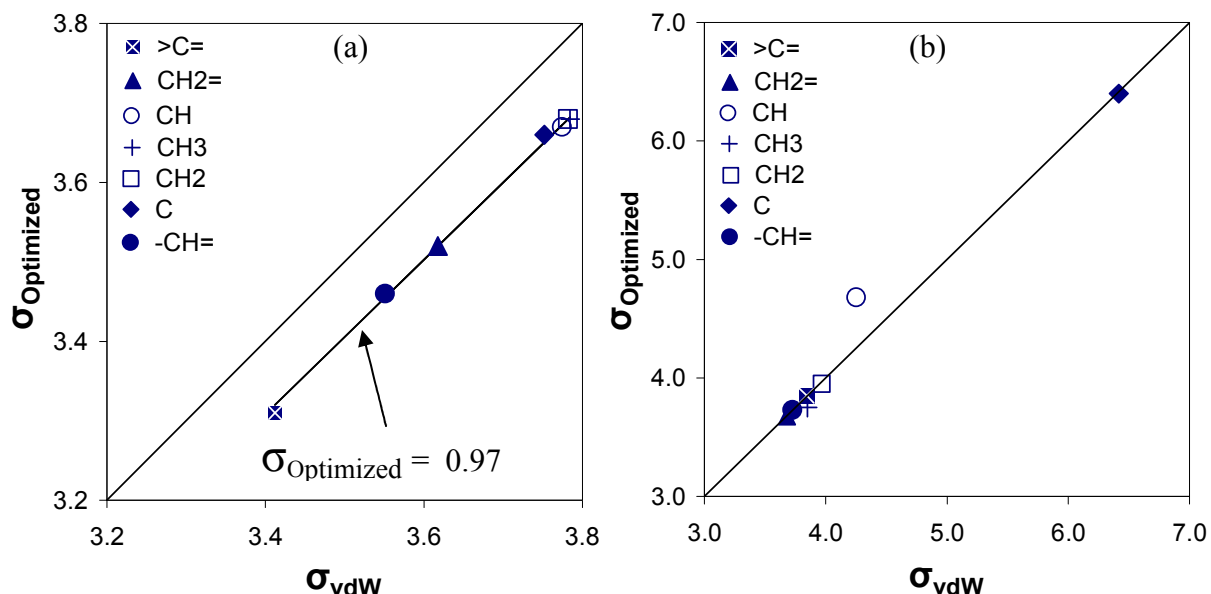


Figure 3.3: Optimized site diameters (ordinate) compared to diameters obtained from van der Waal's volumes (abscissa) in Å; (a) StePPE, based on 20% volume correction per bond, (b) TraPPE, based on 24% volume correction per bond

The molecular core volumes are determined during a run. Prior to a run, the sites are placed at the bond distances given in Table A2.1 in the appendix. The core volume of the free molecule is determined by then vibrating the molecule for 3000-5000 ps and taking 100 snapshots. To prevent translation of the center of mass, the first and last sites in the structure file are accelerated towards each other. The degrees of freedom are reduced by three and when relating the kinetic energy to temperature, the simulation is started at 300K. After an equilibration time ($10000 + 1000 \times \text{Number of molecules per site}$), 100 snapshots are taken at intervals of 30 - 60 ps depending on the size of the molecule. For each snapshot, a grid of points placed $1/20$ Å apart is placed over the molecule. The core volume of the molecule is determined by calculating the fraction of points inside the molecule, which corresponds to the fraction of the cell occupied by the core volume. Different spacings of grid points were tested, and the spacing of $1/20$ Å was determined to be suitable. Due to flexibility of the molecule, the core volume

varies amongst the snapshots. Use of a finer grid took a longer time, and did not result in significantly different core volumes. Further, the free molecule core volume is slightly different than the core volume determined during a simulation. During the simulation, collisions with other molecules affect the core volume and the trend is that the core volume decreases slightly (0.2 %) at high density when the molecules are tightly packed. When each density is run, the core volumes of the first 100 molecules in the simulation box are sampled at the end of the run, and the average core volume is determined. Then the core volumes from the series of densities simulated are averaged to determine the reported core volume. As an example of the results for the core volumes, the core volumes of n-alkanes are plotted against van der Waals volumes tabulated in DIPPR in Figure 3.4. The core volumes in StePPE are smaller than the van der Waal's volumes since the optimized sizes of the CH₃ and the CH₂ groups are slightly smaller than that predicted by the excluded volumes.

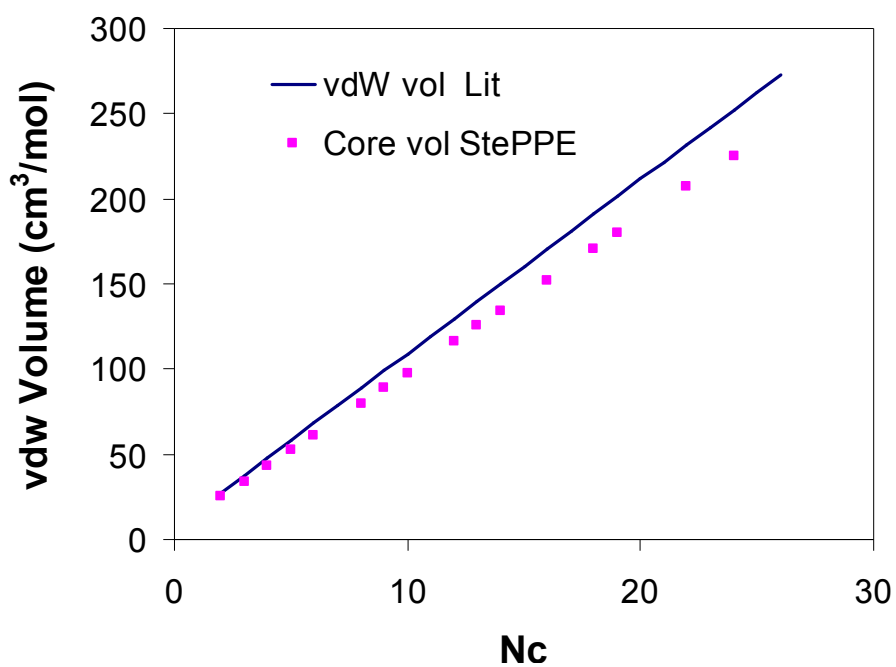


Figure 3.4: Core volumes predicted with StePPE plotted against van der Waal's volumes of alkanes. The x-axis denotes the number of C atoms in the alkane chain

2. Exponential function for A2

The equation of state is obtained from derivatives of the first and second order perturbation terms. Therefore, a good fit to the simulation data for the perturbation terms is essential for the new equation of state to be accurate. For the second order perturbation term, we use a new exponential function given by:

$$A_2 = (a_{21}\eta + a_{22})\exp(-a_{23}\eta^{a_{24}}) - a_{25}$$

where, a_{2i} s are constants to be found from the best fit. It doesn't differ much from the published SPEAD A2 polynomial function for lower and packing factors near 0.35 – 0.4, but in some cases, fits better at moderate densities (Figure 3.5).

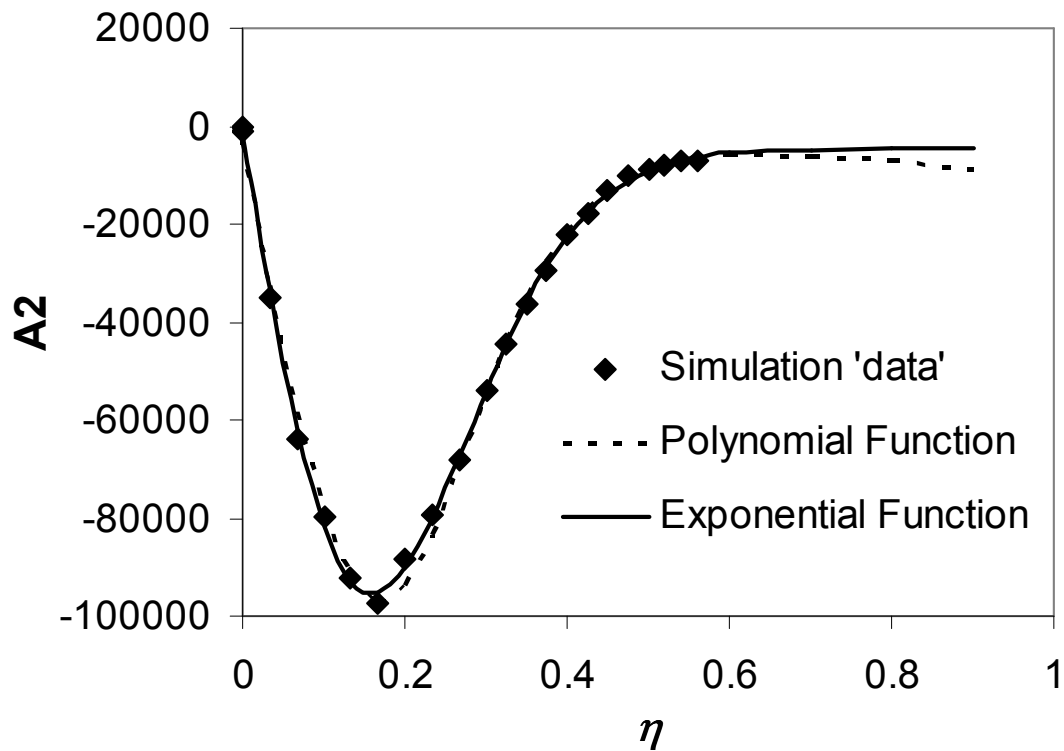


Figure 3.5: Comparison of A2 using polynomial function as in Akron- SPEAD and exponential function as in MSU-SPEAD for trioxane

Also, the fit with the exponential function would be more reasonable if the runs were to be extended to higher densities, though not expected at the current level of detail (note the decreasing A2 in Figure 3.5 for the polynomial function). Overall, the function is used to interpolate and differentiate the simulation results; we don't expect a dramatic change in the overall accuracy of the model with this change, but the exponential function would give a more realistic fit overall. The function was under consideration since we had observed an unrealistic "dip" in the prediction of A2 at higher densities seen in the earliest SPEAD studies[7]. Though the functional form for A2 has changed in SPEAD too, we deemed it reasonable to use the exponential function in our model.

3. Intramolecular interaction parameters

In SPEAD, any two sites separated by less than 6 bonds interact with special reduced diameters (σ_{Intra}). The main purpose of the intra diameters is to let sites flip past each other so as to make the dihedral angle flexible, which in turn imparts flexibility to the chain. In our model, we use intra diameters only for a 1, 4 interactions. Also, the pairwise attractive potential starts at a separation of 3 bonds in our model, as opposed to 7 bonds in SPEAD. The purpose of this change was to incorporate all the intramolecular attractions possible. Bond lengths are taken largely from the NIST Computational Chemistry Comparison and Benchmark DataBase[8]. Average values are used for each class of bond. No special bond lengths were used for specific molecules. In SPEAD, a large table of bond lengths is used to characterize the second-neighbor distances for constraining bond angles. In StePPE, we have instead specified bond angles for given site types. For example, bond angles for sp^3 molecules are typically 109° , but for sp^2 they

are set to 120° . The lengths of pseudobonds are calculated at the start of a simulation run, but matching the bond lengths with the site angles. The pseudobonds are allowed to vibrate $\pm 5\%$.

3.3 Summary of comparison of errors with SPEAD and StePPE

The effect of the improvements discussed above is manifest in the results obtained with StePPE. Not only is the systematic error in the densities removed (Fig 3.6), we have been able to eliminate a significant number of parameters for a number of functional groups, as will be discussed in the third chapter. An overall comparison of errors in vapor pressures and liquid densities with SPEAD and StePPE is shown in Table 3.1

Table 3.1: Summary of errors in vapor pressure and liquid density predictions with SPEAD and StePPE

Compound	P^{sat} Error (%AAD)		ρ Error (%AAD)		N_c range (#compounds simulated)	
	SPEAD	StePPE	SPEAD	StePPE	SPEAD	StePPE
n-Alkanes	4.54	6.15	3.1	0.76	1 – 16 (12)	2 – 24 (16)
n-Alkenes	7.19	10.35	1.61	0.84	3 – 8 (20)	3 – 10 (15)
n-Alcohols	9.01	8.13	2.49	0.65	1 – 10 (10)	1 – 20 (17)
Branched alkanes	-	9.55	-	1.1	-	3 – 10 (24)
Secondary alcohols	-	9.39	-	0.58	-	3 – 9 (10)
Ethers	5.4	8.56	1.83	0.49	2 – 6 (6)	2 – 18 (14)
Ketones	12.2	8.1	3.4	0.37	3 – 9 (15)	3 – 9 (16)
Esters	13.6	10.87	5.5	0.93	3 – 12 (9)	3 – 19 (25)

Some other aspects have been the subject of recent studies, where we have tried to analyze the effect of tail corrections and include the effect of electrostatic charges in the model. These topics are discussed in the “Future work” section in CHAPTER VI, where the implementation procedure and some preliminary results are discussed.

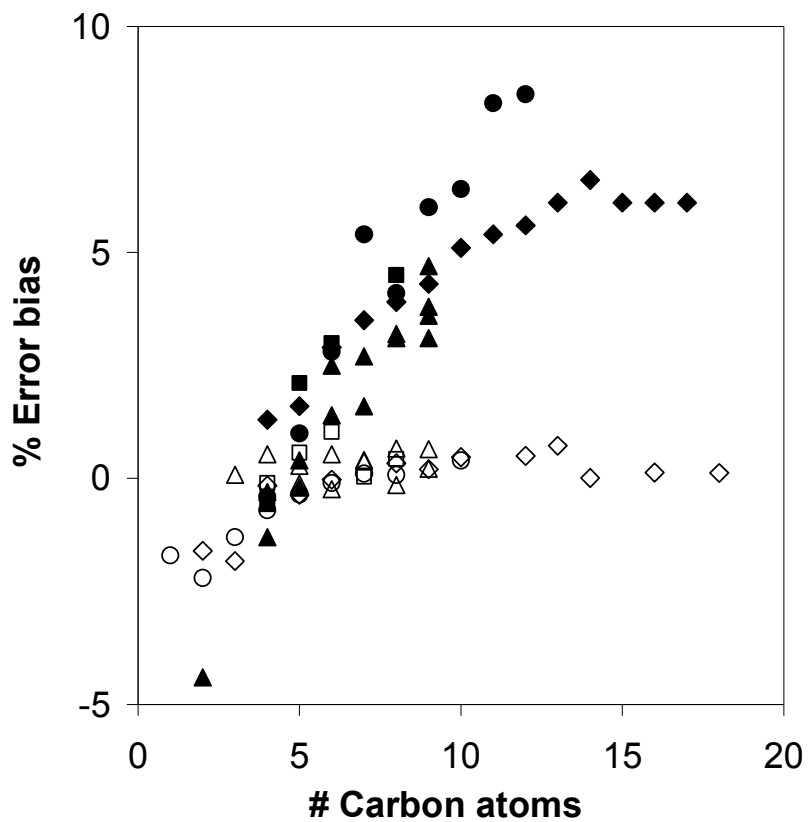


Figure 3.6: Liquid density deviations of selected compounds with SPEAD (filled symbols). Symbols are: diamonds- alkanes[9], circles- 1-alkenes[1], triangles- ketones[2], squares- acetates[2]. The open symbols are with StePPE

REFERENCES

3.4 References

1. Unlu, O.; Gray, N.H.; Gerek, Z.N.; Elliott, J.R., "Transferable Step Potentials for the Straight-Chain Alkanes, Alkenes, Alkynes, Ethers, and Alcohols". *Industrial & Engineering Chemistry Research* **2004**, 43, 1788-1793.
2. Baskaya, F.S.; Gray, N.H.; Gerek, Z.N.; Elliott, J.R., "Transferable Step Potentials for Amines, Amides, Acetates, and Ketones". *Fluid Phase Equilibria*, **2005**, 236 42–52.
3. McCoy, J.D.; Curro, G.J., "Mapping Explicit Atom onto United Atom Potentials". *Macromolecules*, **1998**, 31, 9362-9368.
4. McCoy, J.D.; Mateas, S.; Zorlu, M.; Curro, J.G., "The Role of Excluded Volume in Polyethylene Intermolecular Potentials". *Journal of Chemical Physics*, **1995**, 102.
5. Bondi, A., "van der Waal's Volumes and Radii". *The Journal of Physical Chemistry*, **1964**, 68, 441-451.
6. Slonimskii, G.L.; Askadskii, A.A.; Kitaigordoskii, A.I., "The Packing of Polymer Molecules". *Polymer Science USSR*, **1970**, 12, 556-577.
7. Cui, J.Y.; Elliott, J.R., "Phase Diagrams for a Multistep Potential Model of n-Alkanes by Discontinuous Molecular Dynamics and Thermodynamic Perturbation Theory". *Journal of Chemical Physics*, **2002**, 116, 8625-8631.
8. <http://cccbdb.nist.gov/>.
9. Elliott, J.R.; Gray, N.H., "Asymptotic Trends in Thermodynamic Perturbation Theory". *Journal of Chemical Physics*, **2005**, 123, 184902-1-184902-6.

CHAPTER IV

4. LIQUID DENSITIES AND VAPOR PRESSURES OF PURE COMPOUNDS WITH StePPE MODEL

4.1 Site diameter and step potential optimization: summary

Liquid density and vapor pressure data from DIPPR 801 were used to optimize the site parameters in this work. Comparisons with SPEAD[1], TraPPE[2] and NERD[3] models are made, wherever published data was found with those models. Experimental data obtained from the DIPPR database was used for the optimization, but for simplicity, when comparisons are made with other models, we use the correlations fit to the accepted experimental data available in DIPPR, except when the comparison is only with SPEAD. Only the experimental data that was categorized as “accepted” in the DIPPR database was used, and smoothed data was avoided. The StePPE fits for complete set of molecules in a homologous series are shown in separate plots in Appendix A.3.

Three parameters were optimized for each site, namely the hard site diameter (σ) and the inner (ϵ_I) and the outer (ϵ_O) well depths using the HEEDS optimization software. The optimization method used was proprietary method called SHERPA[4], which stands for Simultaneous Hybrid Exploration that is Robust, Progressive and Adaptive. It is a hybrid method which uses multiple search methods simultaneously using the best attributes of each method. It uses a combination of global and local search methods, and the parameters of the methods used are tuned internally. The number of evaluations to perform is defined by the user. Typically, the SHERPA optimization was followed by a quadratic gradient search to further optimize the parameters.

Table 4.1: Summary of optimized parameters for sites used in this study. The sites within parentheses in the first columns are the sites to which the group in that column is bonded, or a special case. For example ‘CH3 (-CH2-/-CH3)’ represents a methyl group, which is bonded to another methyl or methylene group. The ‘>’ or ‘<’ signs mean two sigma bonds and the ‘=’ sign denotes a double bond. For example, the carbonyl carbon, which has two sigma bonds and a double bond is represented by ‘>C=’. θ is the bond angle. The term ‘ σ ’ denotes the site diameter and the term ‘ k ’ in well energies is the Boltzmann constant.

Site	σ (Å)	σ Intra (Å)	ϵ_1/k (K)	Angle (θ°)	ϵ_4/k (K)
CH3 (-CH2-/-CH3)	3.68	2.63	93.4	109.5	13.0
CH3 (>CH-/>C<)	3.68	2.63	54.7	109.5	27.3
CH3 (>CH- in isobutane only)	3.68	2.63	70.4	109.5	20.4
CH3 (-O-)	3.68	2.63	115.9	109.5	6
CH3 (>C=)	3.68	2.63	115.78	109.5	11
CH3 (-OH in methanol only)	3.68	2.63	103.3	109.5	34.5
CH3 (>C= in acetone only)	3.68	2.63	100.0	109.5	26.5
CH3 (2-butanol only)	3.68	2.63	93	109.5	16
CH2 (-CH3/-CH2-)	3.68	2.63	35.4	109.5	17.2
CH2 (-CH-)	3.68	2.63	35.0	109.5	15.7
CH2 (-O-)	3.68	2.63	54.04	109.5	8.1
CH2 (>C=)	3.68	2.63	69.8	109.5	5.8
CH2 (-OH in ethanol only)	3.68	2.63	44.7	109.5	27.0
CH2 (-OH)	3.68	2.63	36	109.5	25.2
CH (in a branched alkane)	3.67	2.67	15.3	109.5	9.1
CH (-OH in secondary alcohols)	3.67	2.69	20.3	109.5	8.9
C (-CH3/-CH2-/>CH-/>C<)	3.66	2.63	4.0	109.5	0.7
CH2= (-CH=)	3.52	2.52	78.8	125	6.9
CH= (in α -olefins and α,ω -diolefins)	3.4	2.4	56.9	125	12.8
CH= (in cis/trans olefins only)	3.4	2.4	57.3	125	8.9
>C= (in ketone)	3.31	2.92	45.0	120	10
>C= (in ester)	3.31	2.92	40.4	120	2.0
-OH (-CH2- in primary alcohols)	2.8	1.8	140	109.5	34
-OH (-CH- in secondary alcohols)	2.8	1.8	116	109.5	6.2
-O- (-CH2-/CH3 in ester or ether)	2.47	1.83	55.4	109.5	37.3
O= (>C= in ketone or ester)	2.77	1.83	108.9	120	12.8
<u>Association parameters</u>					
	κ	λ	ϵ^{AD} (kcal/mol)		
OH (primary or secondary alcohols)	0.000496	0.994347	4.69423		

The two intermediate well depths were found by interpolating between the inner and the outer well. Wherever possible, a broad range of molecular weights was used in the training set for each functional group, to account for the smallest contributions from a group, and hence to

improve the transferability of the parameters. Table 4.1 shows the optimized parameter values of all the sites that were optimized in this study.

4.2 Discussion of results with StePPE parameters and comparison with other UA models

1. *n*-Alkanes

n-Alkanes, composed of methyl (-CH₃) and methylene (-CH₂-) groups, are saturated hydrocarbons used in the chemical and petrochemical industry as starting materials and solvents, and are also a critical source of energy for industrial, transport, as well as household needs. They are also of vital importance to academic research of organic compounds, since the functional groups in alkanes are also present in other homologous series, like unsaturated hydrocarbons, alcohols, acids, aldehydes, ketones and esters. Because of their importance as such, and ubiquitous presence in organic compounds, large amount of reliable thermodynamic data for alkanes is available in literature. Hence, they are always used as the first class of compounds to test the accuracy and transferability of potential models.

In the UA models, two sites with appropriate bonding parameters are required to define the alkanes. In our model, the CH₃ and CH₂ parameters were obtained by fitting the experimental liquid densities and vapor pressures of ten alkanes. The parameters were then used to predict the liquid densities and vapor pressures of six other alkanes, shown in Table 4.1. The overall deviation for liquid densities is less than 1%, and for vapor pressures is 6.1%. The reduced temperature range shown in Table 4.2 and the following tables is only for accepted experimental data in DIPPR that was used for the optimizations. The comparisons mostly range to wider temperature ranges.

Among the continuous force-fields for alkanes, OPLS[5], which was parameterized for liquid densities and heats of vaporization of short chain alkanes near ambient conditions, has

been observed to show inaccuracies at elevated temperatures and pressures for both, liquid densities[2, 6] and vapor pressures[2]. TraPPE –UA[2] predicts the liquid densities extremely well (AAD < 1%) for the alkanes ranging between ethane and n-decane, but higher errors have been reported[3] for longer normal alkanes. The reported TraPPE vapor pressures on the other hand, show an average deviation of about 26%[1]. The errors appear to be higher for the shorter n-alkanes and at lower reduced temperatures. The NERD[7] force-field predicts the liquid density of alkanes longer than n-dodecane better than TraPPE, but vapor pressure calculations for the long alkanes are less accurate[8].

Table 4.2: Vapor pressures and liquid densities of n-alkanes with StePPE. P^{sat} , T_r^{min} , and T_r^{max} in this and the subsequent tables mean vapor pressure, minimum reduced temperature and maximum reduced temperature

Compound ¹	P^{sat}		ρ		T_r^{min}	T_r^{max}
	%AAD	%Bias	%AAD	%Bias		
nC2	2.27	0.28	3.48	-1.6	0.37	0.9
nC3* ²	9.97	-9.97	1.86	-1.82	0.24	0.97
nC4*	14.94	-14.94	0.94	-0.16	0.33	0.89
nC5*	8.47	-8.47	1.04	-0.36	0.31	0.89
nC6*	7.07	-7.07	0.69	-0.02	0.38	0.9
nC8	6.49	-6.45	0.82	0.33	0.4	0.88
nC9	4.23	-4.16	0.6	0.2	0.38	0.9
nC10*	4.57	-3.47	0.81	0.46	0.39	0.9
nC12*	4.45	-2.31	0.77	0.5	0.4	0.87
nC13	4.2	1.02	0.93	0.72	0.4	0.85
nC14	4.72	0.77	0.21	0	0.4	0.81
nC16*	6.85	3.38	0.19	0.13	0.4	0.82
nC18*	7.27	4.55	0.32	0.12	0.4	0.84
nC19*	7.62	2.11	0.44	0.16	0.4	0.84
nC22	10.19	1.71	0.15	-0.08	0.4	0.85
nC24*	9.26	-6.89	0.09	-0.09	0.43	0.73
Overall	6.14	-2.71	0.75	0.07		

¹ The ‘n’ in ‘nC_x’ implies a normal alkane and ‘x’ denotes the chain length. For example, nC₈ is n-octane

² The compounds with ‘*’ in this and the following tables were used in the training set

Unlu and Elliott[9] first reported vapor pressures and liquid densities of 12 n-alkanes with step potentials between methane and n-hexadecane in 2004. With the optimized parameters, the deviations in vapor pressure and liquid density were 4.3% and 4.0% respectively. They report an improvement in the vapor pressure prediction by an order of magnitude compared to TraPPE. Also, the SPEAD predictions range to lower reduced temperatures in comparison. It should be noted however, that the adjustable parameters for n-alkanes in TraPPE are four, against six in SPEAD. The density deviations in SPEAD on the other hand, showed a systematic overprediction with increasing chain length (see Fig 3.2)). In a later publication[10], the parameters were refined to include larger molecular weight compounds, at the expense of ethane. With the new parameters, we see an improvement in the vapor pressure predictions of the intermediate alkanes- n-heptane to n-dodecane, but the densities still remain overpredicted (Fig 3.5).

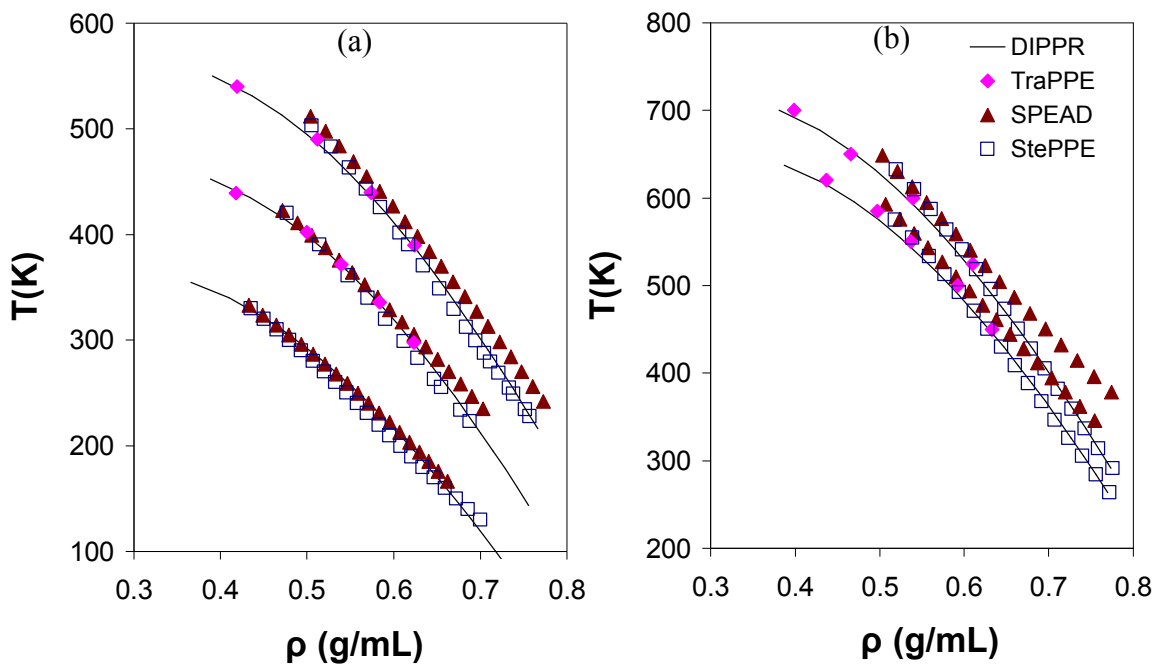


Figure 4.1: Liquid densities from left to right of (a) n-propane, n-pentane and n-octane, and (b) n-dodecane and n-hexadecane. The symbol meanings are same in (a) and (b)

The StePPE liquid densities are significantly improved in comparison to SPEAD, and the vapor pressures are particularly improved for C16 and larger alkanes. Figures 4.1 and 4.2 show a comparison of the liquid densities and vapor pressures for selected alkanes with TraPPE, SPEAD, and StePPE. For molecules larger than propane, the liquid densities are overpredicted with SPEAD and the error is maximum for n-hexadecane. With StePPE, not only is the systematic error in the liquid densities eliminated for all but the smallest compounds, the predictions range to lower temperatures. The densities for n-dodecane with TraPPE and StePPE are very similar, but for n-hexadecane, StePPE seems to be more accurate than TraPPE at lower reduced temperatures. The vapor pressures for the entire range of compounds with StePPE seem to agree well with the experimental data.

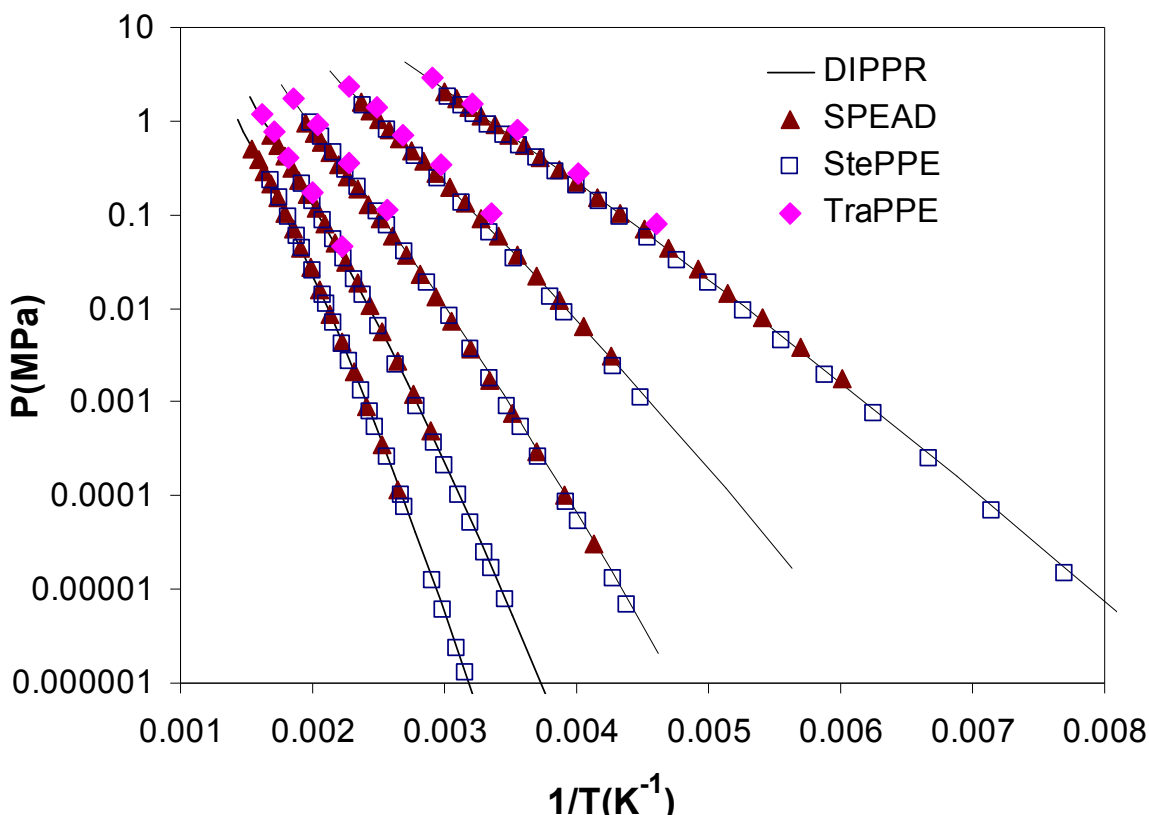


Figure 4.2: Vapor pressures, from right to left, of *n*-propane, *n*-pentane, *n*-octane, *n*-dodecane and *n*-hexadecane. For interpretation of the references to color in this and all other figures, the reader is referred to the electronic version of this dissertation.

In StePPE, the sizes of CH₃ and CH₂ were kept same based on the excluded volume considerations discussed above. Therefore, we have one less adjustable parameter compared to SPEAD for n-alkanes. Also, unlike OPLS and NERD, no special parameters were used for the smaller compounds.

2. Branched alkanes

Branched alkanes are important for the petroleum refining and petrochemical industries, as they are good antiknock agents for gasoline engines, and have good lubrication properties compared to their straight chain counterparts. A good design of the processes technologies for refining and separation of branched alkanes requires reliable phase equilibrium data. The branched alkane isomers also provide an attractive set of compounds to test a force-field for property differences based on differences in molecular arrangements.

Of the force-fields developed so far, not many have been optimized for branched alkanes. SPEAD parameters for branched alkanes have not been published. The TraPPE[11, 12] force – field reproduces the liquid densities of short branched alkanes well (Fig 4.3 (a)), but the vapor pressures are overpredicted, especially for the smaller molecules and at lower reduced temperatures (Fig 4.3 (b)). The %AAD for the vapor pressures of the compounds in their study is about 23%. Also, the liquid densities for compounds with less than six carbon atoms appear to be underpredicted, while for the bigger compounds, an opposite trend is observed. Rather than changing the site diameters, using a different potential depth for the side methyl group could be helpful in rectifying the errors, but might necessitate the use of special parameters for some of the smaller compounds, an approach used in the NERD[13-15] force-field. In comparison to TraPPE, the NERD force-field has been tested for a wider range of branched alkanes and can distinguish between structural isomers, but special parameters have been used for the methyl

groups in isobutane, isopentane, neopentane and neohexane. The vapor pressures of the branched alkanes with NERD, except for a small set of compounds, are still to be tested. StePPE uses a similar approach to NERD, but with special parameters only for isobutane.

Table 4.3: Vapor pressures and liquid densities of branched alkanes with StePPE

Compound ³	P ^{sat}		ρ		T _r ^{min}	T _r ^{max}
	%AAD	%Bias	%AAD	%Bias		
C3-2-Me*	0.85	0.21	0.79	-0.76	0.28	0.89
C3-2.2-diMe*	2.57	-1.08	1.62	1.62	0.59	0.89
C4-2-Me*	5.07	-5.07	1.46	-1.25	0.32	0.86
C5-2-Me	3.12	3.1	1.05	-1.05	0.28	0.88
C5-3-Me	18.45	-18.45	1.52	1.52	0.3	0.88
C4-2.3-diMe	5.05	4.53	0.49	-0.49	0.29	0.89
C4-2.2.3-triMe	9.77	5.94	2.61	2.61	0.47	0.89
C6-2-Me	2.37	1.56	0.51	-0.2	0.29	0.89
C6-3-Me	10.74	-10.74	0.6	0.38	0.32	0.89
C5-3-Et*	6.18	-0.64	1.7	1.7	0.32	0.89
C6-2.5-diMe	4.79	4.79	0.52	0.05	0.33	0.89
C5-2.2.4-triMe	28.36	28.36	1.08	0.38	0.3	0.89
C6-3-Et	7.05	-0.91	0.49	0.46	0.48	0.89
C6-2.4-diMe	6.18	5.3	1.24	1.19	0.49	0.89
C5-2.3.4-triMe	26.01	26.01	1.46	-1.46	0.29	0.89
C7-2-Me	3.3	1.11	0.74	-0.25	0.29	0.89
C6-2.2-diMe*	6.17	-0.42	2.6	2.6	0.31	0.89
C7-4-Me*	4.96	-2.81	0.61	0.32	0.31	0.88
C6-3.4-diMe*	9.62	-7.11	1.57	1.53	0.48	0.89
C6-2.2.5-triMe	9.43	-2.33	2.42	2.42	0.33	0.89
C7-2.6-diMe	9.79	9.79	0.49	-0.49	0.33	0.89
C7-3-Et*	7.48	-7.37	1.18	1.18	0.31	0.88
C9-5-Me*	5.37	-4.49	0.65	0.65	0.34	0.89
C9-2-Me	4.86	4.86	0.16	-0.16	0.33	0.89
Overall	9.55	3.80	1.10	0.35		

³ The first number after ‘C’ denotes the number of carbon atoms in the backbone, the numbers between the dashes denote the location of side groups, and the suffixes denote the type of side group. ‘Me’ stands for a methyl group and ‘Et’ stands for an ethyl group. For example, ‘C6-2.2-diMe’ means, 2,2-dimethylhexane.

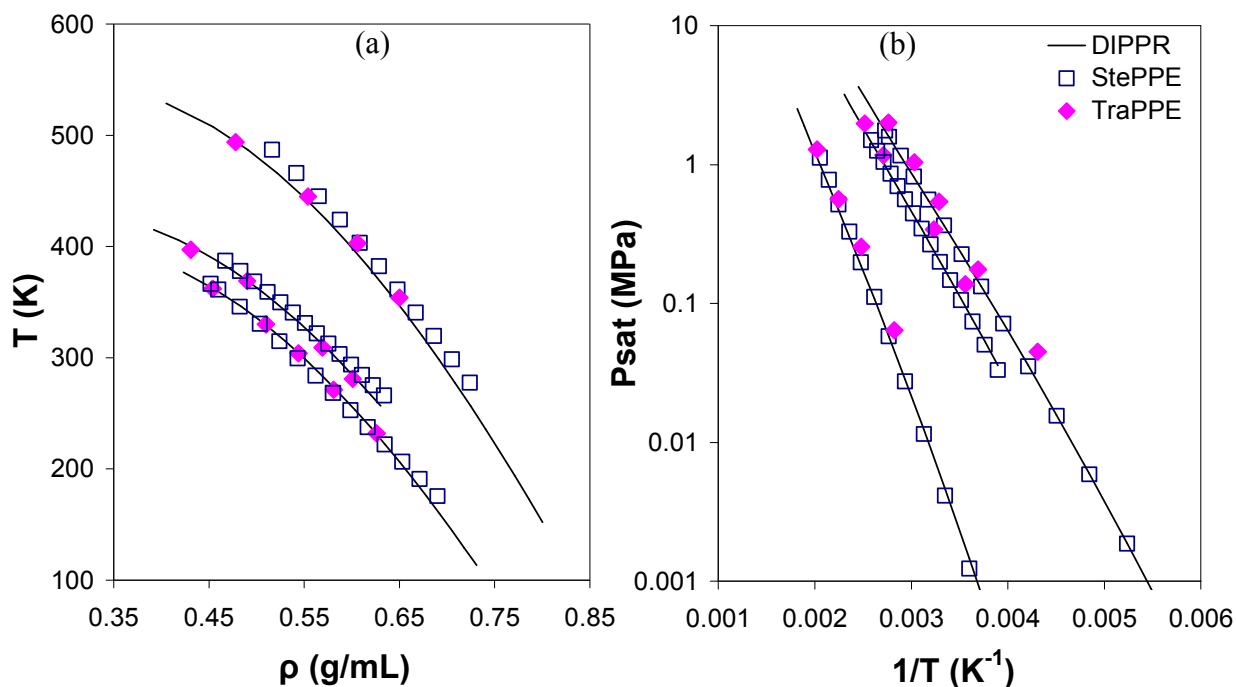


Figure 4.3: (a) Liquid densities of (left to right) isopentane, neopentane and 2,2-dimethylhexane; (b) saturation pressures of (right to left) isopentane, neopentane and 2,2-dimethylhexane. The legend meanings are same in (a) and (b)

The TraPPE parameters, though somewhat inadequate for a wide range of compounds, are able to distinguish isomers with structural differences, without any special parameters (Fig 4.4). The only difference in the compounds in Figure 4.4 is in the intramolecular interactions due to the different arrangement of the CH and CH₃ groups. StePPE also makes this distinction reasonably well, but positive deviations are observed in the liquid density predictions of compounds with a quaternary carbon (Table 4.3). Treating the methyl side chains attached to a quaternary carbon explicitly as in NERD, might alleviate the issue somewhat, but we might have to compromise the accuracy in the vapor pressures of some of these compounds which seem to be slightly underpredicted. Despite the discrepancies, StePPE reproduces the liquid densities and vapor pressures of a wide range of branched alkanes very well.

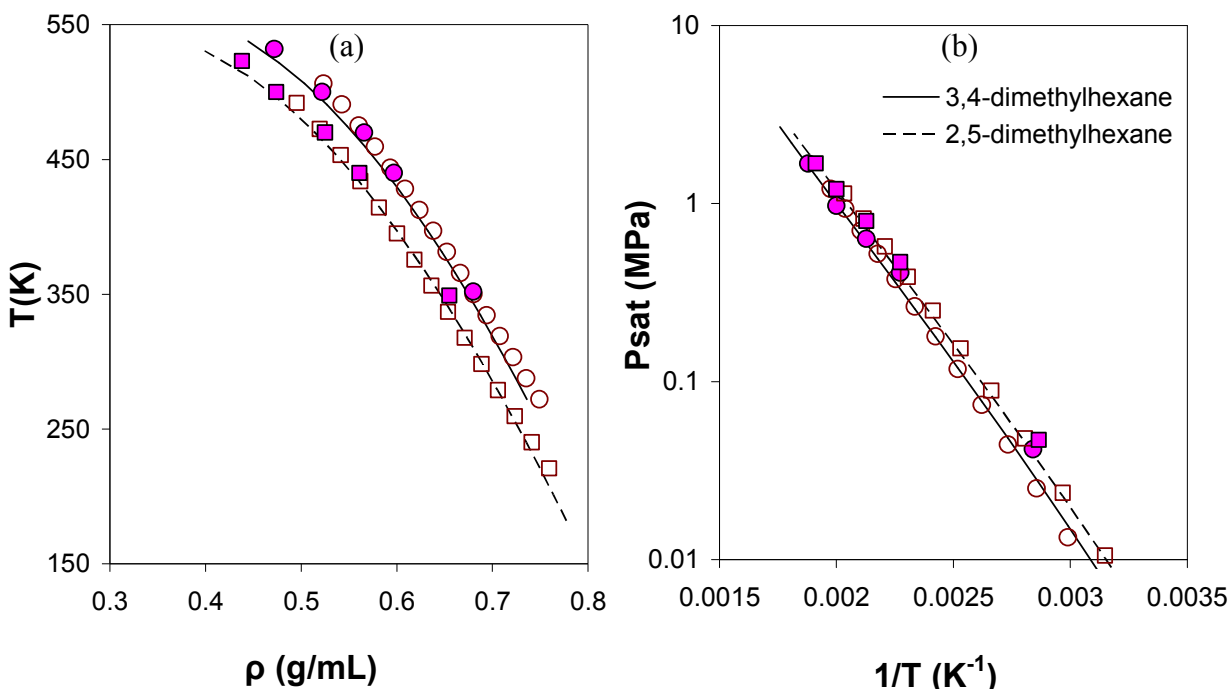


Figure 4.4: Liquid densities (a) and saturation pressures (b) of 3,4-dimethylhexane and 2,5-dimethylhexane. The lines are from correlations in DIPPR, filled symbols are from TraPPE and the open symbols are from StePPE

Optimizing the branched alkanes for a wide range of compounds may not be that trivial after all, because of the multiple factors that need to be taken into account to incorporate the effect of branching on the densities as well as the shapes of the VLCC. For example, with increased branching, naively, we would expect the densities to become smaller because of poor packing and reduced dispersive attractions due to screening. But with much branching, we see an opposite trend. A look at the experimental C9 isomer densities confirms this behavior (Fig 4.5).

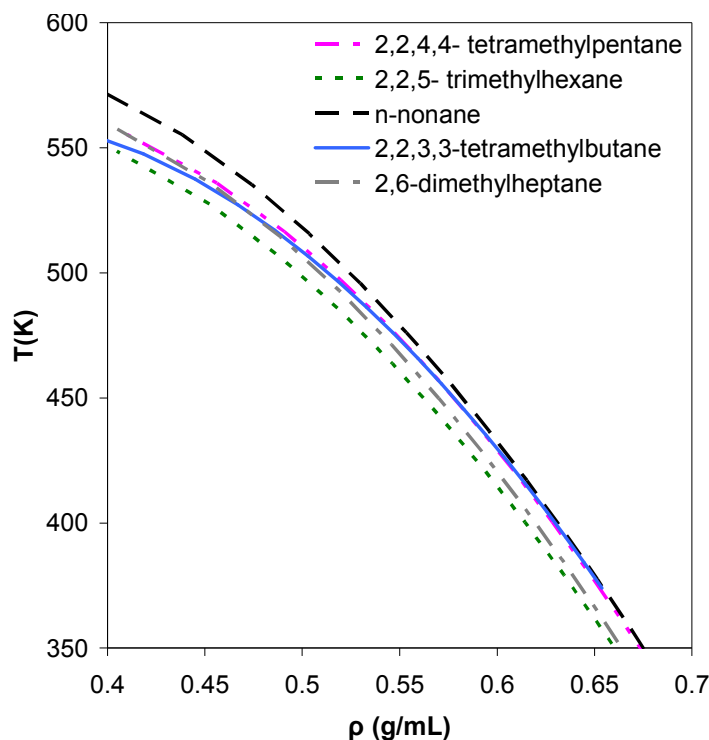


Figure 4.5: Experimental liquid densities of C9 isomers and 2,2,3,3- tetramethylbutane. The curves are from equations in DIPPR 801 database

3. *n*- Alkenes

Because of the unsaturated double bonds present in them, alkenes are at the core of a variety of useful chemical reactions as starting materials and intermediates. They are therefore, aptly called the building blocks of the petrochemical and polymer industries. Reliable thermodynamic data is crucial for industrial processes involving alkenes.

To represent the alkenes, two new sites (-CH= and CH2=) were introduced in the StePPE database. The sp^2 CH parameters were kept the same for the α -olefins, dienes but for cis/trans alkenes, the well depths of the cis/trans sp^2 CH were slightly different. Of the other available force-fields for olefins, OPLS[5], Spyriouni et al's model (SET)[16] and TraPPE[17] use only two unique sites for the olefins. The OPLS parameters were optimized to reproduce

thermodynamic and conformational properties of 1 and 2-butenes at near ambient conditions, and are not transferable to other alkenes[17]. The SET model seems to underpredict the liquid densities of alkenes smaller than n-butene and overpredict the liquid densities of larger alkenes[17, 18] and is increasingly less accurate than TraPPE and NERD for longer chain lengths. The vapor pressure predictions with SET seem to be more accurate than TraPPE and NERD. Like the SET model, NERD too was parameterized for α -olefins only, and represents the vapor liquid coexistence densities of alkenes from propene to 1-octene well. However, NERD uses special parameters for the methyl group in propene and the sp^2 CH₂ in ethylene. A comparison of liquid density and vapor pressure predictions for α -olefins with TraPPE, SPEAD, NERD and StePPE is shown in Figure 4.6.

The SPEAD model reproduces the liquid densities of α and higher olefins and dienes of chain lengths upto C8 with an overall error of about 1.6%, using four new sites for alkenes- sp^2 CH₂ for propylene and other alkenes, and sp^2 CH for α -olefins, and dienes[1]. However, the error in the α -olefins seems to increase with chain length from within 1% in 1-butene to 4.4% in 1-octene. The predictions with TraPPE and StePPE are in close agreement with experimental data for the alkenes shown. The liquid densities with NERD however seem to be somewhat underpredicted for the smaller alkenes at low reduced temperatures. The vapor pressures on the other hand, are consistently overpredicted with TraPPE, while both the step potential models agree well with experiments.

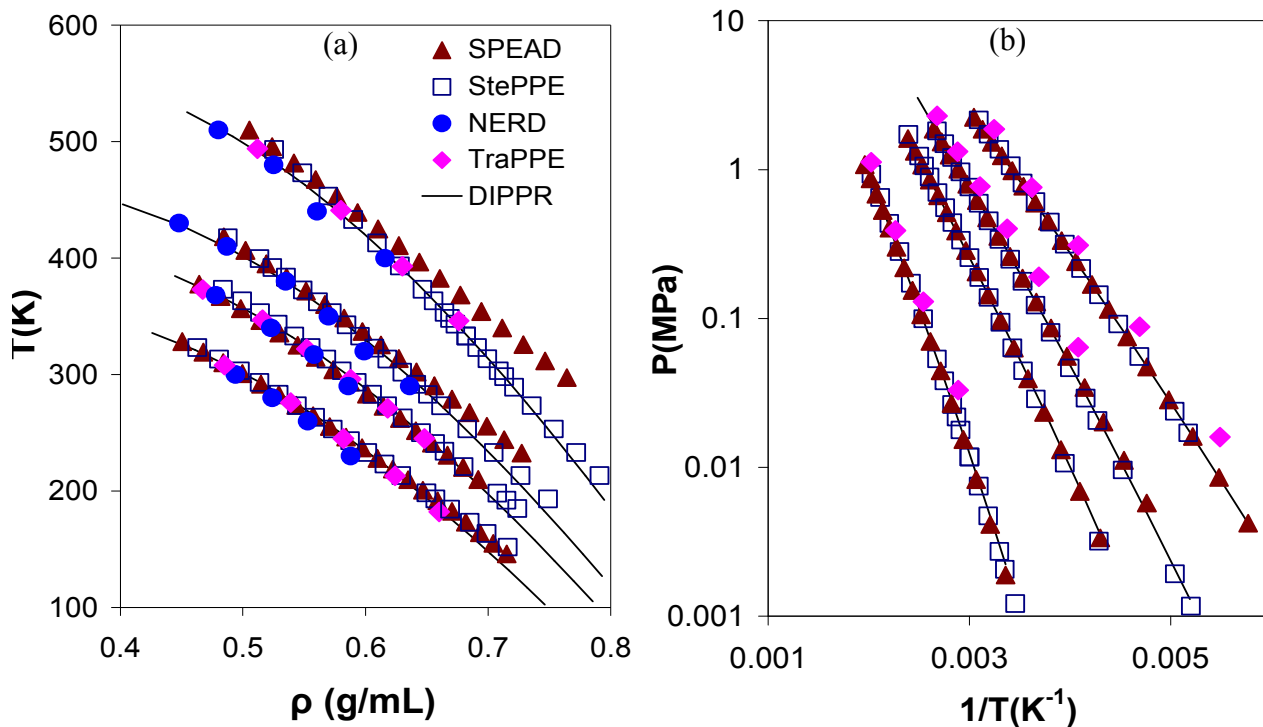


Figure 4.6: (a) liquid densities (left to right) of propene, 1-butene, 1-pentene and 1-octene; (b) vapor pressures of (right to left), propene, 1-butene, 1-pentene and 1-octene. The symbol meanings are same in (a) and (b)

The liquid densities of the α , ω - diolefins seem to agree well with experiments, except 1, 4- pentadiene (Table 4.4). However, there have been very few studies, and in a very limited temperature range, for densities of 1, 4- pentadiene, which show considerable scatter. Vapor pressure measurements are also very rare in literature for 1, 4- pentadiene. In case for 1, 9- decadiene, density data is limited and scattered too, but its vapor pressure data seems to be more reliable.

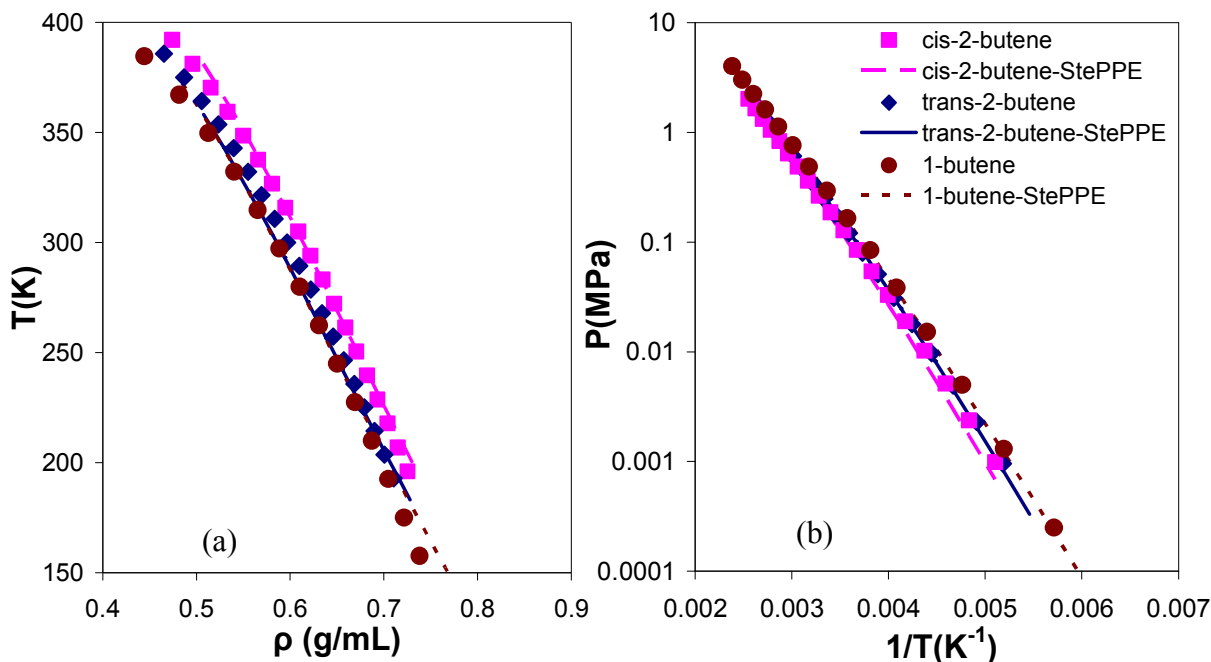


Figure 4.7: liquid densities (a) and vapor pressures (b) of butene isomers. The meanings of the legends are same in (a) and (b)

With the current set of parameters, the errors in cis/trans isomers are low but, it appears that a very clear distinction between the isomers is not made for the liquid densities (Fig 4.7 (a)). The liquid density predictions for cis-2-butene and trans-2-butene almost overlap each other. But the trends in vapor pressures are distinguishable for the isomers (Fig 4.7 (b)). TraPPE parameters for the alkenes are able to make that distinction without special cis/trans parameters, but have not been tested for isomers of alkenes larger than butene. It is not clear whether SPEAD uses separate parameters for the sp^2 CH₂ and CH groups for cis/trans compounds. Perhaps, different sets of parameters for the cis/trans groups may be required to correctly differentiate the trends between those isomers in StePPE, which would be a subject of future study.

Table 4.4: Vapor pressures and liquid densities of alkenes with StePPE

Compound ⁴	P ^{sat}		ρ		T _r ^{min}	T _r ^{max}
	%AAD	%Bias	%AAD	%Bias		
C3-1-ene*	10.93	-10.93	0.47	-0.10	0.28	0.89
C4-1-ene	5.09	-3.40	0.50	0.41	0.30	0.89
C4-1.3-diene*	27.14	27.14	0.71	0.36	0.39	0.89
C4-2c-ene*	12.94	-12.94	0.59	0.53	0.45	0.88
C4-2t-ene*	5.13	2.04	1.50	-1.48	0.43	0.89
C5-1-ene*	3.08	-1.66	0.83	0.57	0.33	0.90
C5-2t-ene	14.64	14.64	1.35	-1.35	0.47	0.72
C6-1.5-diene*	12.40	10.73	0.40	0.07	0.52	0.90
C6-1-ene	3.85	-3.11	1.05	1.04	0.30	0.90
C7-1-ene*	3.53	-3.24	0.26	-0.04	0.48	0.73
C7-2c-ene	6.21	-4.62	0.12	0.04	0.48	0.73
C8-1-ene	3.95	-2.41	0.51	0.43	0.31	0.87
C8-2t-ene	13.93	13.51	1.03	-1.03	0.45	0.88
C5-1.4-diene	20.01	20.01	2.70	2.70	0.65	0.88
C10-1.9-diene	8.98	-7.80	0.54	0.27	0.33	0.58
Overall	10.35	2.38	0.81	0.02		

4. Primary alcohols

The current implementation of StePPE does not include electrostatic interactions due to partial charges, which are expected to be present in compounds with highly electronegative sites like oxygen. In alcohols, partial charges would be present on the hydroxyl group and the α -carbon, which is implemented in many of the continuous potential models which include electrostatic interactions in their force-field, such as OPLS[19], TraPPE[20], and NERD[21]. In StePPE, a hydrogen bonding square well similar to SAFT[22] is used to account for association, and its effect is added to the EoS as discussed in the ‘SPEAD theory’ section in CHAPTER III .

⁴ The prefix ‘Cx’ denotes the chain length, the number(s) in between the dashed denote the position(s) of the double bond and the letters ‘c’ or ‘t’ denote a cis or a trans case, and the suffix ‘ene’ denotes one double bond and ‘diene’ denotes two double bonds. For example, C8-2t-ene denotes trans-2-octene

Also, the alkyl groups bonded to the hydroxyl group are optimized to give well parameters different than those obtained from fitting the alkanes to compensate partially for the effect of the charges. Unlike the UA models listed above, where the hydrogen atom in the hydroxyl group is treated explicitly, OH in SPEAD and StePPE is one group. Special parameters are used for methyl group in methanol in all the models. SPEAD also uses additional special parameters for ethanol and propanol compared to the rest of the primary alcohols studied. Though SPEAD reports a higher number of compounds simulated, the liquid densities are not reproduced well for the longer alcohols (Fig 4.8 (a), 4.9). The vapor pressures deviations however, are generally small with SPEAD (Fig 4.8 (b)). The OPLS parameters developed for the short chain alcohols show poor transferability for vapor pressures and liquid densities for longer alcohols or elevated temperatures [23]. The liquid densities with TraPPE and NERD are in good agreement with the experimental values for methanol to 1-octanol, the longest *n*-alcohol studied in TraPPE and NERD. The vapor pressure predictions with TraPPE seem to show a positive deviation (Fig 4.8 (b)). With NERD, the vapor pressure predictions need verification. With the availability of more reliable data for alcohols larger than 1-octanol, the transferability of the parameters developed for TraPPE and NERD force-fields can be tested in future.

The errors for the liquid densities and vapor pressures with StePPE are summarized in Table 4.5. For the eleven compounds in the training set and six in the validation set, the overall deviation in vapor pressure is about 8%, which is slightly better than SPEAD, where this deviation was 9% for a similar range of reduced temperatures. The deviations in the liquid densities however, are a more significant improvement, where the corresponding value is 0.72%, compared to 2.49% in SPEAD. Also, the StePPE parameters are tested to longer chains. The biggest alcohol tested in SPEAD is 1-hexanol, while in StePPE, it is 1-eicosanol. The liquid

density and vapor pressure data is limited for the longest alcohols, but within the temperature range where data is available, the agreement is excellent with StePPE. The only anomalies are the deviations in liquid density for methanol and vapor pressure of 1-octadecanol (Table 4.4). Except methanol, the individual density errors are less than 1% with StePPE, whereas in SPEAD, half of the compounds studied show a density deviation of above 2.5%. Moreover, the density deviations with SPEAD tend to increase with increasing chain length (Fig 4.8 (a) and Fig 4.9), indicating that the $-\text{CH}_2-$ sizes might have been too small. The discussed improvement in StePPE is achieved with three less site types (corresponding to eight adjustable parameters- six well parameters and two hydrogen bonding parameters) compared to SPEAD, which uses special parameters for the alkyl group in propanol in addition to the hydroxyl group in ethanol and propanol.

Table 4.5: Vapor pressures and liquid densities of primary alcohols with StePPE

Compound	P^{sat}		ρ		T_r^{min}	T_r^{max}
	%AAD	%Bias	%AAD	%Bias		
Methanol*	4.25	-1.04	2.48	2.21	0.40	0.88
Ethanol*	1.39	-0.77	0.60	0.27	0.43	0.89
Propanol*	4.76	3.72	0.86	-0.44	0.34	0.90
1-butanol	9.73	-9.73	0.48	0.28	0.34	0.89
1-pentanol*	12.93	12.93	0.65	-0.52	0.43	0.89
1-octanol*	3.33	3.10	0.26	-0.15	0.40	0.84
1-nonanol	4.15	2.01	0.19	0.10	0.41	0.90
1-decanol	4.45	-2.29	0.19	-0.01	0.41	0.80
1-dodecanol*	8.47	-6.97	0.20	-0.06	0.41	0.86
1-tridecanol	9.96	2.80	0.24	-0.14	0.41	0.90
1-pentadecanol	7.38	4.72	0.27	-0.27	0.44	0.89
1-hexadecanol	5.98	-1.92	0.19	0.09	0.42	0.74
1-heptadecanol	12.32	3.58	0.43	-0.43	0.43	0.90
1-octadecanol	26.66	-26.66	0.49	0.34	0.42	0.73
1-nonadecanol	13.92	-10.21	0.44	-0.44	0.44	0.89
1-eicosanol*	11.77	-7.36	0.21	-0.21	0.43	0.87
Overall	7.95	-1.61	0.72	0.05		

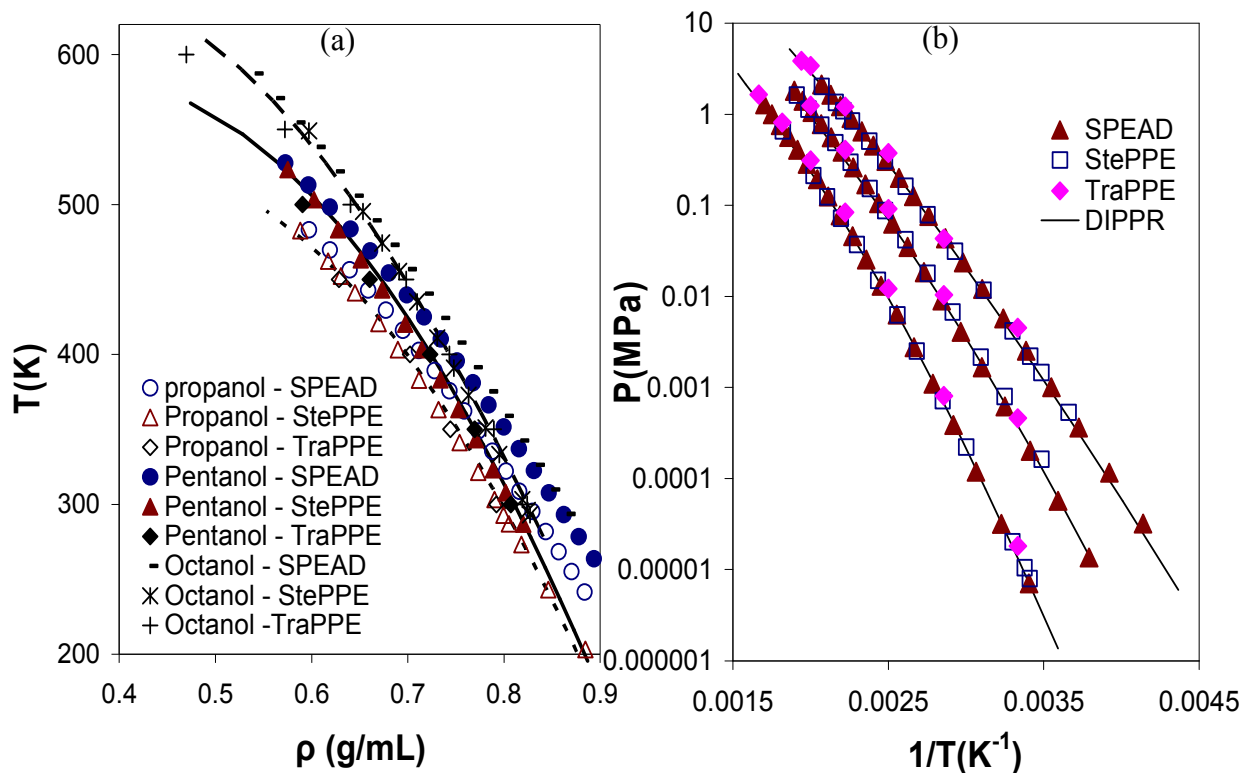


Figure 4.8: Liquid densities (a) and vapor pressures (b) of (right to left) propanol, 1-pentanol and 1-octanol. In (a) the dotted, solid and dashed lines are for propanol, 1-pentanol and 1-octanol respectively

Methanol is the only compound with a better liquid density prediction with SPEAD at lower reduced temperatures (Fig 4.10 (a)). It should be noted however, that only the CH₃ wells are special parameters in StePPE for methanol, compared to the well parameters of both, the CH₃ and OH groups, as well as the hydrogen bonding parameters for the OH in SPEAD. We believe, considering only the temperature dependent hydrogen bonding parameters separately for methanol might be enough to improve the density predictions.

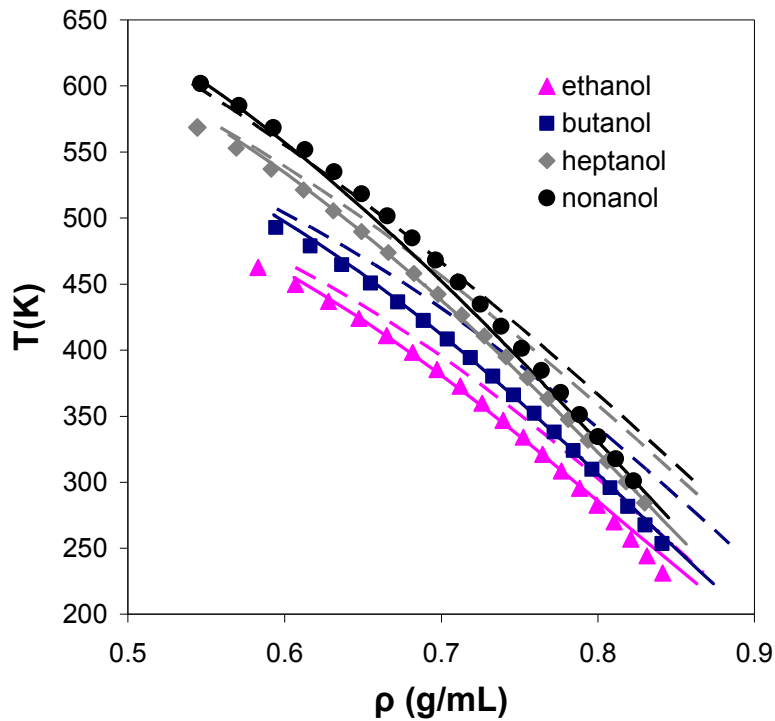


Figure 4.9: Liquid densities of selected 1-alcohols with SPEAD and StePPE. Dashed lines are with SPEAD and the solid lines are with StePPE

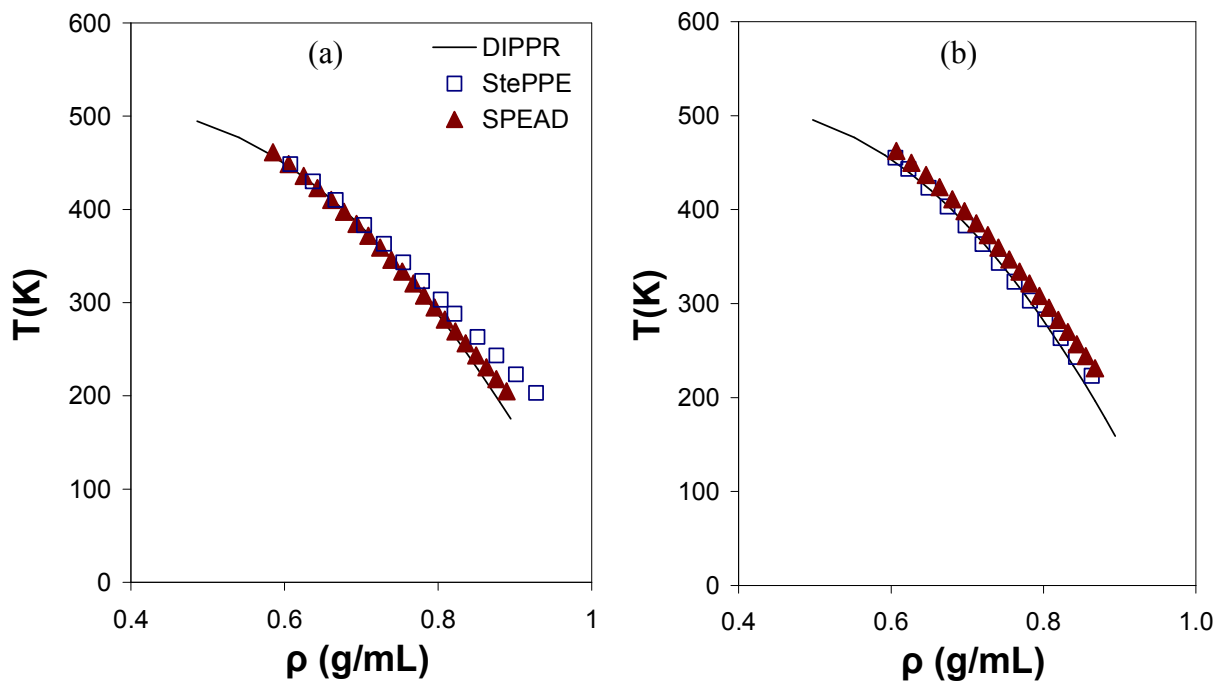


Figure 4.10: Liquid densities of methanol (a) and ethanol (b) with SPEAD and StePPE. The symbol meanings are same in (a) and (b)

5. Secondary alcohols

New sites used in defining the branched alcohols were the side hydroxyl group and the CH group to which it is bonded. The size and the association parameters for the hydroxyl group were borrowed from the optimizations of primary alcohols. The optimized wells of the hydroxyl group were shallower than the hydroxyl in the n-alcohols, possibly because of some steric hindrance, as it is in the middle of the chain. A similar observation was made for the side methyl groups in branched alkanes, which are less exposed than the terminal methyl groups in long alkanes. The CH₃ potential wells were optimized separately for 2-propanol.

Very few force-fields have tested their optimized parameters for branched alcohols. Figure 4.11 shows the liquid densities and vapor pressures of 2-propanol and 2-butanol with TraPPE[20] and StePPE. The liquid densities of both alcohols are overpredicted by about 1% with StePPE, while with TraPPE, the predictions appear to be underpredicted at higher reduced temperatures. The vapor pressures appear to be somewhat overpredicted with both models.

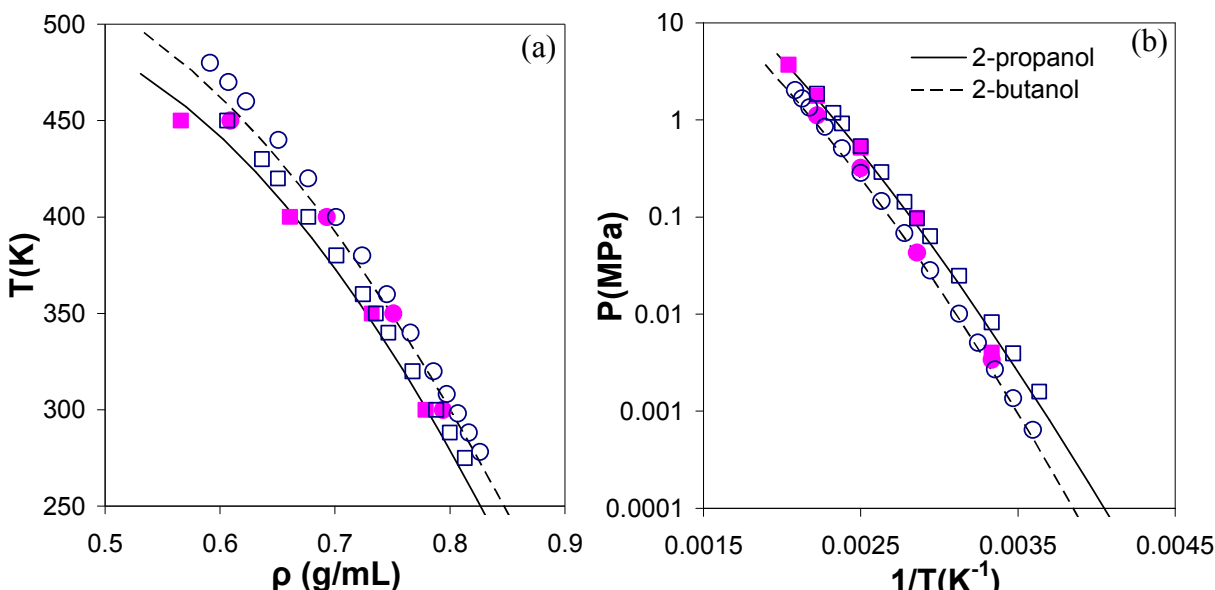


Figure 4.11: Liquid densities and vapor pressures of 2-butanol (circles) and 2-propanol (squares) with TraPPE and SPEAD. The closed symbols are with TraPPE and the open symbols are from StePPE.

Table 4.6: Vapor pressure and liquid density deviations of secondary alcohols with StePPE

Compound ⁵	P^{sat}		ρ		T_r^{min}	T_r^{max}
	%AAD	%Bias	%AAD	%Bias		
C3-2ol*	18.04	9.2	1.16	1.16	0.54	0.9
C4-2ol	10.6	10.6	0.72	0.72	0.52	0.9
C5-2ol*	10.36	10.36	0.46	0.42	0.42	0.7
C6-2ol	5.71	0.83	1.34	1.34	0.41	0.89
C7-2ol*	4.52	2.6	0.67	0.67	0.4	0.71
C8-2ol	5.63	0.4	0.98	0.98	0.4	0.76
C9-2ol*	5.49	-4.24	0.8	0.8	0.41	0.62
C5-3ol	7.99	-7.43	0.23	-0.23	0.44	0.73
C6-3ol*	17.36	-17.29	0.16	0.1	0.45	0.71
C7-3ol	18.03	-16.39	0.56	0.54	0.4	0.71
Overall	9.39	2.65	0.58	0.52		

Table 4.6 shows the liquid density and vapor pressure deviations with StePPE for secondary alcohols with chain lengths from C3 to C9. For the 2-alcohols, the liquid density deviations seem to be positive and increasing with chain length, which can be a result of the CH2 diameter being small. But there isn't a clear trend in the density deviations of the 3-alcohols. On the other hand, the vapor pressures of the 3-alcohols appear to be underpredicted, and the error increases with chain size, suggesting that the potential well for CH2 may be too deep. However, for the 2-alcohols, the vapor pressure deviations seem to be positive and appear to decrease with chain length (if we ignore 2-hexanol, for which very few reliable data points are available in DIPPR), which suggests the -OH or CH potential might be somewhat shallow. Therefore, there is no clear trend about the deviations, but with the availability of more reliable data for longer branched alcohols with the -OH at different locations, a more detailed analysis can be made. A study with an increased diameter of the CH group is shown in the future work section in CHAPTER VI.

⁵ In 'Cx-yol', x denotes the backbone chain length, and y denotes the position of the -OH group in the chain. For example, C5-3ol would mean 3-pentanol.

6. Ethers

Ethers are important industrial solvents and also have medicinal uses as sedatives. Ethers are also used as octane boosters (methyl-tertiary-butyl ether) for gasoline engines and cetane boosters (diethyl ether) for diesel engines. Thermodynamic data of only the smallest aliphatic ethers is available. In this study, the vapor pressures and liquid densities of ethers ranging from dimethyl ether to dinonyl ether are presented.

Table 4.7: Vapor pressure and liquid density deviations of ethers with StePPE

Compound ⁶	P^{sat}		ρ		T_r^{min}	T_r^{max}
	%AAD	%Bias	%AAD	%Bias		
C1OC1*	8.7	8.7	1.4	-1.4	0.45	0.88
C1OC3	2.89	1.92	1.26	-1.26	0.4	0.67
C2OC2*	8.33	8.33	0.59	-0.49	0.43	0.89
C1OC4	8.96	-8.23	0.13	-0.08	0.31	0.86
C2OC3	6.06	6.04	0.61	0.32	0.49	0.89
C1OC5*	15.93	-13.7	0.23	-0.22	0.32	0.86
C3OC3*	9.18	5.45	1.02	-1.02	0.38	0.9
C4OC2	8.71	-5.8	0.21	-0.17	0.38	0.9
C2OC6*	5.09	4.95	0.19	-0.13	0.39	0.85
C4OC4	2.47	0.65	0.21	0.14	0.47	0.71
C5OC5	12.67	-7.54	0.21	0.04	0.36	0.89
C6OC6	9.07	9.07	0.34	0.26	0.45	0.75
C8OC8*	17.85	17.85	0.28	0.23	0.41	0.63
C9OC9	24.47	20.81	0.32	0.32	0.39	0.9
Overall	8.56	4.19	0.49	-0.27		

The new sites to define ethers were the sp^3 oxygen and the alkyl group adjacent to it. The sizes of these alkyl groups were kept the same as in alkanes, and only the well depths were varied, for similar reasons as in the alcohols. The parameters for the rest of the alkyl groups were used from the optimization of the alkanes. The overall deviation in the liquid density prediction

⁶ In 'C_xOC_y', x and y denote the chain length of the alkyl group on each side of the oxygen. For example C2OC3 is ethyl propyl ether

is less than 0.5% (Table 4.7) for the fourteen compounds studied. The largest ether reported in both, TraPPE[24] and SPEAD[1] was dipropyl ether, for which the density deviations appear to be better with StePPE for a broader temperature range (Fig 4.12). For the other compounds common in the three models, the predictions are better with TraPPE and StePPE. The biggest compound in StePPE was dinonyl ether, for which the density is overpredicted at temperatures close to critical. Tuning the parameters further, for a better fit for dinonyl ether, cannot be accomplished without increasing the errors in the smaller compounds, for example, dimethyl ether, whose density is somewhat underpredicted with the current set of parameters. To our knowledge however, no other model has reported such accuracy for such a wide range of ethers.

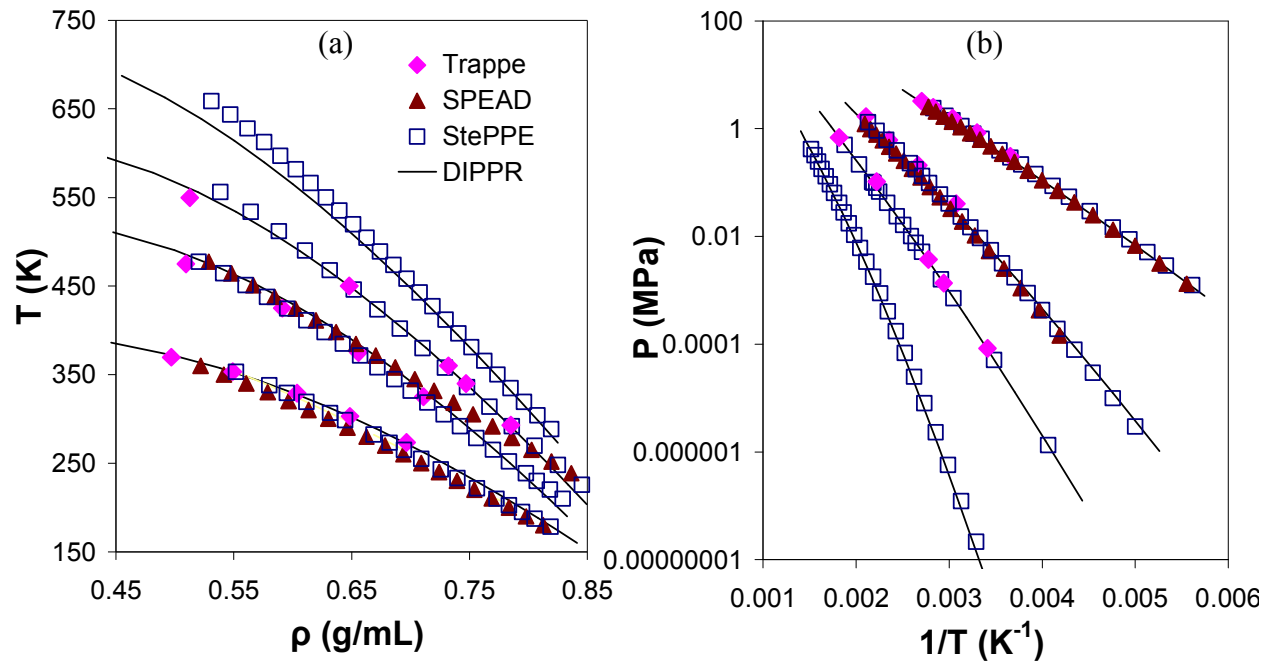


Figure 4.12: (a) liquid densities of (left to right) dimethyl ether, dipropyl ether and di-pentyl ether and di-nonyl ether; vapor pressures of (right to left) dimethyl ether, dipropyl ether and di-pentyl ether and di-nonyl ether

The overall deviation in the vapor pressure for the compounds studied with StePPE is 8.6%, which is significantly better than TraPPE for the relatively smaller compounds reported in reference 24. It appears that the TraPPE parameters for the ethers get better with increasing chain length. For example, the average deviation in the vapor pressure of dipropyl ether was about 40%, but for dipentyl ether, it was within 10%. Both, SPEAD and StePPE agree closely with the experimental vapor pressures for the common ethers. Compared to the liquid densities, the agreement is relatively better for vapor pressures for dinonyl ether with StePPE.

6. Ketones

To represent the ketones, two new sites- carbonyl oxygen (O=) and carbonyl carbon (>C=), were added to the StePPE database. The parameters for the alkyl groups were obtained from alkane optimizations, except for the alkyl groups attached to the carbonyl carbon, whose well depths were readjusted. The ketone oxygen in SPEAD[25] has an additional adjustable parameter, because it is treated as a hydrogen bonding site. Additionally, the wells and the diameter of the CH₂ next to the carbonyl carbon have been reoptimized in SPEAD in order to fit the liquid densities better. As discussed earlier in this work, readjusting the CH₂ size would also help eliminate the systematic trend in the deviations of alkane densities. The overall average error in liquid densities with StePPE is below 0.5%, and all of the individual average deviations are below 1% (Table 4.8) from acetone to 5-nonanone, which is somewhat better than TraPPE[24] for the common compounds in both studies, except at temperatures very close to critical. The StePPE predictions however, span to much lower reduced temperatures compared to TraPPE. The maximum errors observed in the reduced temperature range of about 0.3 to 0.9 for the sixteen ketones are within 1.5%.

Table 4.8: Vapor pressure and liquid density deviations of ketones with StePPE

Compound ⁷	P^{sat}		ρ		T_r^{min}	T_r^{max}
	%AAD	%Bias	%AAD	%Bias		
C3.2one*	2.5	-2.1	1.42	-1.86	0.36	0.90
C4.2one*	9.86	4.7	0.53	0.53	0.36	0.89
C5.2one	6.71	1.29	0.19	-0.11	0.36	0.89
C5.3one*	7.52	5.81	0.28	0.28	0.49	0.89
C6.2one*	5.93	-5.39	0.53	0.53	0.48	0.73
C6.3one	4.88	1.8	0.28	-0.23	0.5	0.72
C7.2one	9.42	-9.36	0.38	0.38	0.41	0.74
C7.3one*	3.42	0.14	0.41	0.41	0.47	0.69
C7.4one	7.7	0.56	0.31	-0.29	0.4	0.88
C8.2one*	9.88	-9.8	0.66	0.66	0.4	0.76
C8.4one	18.48	-11.18	0.3	-0.14	0.47	0.71
C8.3one	20.47	-19.58	0.26	0.11	0.45	0.71
C9.2one	10.3	-10.24	0.65	0.65	0.42	0.77
C9.4one	15.84	-2.06	0.25	-0.25	0.43	0.71
C9.5one*	5.9	0.01	0.3	0.22	0.44	0.76
Overall	8.12	-2	0.37	0.18		

The overall error in vapor pressures with StePPE and SPEAD are better than TraPPE. However, it is important to note that StePPE has three less adjustable parameters in comparison to SPEAD. In both step potential models, the CH₃ in acetone was optimized separately, so it has different well parameters compared to the CH₃ adjacent to >C= in other ketones. If we do not consider these special parameters for acetone, the error in vapor pressure is about 42%, although the density error is still less than 1%. The maximum deviation in vapor pressures with StePPE is observed with 3-octanone, 4-octanone and 4-nonanone, all of which have very scattered experimental vapor pressure data in DIPPR. It should be noted that we used the experimental points, rather than the fitted correlations, to tune the parameters in StePPE.

⁷ In 'Cx.yone' x denotes the chain length and y denotes the position of the ketone group. For example, C6.3one is 3-hexanone

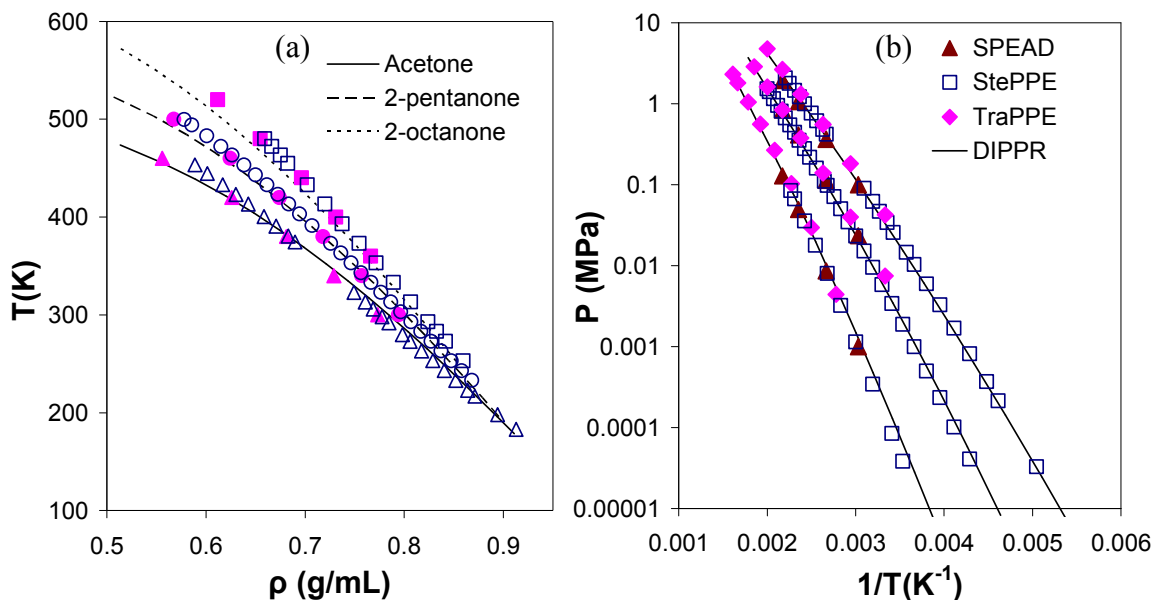


Figure 4.13: Liquid densities (a) and vapor pressures (b) of acetone, 2-pentanone and 2-octanone with SPEAD, TraPPE and StePPE. In (a), the filled symbols are from TraPPE and open symbols are from StePPE. In (b), from top to bottom: acetone, 2-pentanone, 2-octanone

8. Esters

Esters are important compounds in chemical industry with a plethora of applications, like, fragrances, food additives and preservatives, adhesives and polymers. Esters are also the important constituents in biodiesel[26] fuel blends, owing to their relatively desirable combustion properties[27]. They are formed by replacing the hydroxyl group ($-\text{OH}$) in an acid with an alkoxy group ($-\text{OR}$), which comes from an alcohol, or by a transesterification method[28], where a triglyceride is converted to monoglycerides.

The only parameters optimized for esters were the outer well depths of the carbonyl (sp^2) carbon ($>\text{C}=\text{O}$). Its diameter, along with the parameters for the adjacent alkyl groups and the carbonyl (sp^2) oxygen ($\text{O}=\text{O}$), was borrowed from the ketone optimizations. The parameters of the

alkoxy (sp^3) oxygen ($-O-$) and the alkyl group to which it is attached ($-R-(-O-)$) are obtained from the optimization of the ethers. The sp^2 carbon in the ketones is bonded to alkyl groups, whereas in esters, one of the bonds is with the sp^3 oxygen. One would expect, as in the alcohols and ethers, that the well depth for $>C=$ would be higher in the ester in comparison to ketones. However, the optimized well depths show an opposite trend, based on which, it might be expected that the well depths for the carbonyl carbon in the ketones might have been too deep. To test this hypothesis, we tried to reoptimize the ketones with smaller well size for the carbonyl carbon, but we were unable to get a combination of wells for the carbon and oxygen, which gave errors similar to or better than the current parameters for those groups.

The overall deviation in the liquid density predictions for a set of 26 esters was found to be 0.8% and the corresponding deviations in the vapor pressure predictions was 10%. The set includes multiple acetates, propionates and butanoates, along with methyl esters that are relevant to biofuels, namely methyl decanoate to methyl stearate. We believe no other model has considered such a wide range of esters, though the vapor pressure error for some acetates and propionates appears to be high (between 15% and 21%), which is still better than SPEAD and the group contribution methods[29]. Three of the nine acetates reported in SPEAD[25] show a deviation of more than 25% in the vapor pressure prediction. Decylacetate, which is the biggest acetate in the study, shows a deviation of about 27%. The liquid density predictions appear to be consistently better with StePPE (Table 4.7). It should also be noted however, that in SPEAD, the parameters for $>C=$, $O=$, $-O-$, and the methyl group attached to $>C=$ are optimized for the esters. Therefore, the number of sites for which parameters are adjusted in SPEAD is four, compared to one in StePPE. The parameters for the group present in esters have also been

reported for OPLS[30], TraPPE[31] and NERD[32] force-fields. The OPLS parameters were developed for methyl acetate and are inaccurate for liquid densities of ethyl acetate[33]. The NERD parameters have been used to study triglycerides and very limited data is published for monoesters. Only TraPPE reports results for a small set, but the state points are not published, so we're unable to make a comparison.

Table 4.9: Deviations in liquid densities and vapor pressures of esters with StePPE

Compound ⁸	P ^{sat}		ρ		T _r ^{min}	T _r ^{max}
	%AAD	%Bias	%AAD	%Bias		
C2ateC1*	9.38	9.32	1.31	-1.28	0.39	0.89
C2ateC2*	14.35	14.35	1.62	-1.62	0.52	0.89
C3ateC1*	7.92	3.94	1.22	-1.22	0.48	0.89
C2ateC3	7.46	7.23	1.04	-0.95	0.48	0.90
C4ateC1	7	-3.75	1.05	-1.05	0.47	0.89
C3ateC2*	13.09	13.09	1.22	-1.22	0.48	0.88
C2ateC4	2.71	-1.03	0.41	-0.41	0.47	0.71
C3ateC3	9.35	5.39	1.28	-1.28	0.46	0.74
C4ateC2	11.67	-1.72	1.1	-1.1	0.45	0.74
C3ateC4	5.82	3.64	0.49	-0.49	0.46	0.73
C6ateC1	16.33	-16.33	0.2	0.16	0.78	1.00
C2ateC5*	11.56	-10.44	0.17	-0.08	0.46	0.81
C4ateC3*	8.52	6.33	0.9	-0.9	0.46	0.75
C2ateC6	21.79	-21.79	0.19	0.15	0.44	0.62
C4ateC4	18.36	-5.38	0.42	-0.31	0.41	0.89
C2ateC7	5.21	-5.07	0.35	0.35	0.43	0.73
C5ateC4	16.31	-9.85	0.3	0.11	0.42	0.81
C8ateC1*	15.08	-15.08	0.54	0.54	0.70	1.00
C8ateC2	7.43	-2.88	0.07	-0.01	-	-
C2ateC8*	14.84	-14.84	0.27	0.27	0.45	0.74
C10ateC1	17.5	-17.13	0.68	0.68	0.38	0.86
C2ateC10	18.41	-18.41	0.54	0.54	0.57	0.87
C12ateC1*	17.24	-17.24	0.84	0.84	0.41	0.68
C14ateC1*	5.14	-4.12	0.82	0.82	0.57	1.00
C16ateC1	5.19	-2.93	0.72	0.72	0.61	1.00
C18ateC1*	4.14	-0.49	0.64	0.64	0.61	1.00
Overall	10.03	-2.78	0.8	-0.55		

⁸ 'CxateCy' is ROOR'. Cx (R) is from acid, Cy (R') is from alcohol part in the saturated ester. For example, C3ateC2 means propanoic acid ethyl ester

REFERENCES

4.3 References

1. Unlu, O.; Gray, N.H.; Gerek, Z.N.; Elliott, J.R., "Transferable Step Potentials for the Straight-Chain Alkanes, Alkenes, Alkynes, Ethers, and Alcohols". *Industrial & Engineering Chemistry Research* **2004**, 43, 1788-1793.
2. Martin, M.G.; Siepmann, J.I., "Transferable Potentials for Phase Equilibria. 1. United-Atom Description of n-Alkanes". *Journal of Physical Chemistry B*, **1998**, 102, 2569-2577.
3. Nath, S.K.; Escobedo, F.A.; de Pablo, J.J., "On the Simulation of Vapor-Liquid Equilibria for Alkanes". *Journal of Chemical Physics*, **1998**, 108, 9905-9911.
4. *SHERPA – An Efficient and Robust Optimization/Search Algorithm*, Red Cedar Technologies: www.redcedartech.com.
5. Jorgensen, W.L.; Madura, J.D.; Swenson, C.J., "Optimized Intermolecular Potential Functions for Liquid Hydrocarbons". *Journal of the American Chemical Society*, **1984**, 106, 6638-6646.
6. Benet, J.; MacDowell, L.G.; Menduin, C., "Liquid-Vapor Phase Equilibria and Surface Tension of Ethane as Predicted By the Trappe and OPLS Models†". *Journal of Chemical & Engineering Data*, **2010**, 55, 5465–5470.
7. Nath, S.K.; Escobedo, F.A.; de Pablo, J.J.; Patramai, I., "Simulation of Vapor-Liquid Equilibria for Alkane Mixtures". *Industrial & Engineering Chemistry Research* **1998**, 37, 3195-3202.
8. Errington, J.R.; Panagiotopoulos, A.Z., "A New Intermolecular Potential Model for the n-Alkane Homologous Series". *Journal of Physical Chemistry*, **1999**, 103, 6314-6322.
9. Cui, J.Y.; Elliott, J.R., "Phase Diagrams for a Multistep Potential Model of n-Alkanes by Discontinuous Molecular Dynamics and Thermodynamic Perturbation Theory". *Journal of Chemical Physics*, **2002**, 116, 8625-8631.
10. Elliott, J.R.; Gray, N.H., "Asymptotic Trends in Thermodynamic Perturbation Theory". *Journal of Chemical Physics*, **2005**, 123, 184902-1-184902-6.

11. Martin, M.G.; Siepmann, J.I., "Novel Configurational-Bias Monte Carlo Method for Branched Molecules. Transferable Potentials for Phase Equilibria. 2. United-Atom Description of Branched Alkanes". *Journal of Physical Chemistry B*, **1999**, 103, 4508-4517.
12. Zhuravlev, N.D.; Martin, M.G.; Siepmann, J.I., "Vapor-Liquid Phase Equilibria of Triacontane Isomers: Deviations from Principle of Corresponding States". *Fluid Phase Equilib.*, **2002**, 202, 307-324.
13. Nath, S.K.; de Pablo, J.J., "Simulation of Vapor-Liquid Equilibria for Branched Alkanes". *Molecular Physics*, **2000**, 98, 231-238.
14. Nath, S.K.; Khare, R., "New Forcefield Parameters for Branched Hydrocarbons". *Journal of Chemical Physics*, **2001**, 115, 10837-10845.
15. Wescott, J.T.; Kung, P.; Nath, S.K., "Vapour-Liquid Coexistence Properties and Critical Points of Two Branched Alkanes Series". *Fluid Phase Equilibria*, **2003**, 208, 123-139.
16. Spyriouni, T.; Economou, I.G.; Theodorou, D.N., "Molecular Simulation of α -Olefins Using a New United-Atom Potential Model: Vapor-Liquid Equilibria of Pure Compounds and Mixtures". *Journal of the American Chemical Society*, **1999**, 121, 3407-3413
17. Wick, C.D.; Martin, M.G.; Siepmann, J.I., "Transferable Potentials for Phase Equilibria. 4. United-Atom Description of Linear and Branched Alkenes and alkylbenzenes". *Journal of Physical Chemistry B*, **2000**, 104, 8008-8016.
18. Nath, S.K.; Banaszak, B.J.; de Pablo, J.J., "A New United Atom Force Field for α -Olefins". *Journal of Chemical Physics*, **2001**, 114, 3612-3617.
19. Jorgensen, W.L., "Optimized Intermolecular Potential Functions for Liquid Alcohols". *Journal of Physical Chemistry*, **1986**, 90, 1276-1284.
20. Chen, B.; Potoff, J.J.; Siepmann, J.I., "Monte Carlo Calculations for Alcohols and Their Mixtures with Alkanes. Transferable Potentials for Phase Equilibria. 5. United-Atom Description of Primary, Secondary, and Tertiary Alcohols". *The Journal of Physical Chemistry*, **2001**, 105, 3093-3104.

21. Khare, R.; Sum, A.K.; Nath, S.K.; de Pablo, J.J., "Simulation of Vapor-Liquid Phase Equilibria of Primary Alcohols and Alcohol-Alkane Mixtures". *Journal of Physical Chemistry*, **2004**, 108, 10071-10076.
22. Liu, J.; Bowmann II, T.L.; Elliott, J.R., "Discontinuous Molecular Dynamics Simulation of Hydrogen-Bonding Systems". *Ind. Eng. Chem. Res.*, **1994**, 33, 657-964.
23. van Leeuwen, M.E., "Prediction of the Vapour- Liquid Coexistence Curve of Alkanols by Molecular Simulation". *Molecular Physics*, **1996**, 87, 87-101.
24. Stubbs, J.M.; Potoff, J.J.; Siepmann, J.I., "Transferable Potentials for Phase Equilibria. 6. United-Atom Description for Ethers, Glycols, Ketones, and aldehydes". *Journal of Physical Chemistry B*, **2004**, 108, 17596-17605.
25. Baskaya, F.S.; Gray, N.H.; Gerek, Z.N.; Elliott, J.R., "Transferable step potentials for amines, amides, acetates, and ketones". *Fluid Phase Equilib.*, **2005**, 236, 42-52.
26. Demirbas, A., "Biodiesel from Vegetable Oils via Transesterification in Supercritical Methanol". *Energy Conversion and Management*, **2002**, 43, 2349-2356
27. Dagaut, P.; Gail, S., "Chemical Kinetic Study of the Effect of a Biofuel Additive on Jet-A1 Combustion". *Journal of Physical Chemistry A*, **2007**, 111, 3992-4000.
28. Demirbas, A., "Biodiesel Fuels from Vegetable Oils via Catalytic and Non-Catalytic Supercritical Alcohol Transesterifications And Other Methods: A Survey". *Energy Conversion and Management*, **2003**, 44, 2093-2109.
29. Bureau, N.; Jose, J.; Mokbel, I.; de Hemptinne, J.-C., "Vapour Pressure Measurements and Prediction for Heavy Esters". *J. Chem. Thermodyn.*, **2001**, 33, 1485-1498.
30. Briggs, J.M.; Nguyen, T.B.; Jorgensen, W.L., "Monte Carlo Simulations of Liquid Acetic Acid and Methyl Acetate with the OPLS Potential Functions". *The Journal of Physical Chemistry*, **1991**, 95, 3315-3322.
31. Kamath, G.; Robinson, J.; Potoff, J.J., "Application of Trappe-UA Force Field for Determination of Vapor-Liquid Equilibria of Carboxylate Esters". *Fluid Phase Equilibria*, **2006**, 240, 46-55.

32. Sum, A.K.; Bidy, M.J.; de Pablo, J.J., "Predictive Molecular Model for the Thermodynamic and Transport Properties of Triacylglycerols". *Journal of Physical Chemistry*, **2003**, 107, 14443-14451.
33. Kamath, G.; Cao, F.; Potoff, J.J., "An Improved Force Field for the Prediction of the Vapor-Liquid Equilibria for Carboxylic Acids". *Journal of Physical Chemistry*, **2004**, 108, 14130-14136.

CHAPTER V

5. MEASUREMENTS OF VAPOR PRESSURES AND BUBBLE POINTS WITH EBULLIOMETRY

5.1 Introduction

Vapor pressures of pure compounds can be measured experimentally by using static or dynamic methods. In the static method, the liquid is degassed to eliminate dissolved gases, so that the vapor space in the equilibrium chamber is filled only with the vapors of the liquid of interest and the pressure of the system is measured to give the vapor pressure. In dynamic methods, the system pressure is fixed and the liquid is heated to bring it to boil. The corresponding pressure gives the vapor pressure of the system at the measured boiling temperature. Though static methods are more accurate, they are tedious to degass and the auxiliary equipment needed is expensive[1]. Ebulliometry[2, 3] on the other hand, which is the most widely used dynamic method, is fast and has undergone considerable developments in recent years to give accuracies[4-6] close to static methods.

One of the major issues in ebulliometry is effective removal of superheat[3]. It can be removed with the help of Cottrell[7], or Washburn[8] type tubes, which carry slugs of liquid and vapor to an equilibrium chamber where the temperature is measured. On the way to this chamber, the superheat in the liquid is used to vaporize extra liquid in the Cottrell pump, so that the temperature being measured is the true equilibrium temperature. Another way to alleviate the problem is to “activate” the heated surface with powdered glass[2] and use stirring to facilitate nucleation points for the vapor and provide good mixing. At low pressures getting rid of the superheat becomes difficult, because even a small liquid head inside the boiling chamber can create large enough superheat to cause ‘bumping’, which can flash the entire sample at once and

lead to cooling of the equilibrium chamber. Measuring the equilibrium temperature under such circumstances may require combining various methods to reduce the superheat.

In this study, we constructed ebulliometers based on previous models with two important design considerations, effective removal of superheat at low pressures and use of small amount of sample, since many of the compounds in high purity form are very expensive. At several instances during the optimization of parameters in the StePPE model, we encountered scattered or limited vapor pressure data, which needed measurements. Another important objective of this study is to make the ebulliometer developed for pure compounds usable for measurements of bubble points of binary mixtures. Adding the capability to measure bubble points of binary mixtures would be helpful in achieving that goal and would also be helpful in validating the StePPE model for binary mixtures in future.

5.2 Ebulliometer designs for pure compounds

The first ebulliometer studied in this work was based on Hoover's[9] design, which uses a tungsten wire to heat the liquid (Fig 5.1). The total height of the apparatus is about 8 inches. The sample holder has an inside diameter of about 1 cm and requires about 10 mL of sample. It works well when the wire is heated using a flame (Fig 5.5) at pressures as low as 30 mbar, below which, removing the superheat becomes difficult and bumping is observed. However, owing to safety concerns with the use of flames in a lab that handles large amounts of flammable liquids, this design was abandoned.

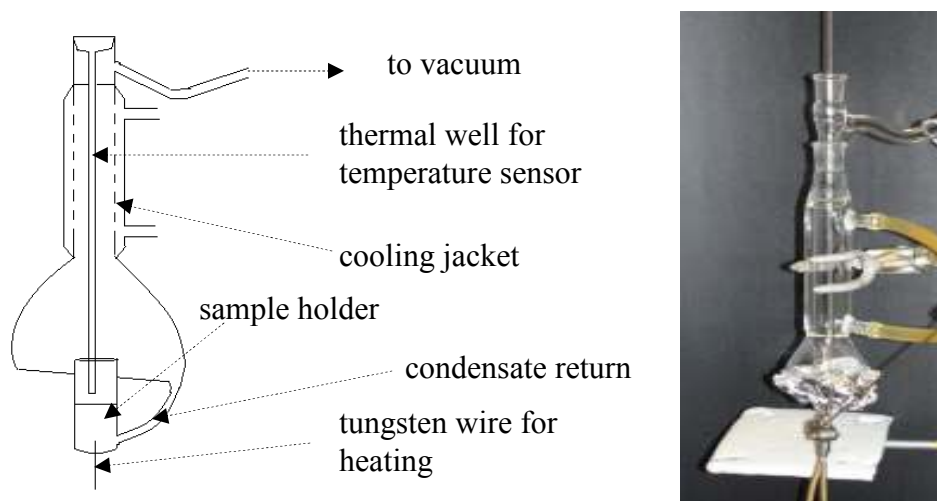


Figure 5.1: Ebulliometer based on Hoover's[9] design for vapor pressure measurement

Three other designs based on Cottrell's (Fig 5.2), Washburn's (Fig 5.3) and stirred flask (Fig 5.4) designs were tested, and they all work well in a pressure range of approximately 50 – 1000 mbar (Fig 5.5, 5.6). With the Cottrell tube apparatus, foaming was observed at pressures below 100 mbar for esters. Boiling chips, which were used in that design in order to facilitate nucleation of vapors, might have added impurities like moisture to the sample. In the Washburn and the stirred flask design, the heated surface is activated using powdered glass, in order to provide nucleation points for vaporization, so that boiling chips can be avoided. In the stirred tank apparatus, stirring is used in addition to the activation to help create good and rapid mixing, which is the key to effective superheat removal. Since the mixing is good in this design, the equilibrium temperature is measured by inserting the temperature probe in the liquid itself, rather than in a separate chamber, as in the Cottrell or Washburn design.

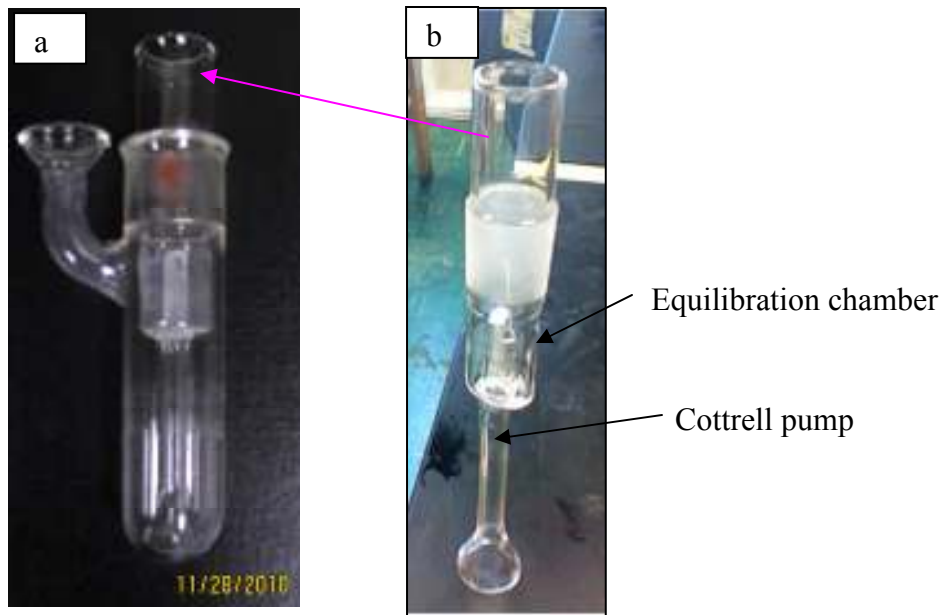


Fig 5.2: Cottrell tube ebulliometer. In (a), the entire assembly is shown, (b) shows the Cottrell tube insert with a funnel shaped bottom to catch the vapors, which get carried to the equilibrium chamber with the boiling liquid. The contents get squirted on the temperature probe (not shown) in this chamber. The height of the outside tube is about 6” and the diameter is about 1”



Figure 5.3: Ebulliometer with Washburn pump

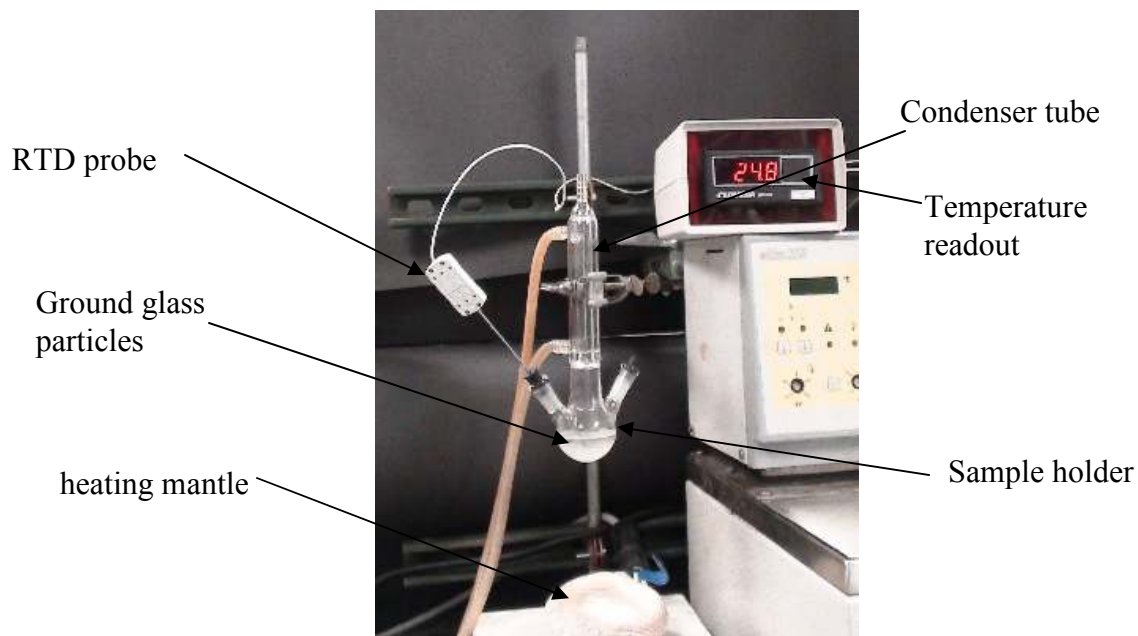


Figure 5.4 Stirred round bottom flask ebulliometer for vapor pressure measurements

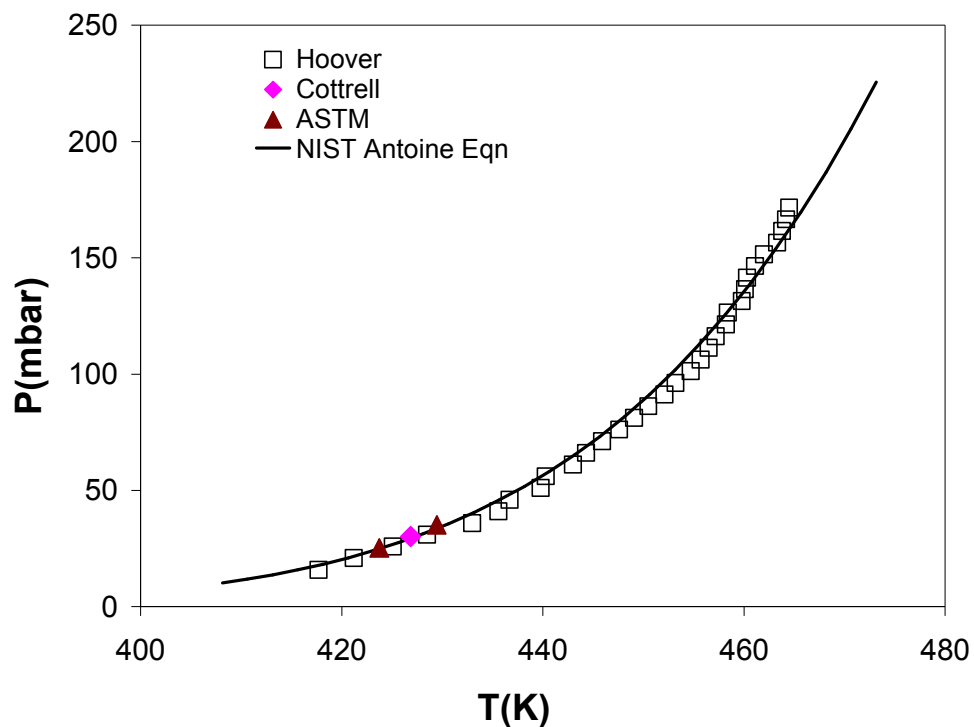


Figure 5.5: Measurement of P^{sat} of monoethyl succinate with Cottrell, Hoover and stirred flask ebulliometers

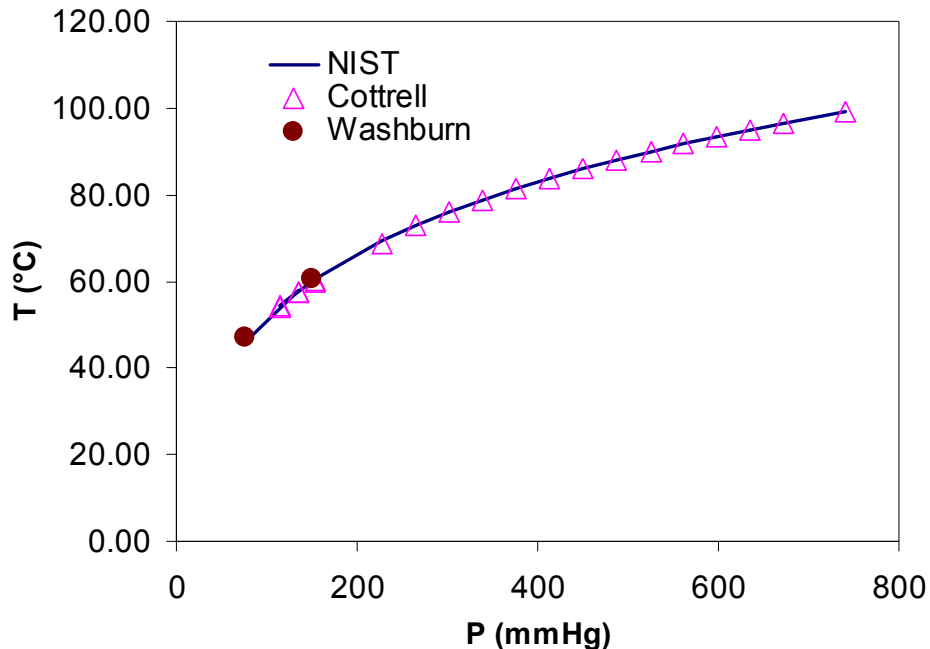


Figure 5.6: Measurements of water P^{sat} with Cottrell and Washburn ebulliometers

5.3 Ebulliometer for measuring T-x of a binary liquid

In addition to errors arising from superheat, compositional errors are also of concern when measuring the boiling temperature of a binary mixture. The major source of compositional error is the condensate hold-up on the walls of the ebulliometer. A relatively smaller error is incorporated due to evaporation of the liquid to fill the vapor space, which can be neglected if the relative volatilities of the components in the binary mixture do not differ significantly. Olson[10] gives a guideline for the use of different ebulliometric methods based on the difference in the boiling points of the compounds of interest, and suggests the use of static methods in case this difference is above about 120 K, where the errors due to evaporation and condensed liquid hold-up would be high.

Based on simple material balances, the condensed liquid hold-up can be calculated using Olson's[10] or Rogalski's[11] method, which differ slightly in the approach, but practically give the same result. For one mole of a sample feed, with V moles of vapor and L moles of liquid:

$$V + L = 1 \quad (1)$$

Applying material balance on component i , we get:

$$V.y_i + L.x_i = 1.q_i \quad (2)$$

where, y_i , x_i and q_i are the mole fractions of i in the vapor phase, the liquid phase and the feed, respectively. Using the equilibrium ratio $K_i = y_i/x_i$, equation 2 can be written as:

$$q_i = V.K_i x_i + L.x_i \quad (3)$$

or:

$$x_i = \frac{q_i}{V.K_i + L} = \frac{q_i / L}{(V / L).K_i + 1} \quad (4)$$

Defining vapor-to-liquid mole ratio as $f = V/L$, (4) can be simplified to:

$$x_i = \frac{q_i(1 + f)}{f.K_i + 1} \quad (5) \quad (\because L + V = 1 \Rightarrow 1/L = 1 + V/L = 1 + f)$$

or:

$$f = \frac{q_i - x_i}{y_i - q_i} \quad (6)$$

The fraction f depends on the construction of the ebulliometer and the rate of heat supplied. In other words, for a given ebulliometer and an approximate heating rate, f should be independent of the system. Generally, the heating rate is monitored using a drop counter in the condensate

return line of the ebulliometer. Once f is known, equation (5) can be used to calculate x_i iteratively for a given feed composition (q_i) for an unknown system, without having to measure the equilibrium liquid or vapor compositions, given by:

$$x_i^{n+1} = \frac{q_i(1+f)}{f \cdot (y_i^n / x_i^n) + 1} \quad (7)$$

where, n is the iteration number. The first guess of x_i can be the feed composition (q_i) and the corresponding vapor composition (y_i) can be found by using any activity model, using the following equation:

$$\gamma_i x_i P_i^{sat} = y_i P \quad (8)$$

In equation (8), γ_i is the activity coefficient of component i , P_i^{sat} is the vapor pressure of pure component i at the measured bubble temperature and P is the bubble pressure.

This approach has been used in many studies [4, 12, 13], where, first, f is determined using equation (9) either by measuring both, the liquid and vapor compositions, or by measuring the liquid composition and using an activity model to find the vapor composition, then equations (7) and (8) are used to get the T-x-y data of a system for a given pressure.

The flask ebulliometer (Fig 5.4) uses a small amount of sample, is the simplest among the ones studied and easiest to operate. Also, it has the smallest amount of vapor space. Therefore corrections due to evaporation would be negligible, if it were to be used to measure the bubble pressures of binary mixtures. The correction due to the condensate hold-up would be relatively small too, but important enough to be evaluated. However, neither the equilibrium liquid nor

vapor compositions can be measured easily with this ebulliometer. If a thermodynamically stable and well known binary system is used, the factor f in equation (6) can be calculated by measuring the T, P and q_i only. The key is measuring these quantities accurately. We will test this ebulliometer with methyl palmitate – methyl myristate system, for which P-T-x data are available[14]. If f stays stable, the ebulliometer can be used to measure the P-T-x of unknown systems.

REFERENCES

5.4 References

1. Hala, E.; Pick, J.; Fried, V.; Vilim, O., "Vapor- Liquid Equilibrium". **1958**, Pergammon Press: New York.
2. Swietoslowski, W., "Ebulliometric Measurements". **1945**, Reinhold Publishing: New York.
3. Ambrose, D., "Vapor Pressures", in *Experimental Thermodynamics*. 1975, Butterworths: London. 607-656.
4. Rogalski, M.; Malanowski, S., "Ebullimeters Modified for the Accurate Determination of Vapor-Liquid Equilibrium". *Fluid Phase Equilibria*, **1980**, 5, 97-112.
5. Chernyak, Y.; Clements, J.H., "Vapor Pressure and Liquid Heat Capacity of Alkylene Carbonates". *Journal of Chemical & Engineering Data*, **2004**, 49, 1180-1184.
6. Raal, J.D.; Gadodia, V.; Ramjugernath, D.; Jalari, R., "New Developments in Differential Ebulliometry: Experimental and Theoretical". *Journal of Molecular Liquids*, **2006**, 125, 45 – 57.
7. Cottrell, F.G., "On the Determination of Boiling Points of Solutions". *Journal of the American Chemical Society*, **1919**, 41, 721-729.
8. Washburn, E.W.; Read, J.W., ""Concentrated" Solutions. IV. The General Boiling Point Law". *Journal of the American Chemical Society* **1919**, 41, 729-741.
9. Hoover, S.R.; John, H.; Mellon, E.F., "Vapor Pressure Ebulliometer for Milliliter Samples". *Analytical Chemistry* **1953**, 25, 1940-1941.
10. Olson, J.D., "Measurement of Vapor-Liquid Equilibria by Ebulliometry". *Fluid Phase Equilibria*, **1989**, 52, 209-218.
11. Rogalski, M.; Rybakiewicz, K.; Malanowski, S., "Rapid and Accurate Method for Determination of Vapour-Liquid Equilibrium". *Berichte der Bunsen-Gesellschaft für Physikalische Chemie*, **1977**, 81, 1070-1073.

12. Zhenghong, G.; Zhonglong, M.; Qin, C.L.W., "Isothermal Vapor–Liquid Equilibria of Benzene-Dimethylformamide and Toluene-Dimethylformamide Systems Using a Small Modified Ebulliometer". *Fluid Phase Equilibria*, **2000**, 173, 253–262.
13. Kim, I.; Svendsen, H.F.; Børresen, E., "Ebulliometric Determination of Vapor-Liquid Equilibria for Pure Water, Monoethanolamine, N-Methyldiethanolamine, 3-(Methylamino)-Propylamine, and Their Binary and Ternary Solutions". *Journal of Chemical & Engineering Data*, **2008**, 53, 2521–2531.
14. Rose, A.; Supina, W.R., "Vapor Pressure and Vapor-Liquid Equid Equilibrium Data for Methyl Esters of the Common Saturated Normal Fatty Acids". *Journal of Chemical & Engineering Data*, **1961**, 6, 173-179.

CHAPTER VI

6. CONCLUSIONS AND RECOMMENDATIONS FOR FUTURE WORK

This chapter is divided in two sections. The first part deals with the StePPE simulations and the second part is about ebulliometric measurements of vapor pressures.

6.1. VLE calculations with StePPE

1. Conclusions

Robust thermodynamic property prediction is at the core of developing good process technologies in the chemical industry. Molecular simulations with UA Lennard-Jones potential[1-4], have come a long way in accurately predicting equilibrium liquid densities, vapor pressures, and heats of vaporization for pure compounds and mixtures. Recently, molecular dynamics simulations with step potentials[5], in conjunction with TPT has proven to be a fast alternative to continuous potential simulations. The step potential model, called SPEAD, though reproduces vapor pressures relatively better than other methods, the liquid density predictions lack accuracy. Vapor –liquid coexistence densities provide a stringent test for accuracy of a force-field, since thermodynamic properties are sensitive to changes in densities. A new UA step potential model, named StePPE, has been developed aimed at addressing the discrepancies in the SPEAD model, so that it can be used not only for vapor pressures, but also for accurate predictions of liquid densities. A new guideline has been outlined for selecting the site sizes, based on Bondi's[6] tabulated excluded volumes of the sites. Compared to SPEAD, the number of adjustable parameters has been reduced in StePPE for the alkenes, alcohols, ketones and esters. With the changes, a significant improvement in the liquid density predictions is achieved, while the accuracy in vapor pressure predictions is better than macroscopic group contribution

methods, especially for some of the complex compounds studied. The improvements have also helped ameliorate the transferability of the parameters to a broad range of compounds, and a broad chain length range within a homologous series, as discussed in CHAPTER IV.

Comparisons have been made with the more detailed continuous potential models. A good agreement is observed for the liquid densities compared to the accurate continuous potential models, and the vapor pressure predictions are generally more accurate with StePPE.

2. Future work

Many of pure compounds like, alkynes, aldehydes, naphthenes, aromatics and amines may not need any changes to the model parameters or the theory. The new parameters for those compounds should be optimized first, as experimental data for many of them is readily available.

For the pure compounds reported in this study, though the StePPE model reproduces the vapor pressures and liquid densities very well, some limitations were observed in the predictions for branched compounds and esters. Some improvements can be made for the charge neutral compounds by revisiting some of the model parameters, while improving the predictions of compounds with charges might involve some improvement to the theory itself.

a) Branched compounds and site sizes

The agreement with the experimental liquid densities and vapor pressures for branched compounds with StePPE is generally excellent for a broad range of compounds and with fewer special parameters compared to some other models. However, a closer look at the density predictions reveals a systematic overprediction for compounds with quaternary carbon (Fig 6.1). One remedy would be to treat the side methyl groups attached to the quaternary carbon with

reduced well parameters. Alternatively, the size of the quaternary carbon can be increased. The experimental liquid densities of branched alkanes decrease with branching, which suggests that among structural isomers, the core volume should increase with branching. The current sizes however, show an opposite trend, and the expected error is apparently compensated for by the potential wells of the CH and CH₃s groups.

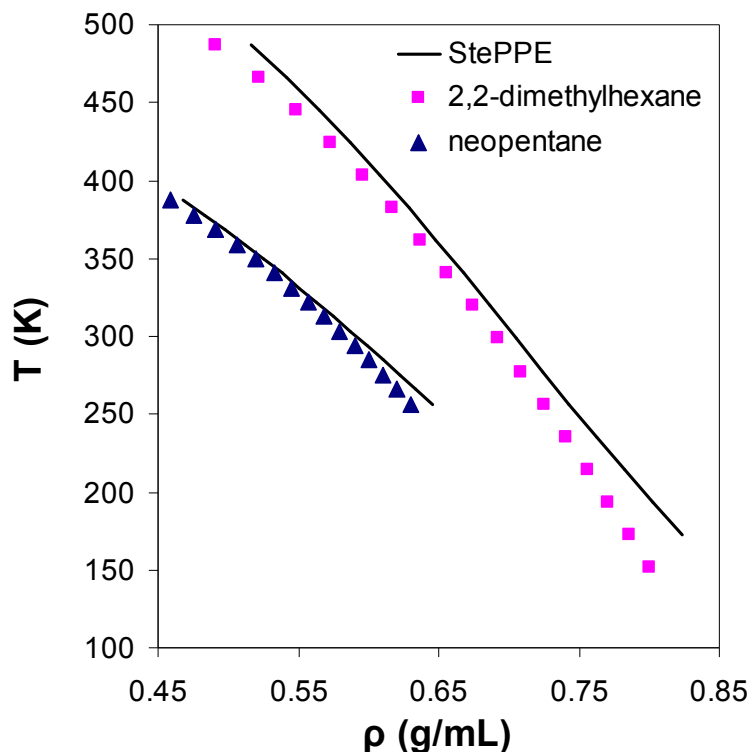


Fig 6.1: Liquid densities of neopentane and 2,2-dimethylhexane with StePPE. The symbols are from DIPPR 801 correlations

A similar observation was made for the secondary alcohols. An optimization with an increased size of the methine group was done. The results show a better agreement with the increased CH size than what is obtained with the current set of parameters for the liquid densities as well as the vapor pressures (Table 6.1). Additionally, unlike the current implementation, no special parameters were used for 2-methanol.

From a fundamental viewpoint, increasing the site diameters appears more justifiable than changing the well parameters to overcome the errors, which can be achieved by setting the volume correction factor, as discussed in CHAPTER III, to above 20%. A reasonable value would be 20.5%, which would affect the CH3 and CH2 diameters only by a small amount.

Table 6.1: Comparison of errors of secondary alcohols with two different sizes of the methine group

Compound	P^{sat}				ρ			
	$\sigma_{\text{CH}} = 3.9\text{\AA}$		$\sigma_{\text{CH}} = 3.9\text{\AA}$		$\sigma_{\text{CH}} = 3.9\text{\AA}$		$\sigma_{\text{CH}} = 3.9\text{\AA}$	
	%AAD	%Bias	%AAD	%Bias	%AAD	%Bias	%AAD	%Bias
2-propanol	8.68	8.60	9.20	9.20	1.41	-1.39	1.84	1.84
2-butanol	3.20	3.07	12.53	12.53	0.26	0.10	1.25	1.25
2-pentanol	3.20	2.94	14.96	14.96	0.35	-0.25	0.79	0.77
2-hexanol	7.10	-6.86	7.80	4.99	0.70	0.70	1.64	1.64
2-heptanol	7.68	-7.63	7.46	6.73	0.27	0.21	0.94	0.94
2-octanol	10.45	-9.73	6.55	4.65	0.55	0.55	1.25	1.25
2-nonanol	14.98	-14.98	3.43	-0.07	0.46	0.46	1.04	1.04
3-pentanol	9.76	9.34	4.69	-2.50	0.31	-0.31	0.17	0.16
3-hexanol	9.73	-0.72	12.25	-10.64	0.15	-0.02	0.37	0.34
3-heptanol	9.17	-1.45	13.67	-9.69	0.45	0.42	0.75	0.75

b) Including the analytical tail correction

For a Lennard– Jones particle, the potential well extends to infinity, while the simulation box is limited. The general practice therefore is to truncate the potential function at a cut-off distance (r_c), and add a tail correction to compensate for the truncation error, such that the energy due to a particle can be given by,

$$\frac{E}{NkT} = \frac{\rho}{2kT} \int_0^{r_c} u(r)g(r)4\pi r^2 dr + \frac{\rho}{2kT} \int_{r_c}^{\infty} u(r)g(r)4\pi r^2 dr$$

where, N is the total number of particles, ρ is the average number density of particles, $g(r)$ is the radial distribution function (rdf) at a distance r , and $u(r)$ is the potential function. The second integral is the tail correction, which can be calculated analytically. Assuming $g(r)=1$ beyond the cutoff separation, the contribution of the tail to the configurational energy per particle can be given by,

$$\frac{\rho}{2kT} \int_{r_c}^{\infty} u(r) 4\pi r^2 dr = \frac{E^{tail}}{NkT}$$

Generally, r_c is chosen to be around 2.5σ , where the potential is about 1.6% of the minimum. Though seemingly negligible, the tail correction due to the potential beyond r_c can be significant at liquid-like densities[7]. For the step potentials, with $r_c = 2\sigma$, used in SPEAD and StePPE, the tail correction for a pair i is given by (for a complete derivation, see Appendix A.2),

$$\frac{E_i^{tail}}{NkT} = -\frac{32\rho_i\sigma_i^3\epsilon_{4i}}{3kT}$$

where, ϵ_{4i} is the fourth well, ρ_i is the number density of pair i and σ_i is the adjusted diameter for the pair. The contribution from each pair can be added to the Helmholtz energy equation from TPT.

To replicate a Lennard-Jones type potential more realistically, an optimization with tail corrections for the alkanes was done, keeping the fourth well close to about 6% of the first, (which is the potential at 2σ for Lennard-Jones potential). The preliminary results are shown in Table 6.2. Though the overall agreements for the vapor pressures and the liquid densities are

good, the density deviations seem to increase with increasing molecular weight. This might need a reoptimization of the CH2 site size. The analysis can then be extended to ether, ketones and esters.

Table 6.2: Errors in liquid densities and vapor pressures of n-alkanes with StePPE with tail corrections

Compound	% AAD P^{sat}	% Bias P^{sat}	%AAD ρ	%Bias ρ
propane	6.48	-2.82	1.03	-1.03
n-butane	11.14	-7.87	0.71	0.71
n-octane	9.04	4.26	0.53	0.53
n-decane	8.05	3.41	1.42	1.42
n-tetradecane	11.19	1.46	2.45	2.45
Overall	9.18	1.69	1.34	1.07

Optimized well parameters

Site	ϵ_1 (K)	ϵ_4 (K)
CH3	86.94	5.4
CH2	44	4.4

c) Intramolecular attraction parameters

Reduced diameters are used for non-bonded interactions between third neighbors in order to impart flexibility to the chain. Using reduced diameters for up to six neighbors is not expected to affect the simulation results noticeably. The non-bonded intramolecular attractions on the other hand, are expected to affect the results more. In StePPE, the attractive interactions start with neighbors separated by three bonds (collectively, we call it a ‘34’ interaction, meaning that the attractive interactions start at the third bond and the full-diameter repulsions start at the fourth bond). In order to explore this effect, ester simulations were run with ‘77’ intramolecular interactions and the results were compared with those with the ‘34’ interactions (Fig 6.2). The errors with ‘77’ interactions show an increasing trend with increasing number of carbon atoms in the chain, while the trend is more scattered with the ‘34’ interactions, though the vapor pressures

appear to be overpredicted and the densities are underpredicted for the smallest esters with the ‘34’ interactions.

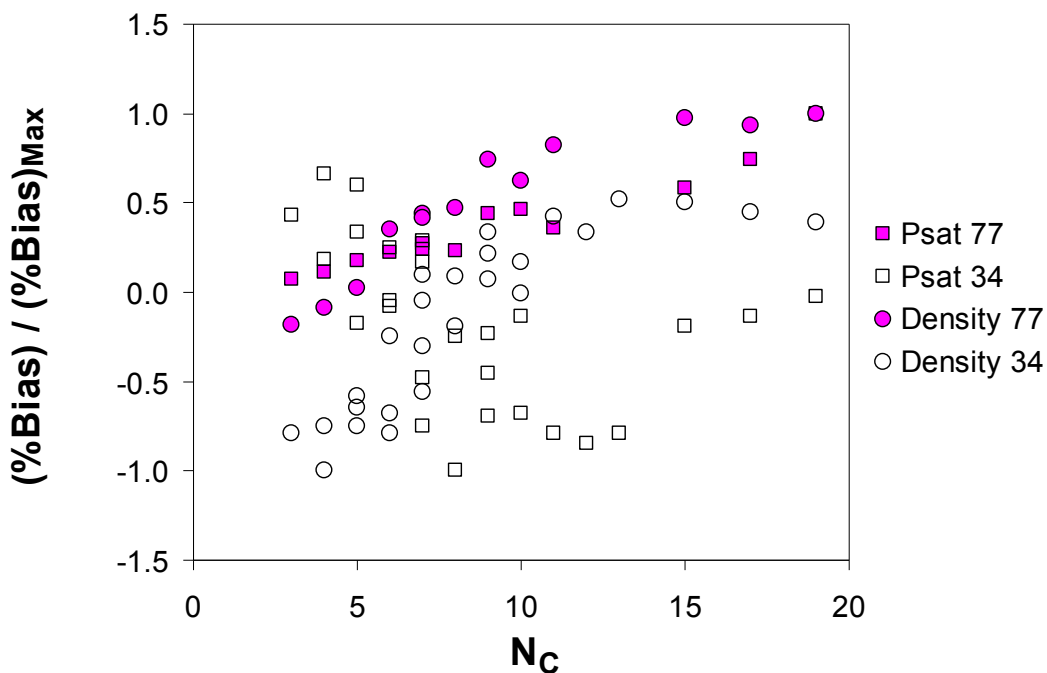


Fig 6.2: Vapor pressure and liquid density deviations with StePPE, using ‘34’ and ‘77’ intramolecular interactions; x-axis denotes the total number of carbon atoms in the ester chain

Intuitively, increasing the number counts for the intramolecular attractions would help reduce the errors in the densities and vapor pressures of the small esters, without affecting the predictions of the bigger molecules as much. For a system of M molecules, with N_s number of sites per molecule, the ratio r of the intramolecular attractive interactions to the total attractive interaction can be given by (see Appendix A.3),

$$\frac{N_s(N_s - 1) - 2 \sum_{i=1}^{x-1} (N_s - i)}{N_s(MN_s - 1) - 2 \sum_{i=1}^{x-1} (N_s - i)}$$

where, x is the bond distance where the intramolecular attractions begin to be counted. Currently x is set at 3. Fig 5.3 shows a plot of the ratio given by the above equation with changing x for different molecular sizes. The plot is not completely quantitative since the equation developed above includes all pairs whether they fall inside or out of the pair-potential. In a real situation, the ratio should scale down by some factor. The smaller molecules would be affected the most by changing the position since they have steeper slopes. In order to increase the intramolecular attractions, the ratio r has to be increased. But the current parameters are set at the minimum bond distance possible for the intramolecular attractions. It is to be noted that the esters use the optimized parameters from alkanes, ethers and ketones, all optimized with '34' interactions. So, the parameters of these functional groups would have to be optimized first with the desired value of x , in order to get a more complete picture of the effect of x on the results.

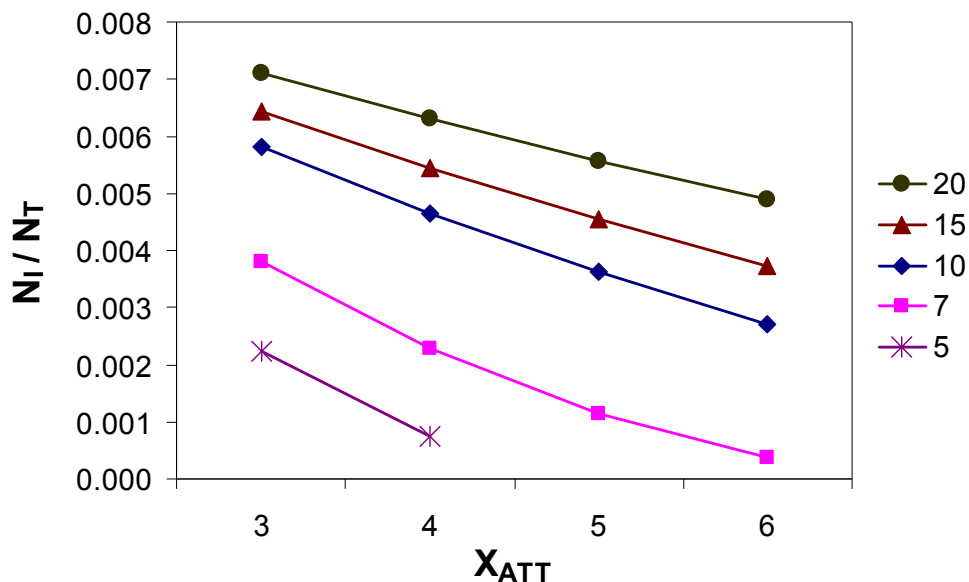


Fig 6.3: Ratio of intramolecular attractive pairs (N_I) to total number of attractive pairs (N_T) with x . The legends denote the total number sites in the molecule

d) Including electrostatic interactions in TPT

The pair-potential in StePPE is truncated at 2σ . The potential due to electrostatic interactions dies off much slowly and is multiple orders of magnitude higher than the dispersion potential in the range $0-2\sigma$. For systems where partial charges are expected, it is therefore important to include electrostatic interactions in the force-field. Since the current StePPE implementation does not include electrostatic interactions, adjusting the step wells based on the type of interaction can somewhat compensate the effect of the partial charges. For example, in dimethyl ether, the oxygen is expected to have a partial negative charge and the CH3 group is expected to have a partial positive charge. For non-bonded interactions between oxygen and a CH3 group, the potential well can be made deeper to compensate for the attraction between these two sites, and likewise, the potential wells for the oxygen-oxygen, or CH3-CH3 interactions can be made shallower as shown below,

$$\varepsilon_{ij,m} = \varepsilon_{ij,m}^0 - K \frac{q_i q_j}{\sigma_{ij,m}}$$

where, $\varepsilon_{ij,m}^0$ is the original well depth of well m of pair $i-j$, q_i, q_j are the charges, $\sigma_{ij,m}$ denotes the location of well m for pair $i-j$ and K is a scaling factor.

Figure 6.4 shows a comparison of results for ethers based on this approach with the original StePPE results. Charges were borrowed from the OPLS force-field[8]. These results are preliminary and more detailed study needs to be done in order to incorporate the effect of charges in the code. For better results, the factor K in the above equation should be made an adjustable parameter or a more sophisticated method should be developed. Parameters obtained from ethers and ketones can then be used for esters in order to test the transferability.

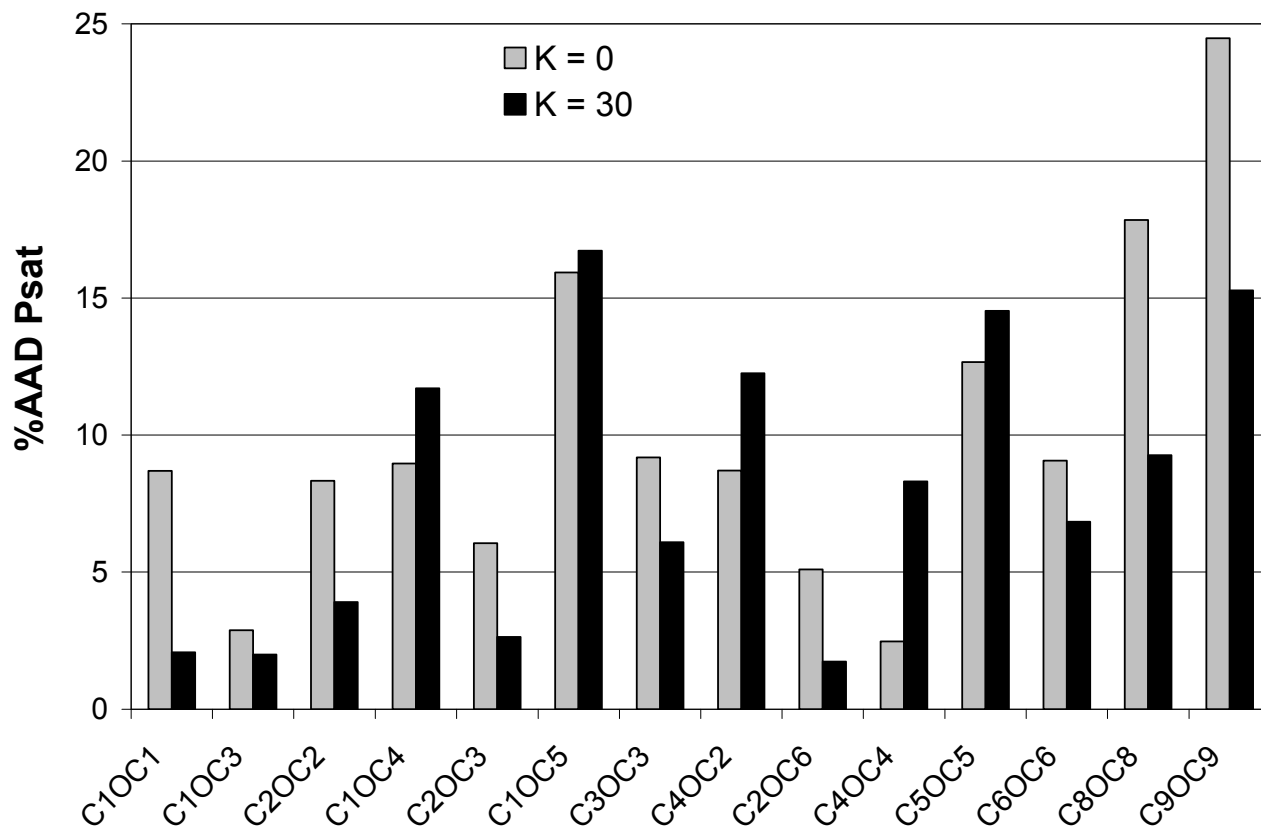


Figure 5.4: Vapor pressures of ethers with StePPE with and without correction for partial charges

e) Radius of Gyration

Another interesting study would involve comparison of the radius of gyration for StePPE simulations with the reported radius of gyration. Below are some comparisons of the radius of gyration reported by DIPPR to the most likely end-to-end distance from the intramolecular distribution function for the n-alkanes. The values appear to be consistently lower with StePPE. This is however a crude method of obtaining the radius of gyration using only the end-to-end distance, and more precise method is needed to calculate it during the simulations.

Table 6.3: Comparison of the radius of gyration of n-alkanes with the most likely end-to-end distance in StePPE simulations

Compound	R_G (Å)	
	StePPE	DIPPR
butane	1.93	2.88
pentane	2.15	3.34
hexane	2.7	3.77
octane	3.69	4.55
nonane	4.68	4.81
decane	4.13	5.15

6.2 Ebulliometric measurements

1. Conclusions and recommendations

To measure vapor pressures of pure components and bubble pressures of binary mixtures, ebulliometry provides a fast and reasonably accurate method, compared to static methods. Commercially available ebulliometers are generally complicated and require sample sizes in the range of about 150 – 200 mL[9, 10]. Several other ebulliometers have been used for laboratory measurements with smaller samples[11].

For the measurement of pure component vapor pressures, our designs with a Cottrell[12] or Washburn[13] type pump were found to be effective in removing superheat. Similar accuracy was achieved with our stirred flask type design, which is the simplest among the three. The design is a scaled-down form of the stirred-type ebulliometer discussed in the ASTM E1719 method. The heated surface of the flask was activated with powdered glass to facilitate the nucleation of bubbles. The activation coupled with vigorous stirring was found to be very effective in removing the superheat from the boiling liquid, and temperature measurement was

possible by putting the probe in the liquid itself rather than in a separate equilibrium chamber, as in Cottrell's or Washburn's design.

Based on an analysis similar to the stirred flask design for binary mixtures, the condensate hold-up in the Washburn apparatus can be estimated. And used for the measurement of bubble pressures of unknown systems.

REFERENCES

6.3 References

1. Siepmann, J.I.; Karaborni, S.; Smit, B., "Simulating the Critical Behaviour of Complex Fluids". *Nature* **1993**, 365, 330- 332.
2. Jorgensen, W.L.; Madura, J.D.; Swenson, C.J., "Optimized Intermolecular Potential Functions for Liquid Hydrocarbons". *Journal of the American Chemical Society*, **1984**, 106, 6638-6646.
3. Martin, M.G.; Siepmann, J.I., "Transferable Potentials for Phase Equilibria. 1. United-Atom Description of n-Alkanes". *Journal of Physical Chemistry B*, **1998**, 102, 2569-2577.
4. Nath, S.K.; Escobedo, F.A.; de Pablo, J.J., "On the Simulation of Vapor–Liquid Equilibria for Alkanes". *Journal of Chemical Physics*, **1998**, 108, 9905-9911.
5. Unlu, O.; Gray, N.H.; Gerek, Z.N.; Elliott, J.R., "Transferable Step Potentials for the Straight-Chain Alkanes, Alkenes, Alkynes, Ethers, and Alcohols". *Industrial & Engineering Chemistry Research* **2004**, 43, 1788-1793.
6. Bondi, A., "van der Waal's Volumes and Radii". *The Journal of Physical Chemistry*, **1964**, 68, 441-451.
7. Frenkel, D.; Smit, B., "Understanding Molecular Simulation". 2nd ed. **1996**, Academic Press: San Diego.
8. Briggs, J.M.; Matsui, T.; Jorgensen, W.L., "Monte Carlo Simulations of Liquid Alkyl Ethers with the OPLS Potential Functions". *Journal of Computational Chemistry*, **1990**, 11, 958–971.
9. Olson, J.D., "Measurement of Vapor-Liquid Equilibria by Ebulliometry". *Fluid Phase Equilibria*, **1989**, 52, 209-218.
10. ASTM Standard E1719, *Standard Test Method for Vapor Pressure of Liquids by Ebulliometry*. 2005, www.astm.org; West Conshohocken, PA.
11. Swietoslawski, W., "Ebulliometric Measurements". **1945**, Reinhold Publishing: New York.

12. Cottrell, F.G., "On the Determination of Boiling Points of Solutions". *Journal of the American Chemical Society*, **1919**, 41, 721-729.
13. Washburn, E.W.; Read, J.W., "'Concentrated' Solutions. IV. The General Boiling Point Law". *Journal of the American Chemical Society* **1919**, 41, 729-741.

APPENDICES

APPENDICES

A.1 Angle distribution in butyl propionate

To demonstrate that the bonds in the DMD are flexible, the following figure shows the bond distribution from 10 snapshots from the simulation of butyl propionate. The curves are not smooth due to the small sample.

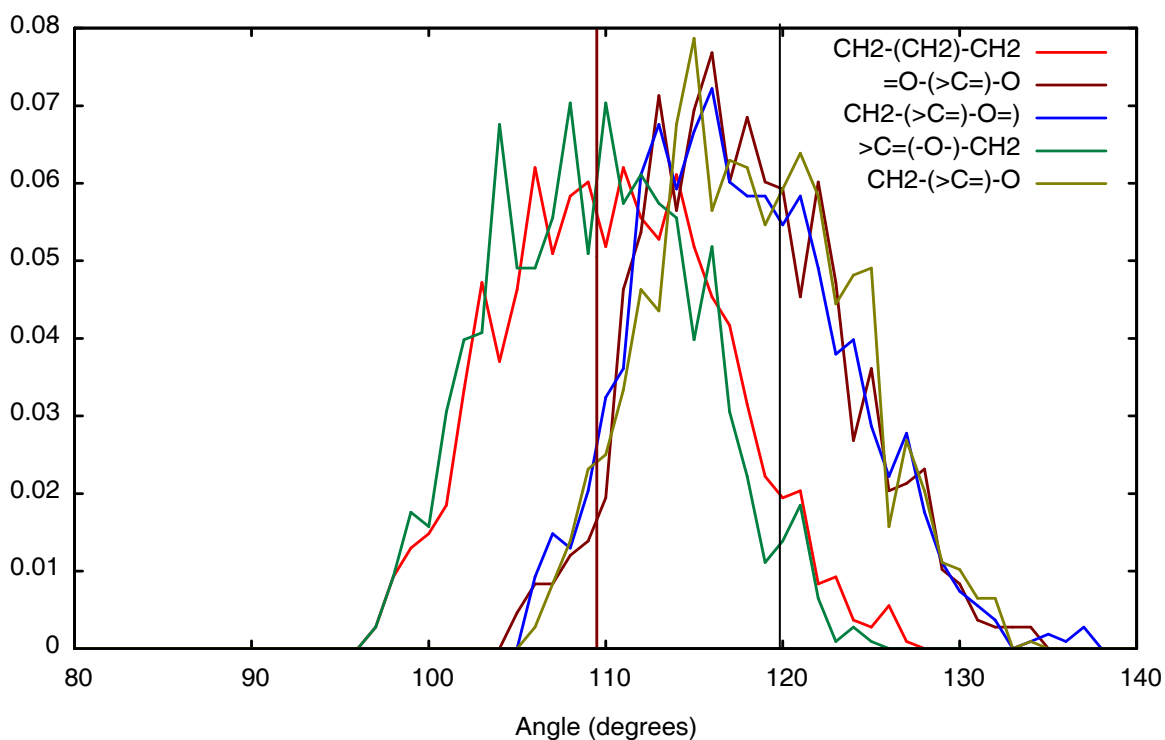


Figure A.1: Distribution of some angles in butyl propionate. The legends denote the three sites that form the angle, and the site within the parentheses is the central angle. The vertical lines denote the equilibrium values (109.5° and 120°)

A2. Bond lengths

Table A2.1 Bond lengths used in StePPE model

SiteA	SiteB	Length(Å)	Remarks
C	C/CH/CH2/CH3	1.54	Any bond in a saturated alkane
>C=(ester/ketone)	CH2/CH3	1.54	Bond between carbonyl carbon in an ester or ketone and a CH3 or a CH2 group
>C=(ester)	O-(ester)	1.43	
>C=(ester/ketone)	O=(ester/ketone)	1.21	
CH	C/CH/CH2/CH3	1.54	
CH=	CH=/CH=c/CH=t	1.54	CH=c and CH=t denote a CH= in a cis or trans alkene
CH=c	CH=c	1.34	
CH=t	CH=t	1.34	
CH=	CH2	1.54	
CH=	CH2=	1.34	
CH(OHs)	CH2	1.54	
CH=c	CH2	1.54	
CH=t	CH2	1.54	
CH(OHs)	CH3	1.54	CH(OHs) denotes a CH in a secondary alcohol
CH=c	CH3	1.54	
CH=t	CH3	1.54	
CH=	CH3	1.54	
CH(OHs)	OHs	1.43	
CH2	C/CH/CH2/CH3	1.54	
CH2(OH)	CH2	1.54	
CH2(r)	CH2(r)	1.54	Bonds between CH2 groups in ring compounds
CH2e(OH)	CH3	1.54	
CH2	O-(ester/ether)	1.43	
CH2e(OH)	OH	1.43	Only in ethanol
CH2(OH)	OH	1.43	
CH3	C/CH/CH2/CH3	1.54	
CH3	O-(ether/ester)	1.43	
CH3(OH)	OH	1.43	Only in methanol

A3. Finding the first guess of site sizes from excluded volumes

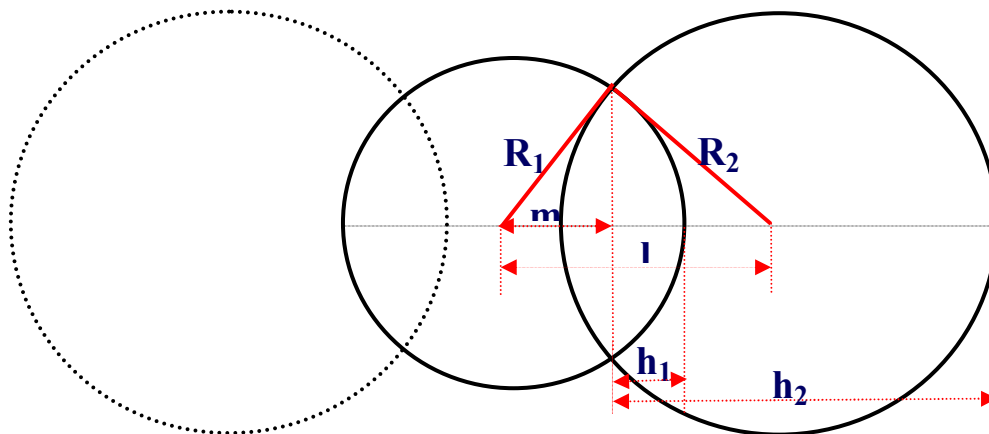


Fig A3.1: Schematic for finding site diameters from given excluded volumes

In Fig A3.1, we use a propane molecule to illustrate the calculation of the volume correction factor for each covalent bond. The outer two spheres are CH₃ groups and the middle sphere is CH₂. The excluded volumes of these sites and the bond length (l in the figure above) are known. With use of simple geometry, R_1 and R_2 can be calculated. Once the diameters are known, the volume lost by each site due to overlap can be calculated. The method is described below.

The volume of a section of a sphere of height h and radius R can be given by:

$$V = \frac{\pi}{3} h^2 (3R - h)$$

We can use the auxiliary parameter m to calculate R_1 and R_2 from the given excluded volumes

V_1 and V_2 using the following equations:

$$m = \frac{R_1^2 + l^2 - R_2^2}{2l}$$

$$h_1 = R_1 - m$$

$$h_2 = l + R_2 - m$$

$$V_1 = \frac{4}{3}\pi R_1^3 - 2\frac{\pi}{3}h_1^2(3R_1 - h_1)$$

$$V_2 = \frac{\pi}{3}h_2^2(3R_2 - h_2)$$

A.4. Liquid density and vapor pressure plots

In all the plots in this section, the experimental data is shown as points and the StePPE predictions are shown as solid lines. The lines and symbols are of the same color for a molecule.

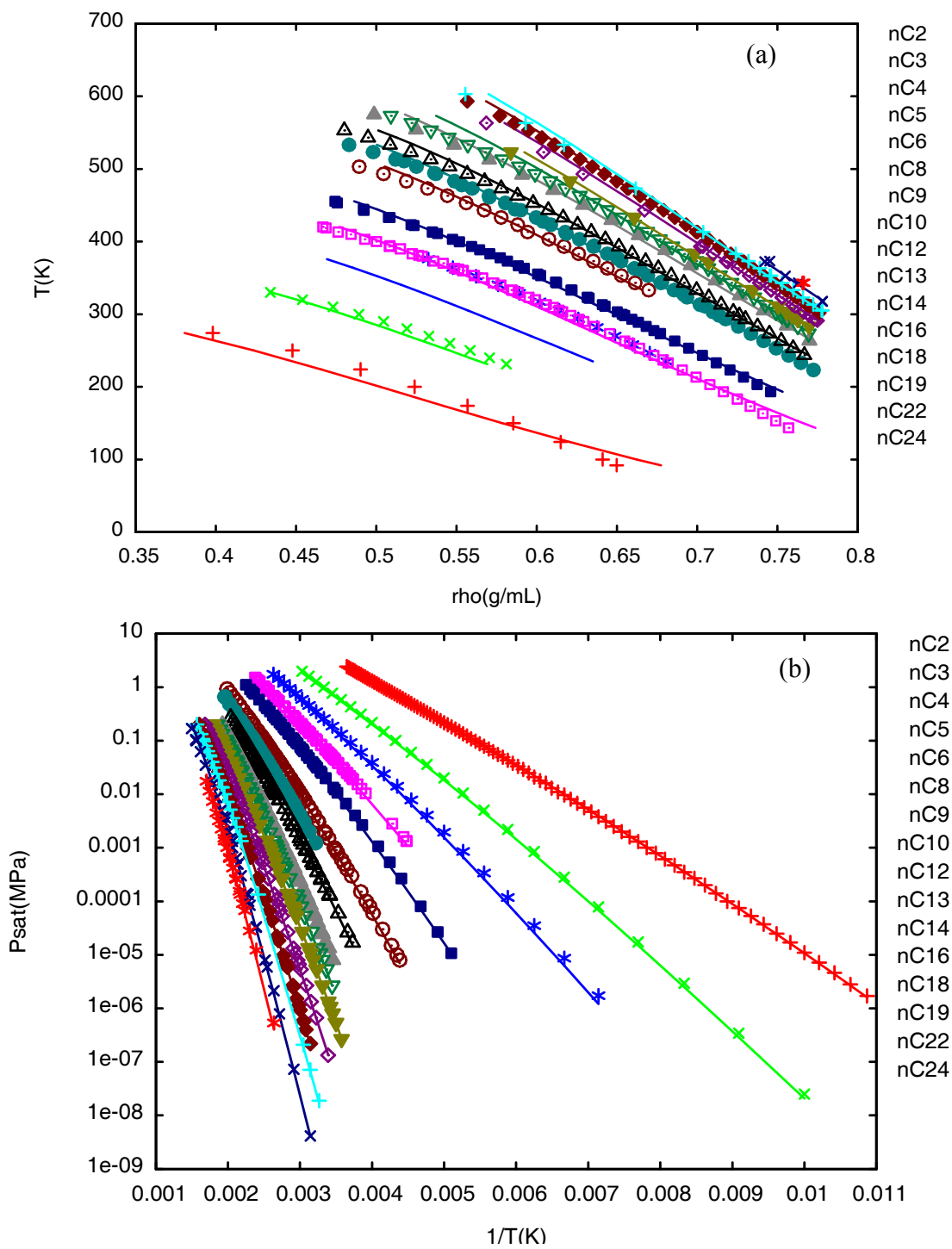
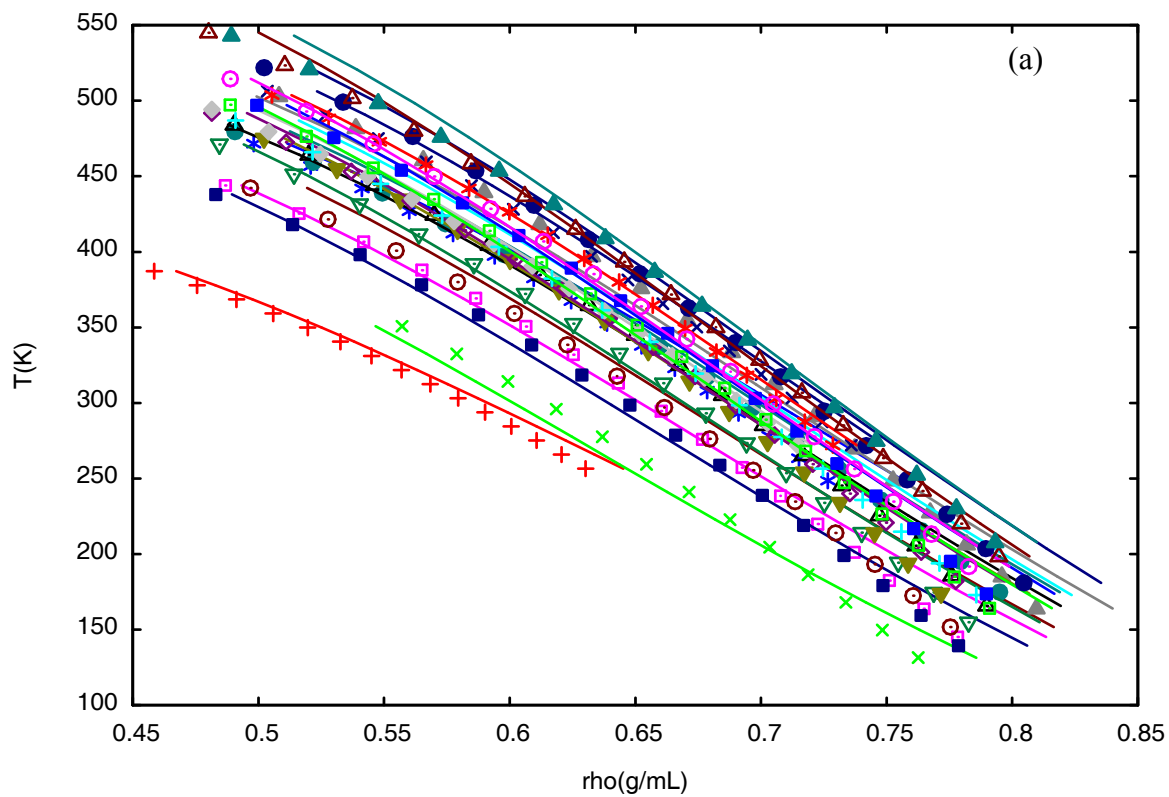


Figure A.4. 1: Liquid densities (a) and vapor pressures (b) of *n*-alkanes



C3-2.2-diMe	+	C5-2.3.4-triMe	▲	C7-2-Me	◻
C4-2-Me	x	C6-2-Me	▼	C7-4-Me	■
C4-2.2.3-triMe	*	C6-3-Me	▼	C7-2.6-diMe	○
C4-2.3-diMe	◻	C6-2.5-diMe	◊	C7-3-Et	●
C5-2-Me	■	C6-2.4-diMe	◊	C9-2-Me	▲
C5-3-Me	○	C6-2.2-diMe	+	C9-5-Me	▲
C5-3-Et	●	C6-3.4-diMe	x		
C5-2.2.4-triMe	▲	C6-3-Et	*		

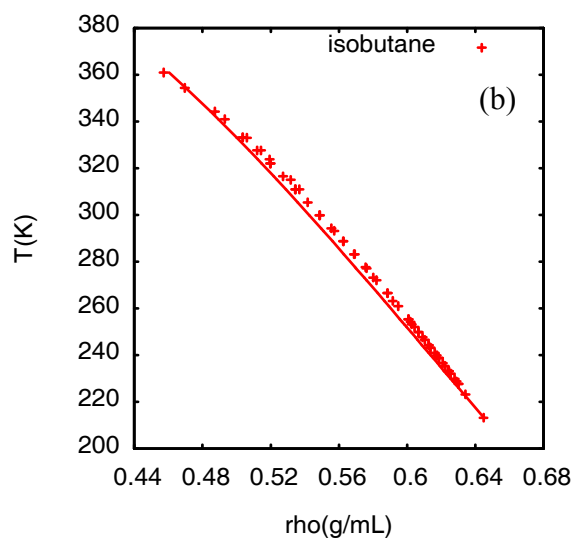
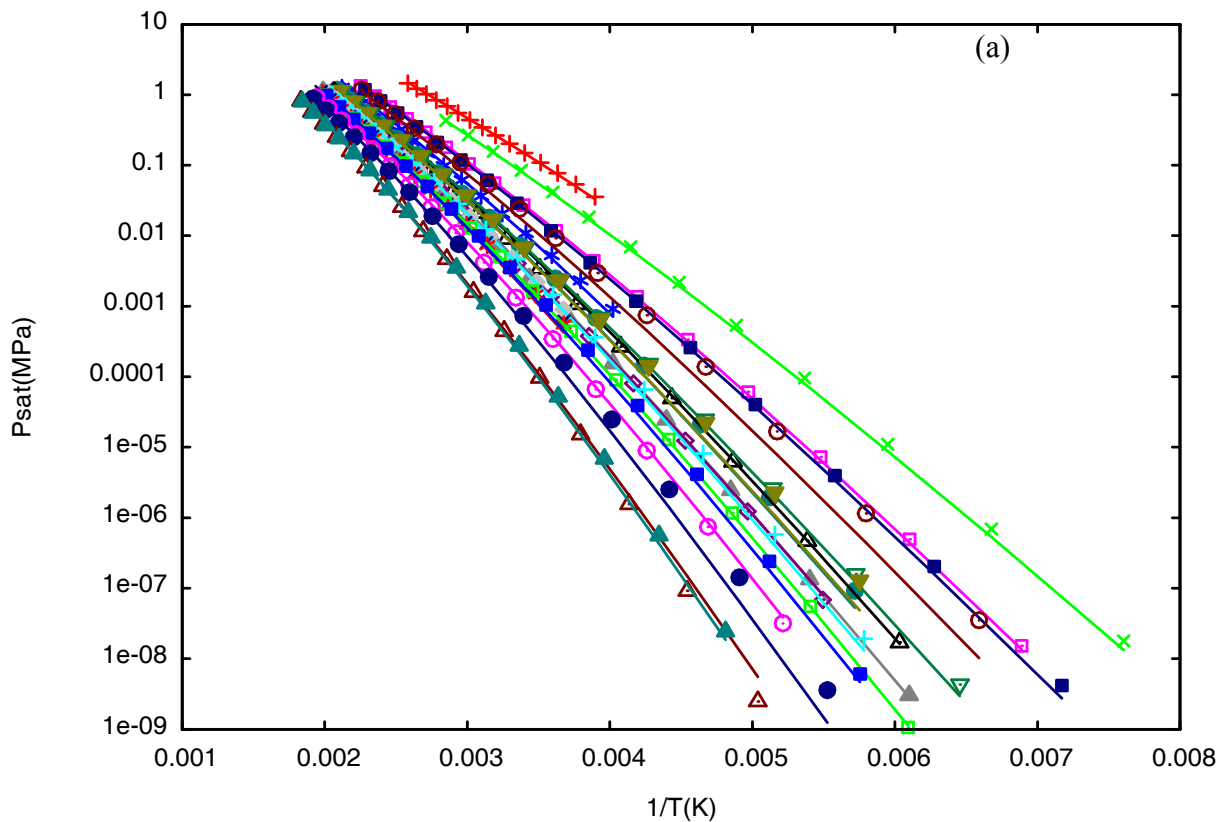


Fig A.4.2: Liquid densities of branched alkanes (a); isobutane (b)



- | | | | | | |
|----------------|---|----------------|---|-------------|---|
| C3-2.2-diMe | + | C5-2.3.4-triMe | ▲ | C7-2-Me | ◻ |
| C4-2-Me | x | C6-2-Me | ▼ | C7-4-Me | ■ |
| C4-2.2.3-triMe | * | C6-3-Me | ▼ | C7-2.6-diMe | ○ |
| C4-2.3-diMe | ◻ | C6-2.5-diMe | ◇ | C7-3-Et | ● |
| C5-2-Me | ■ | C6-2.4-diMe | ◇ | C9-2-Me | △ |
| C5-3-Me | ○ | C6-2.2-diMe | + | C9-5-Me | ▲ |
| C5-3-Et | ● | C6-3.4-diMe | x | | |
| C5-2.2.4-triMe | △ | C6-3-Et | * | | |

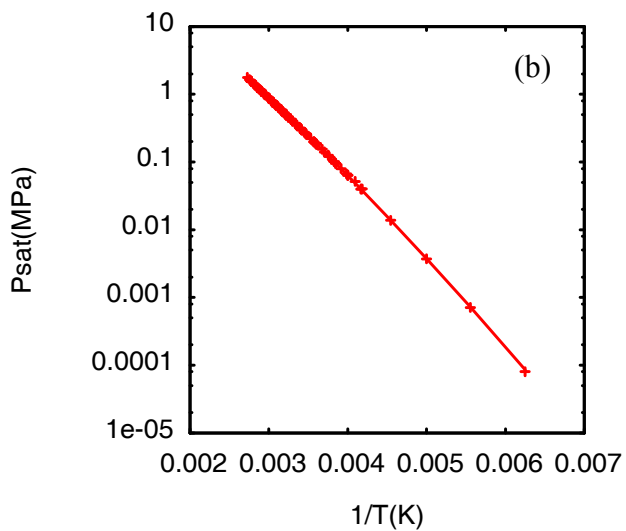


Fig A.4.3: Vapor pressures of branched alkanes (a); isobutane (b)

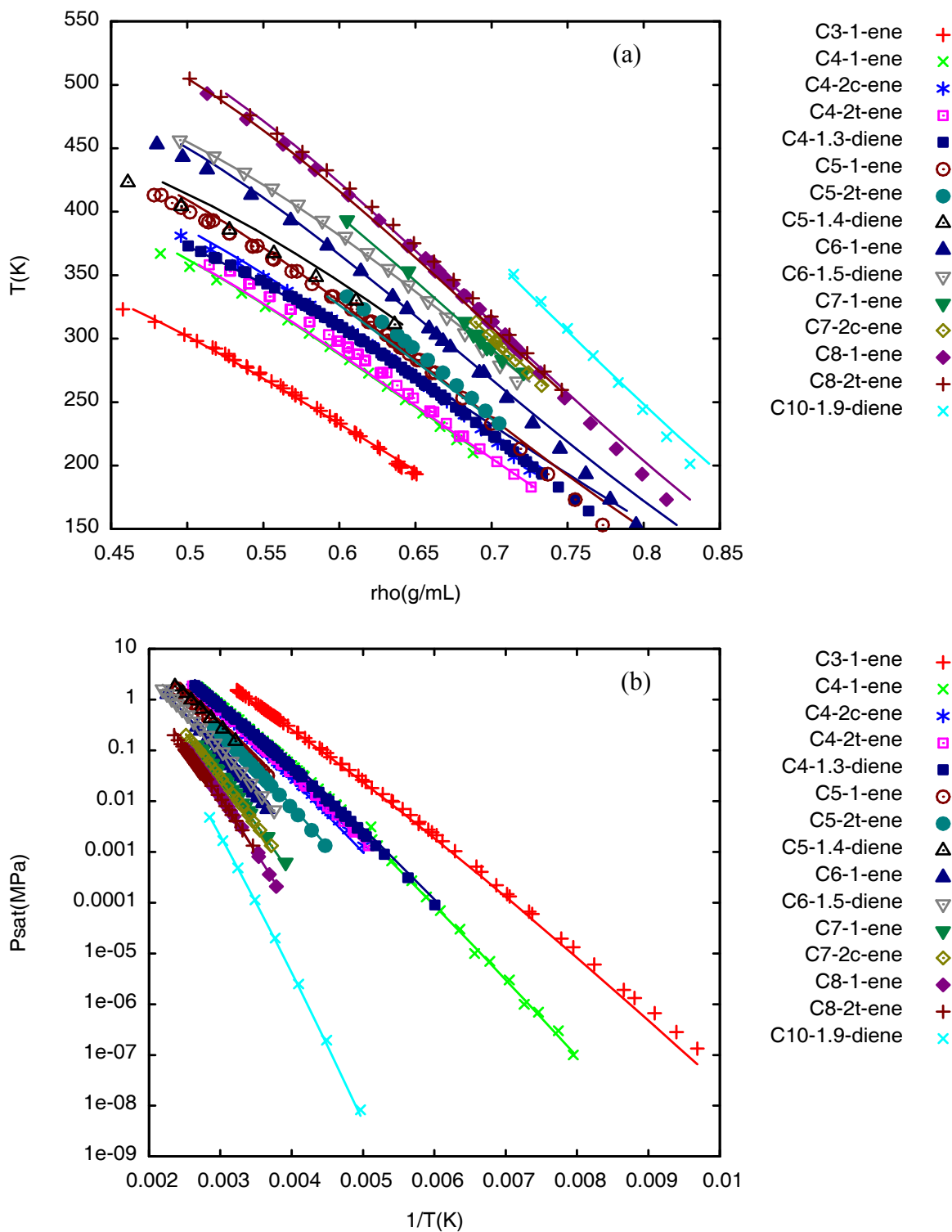


Figure A.4.4: Liquid densities (a) and vapor pressures (b) of alkenes

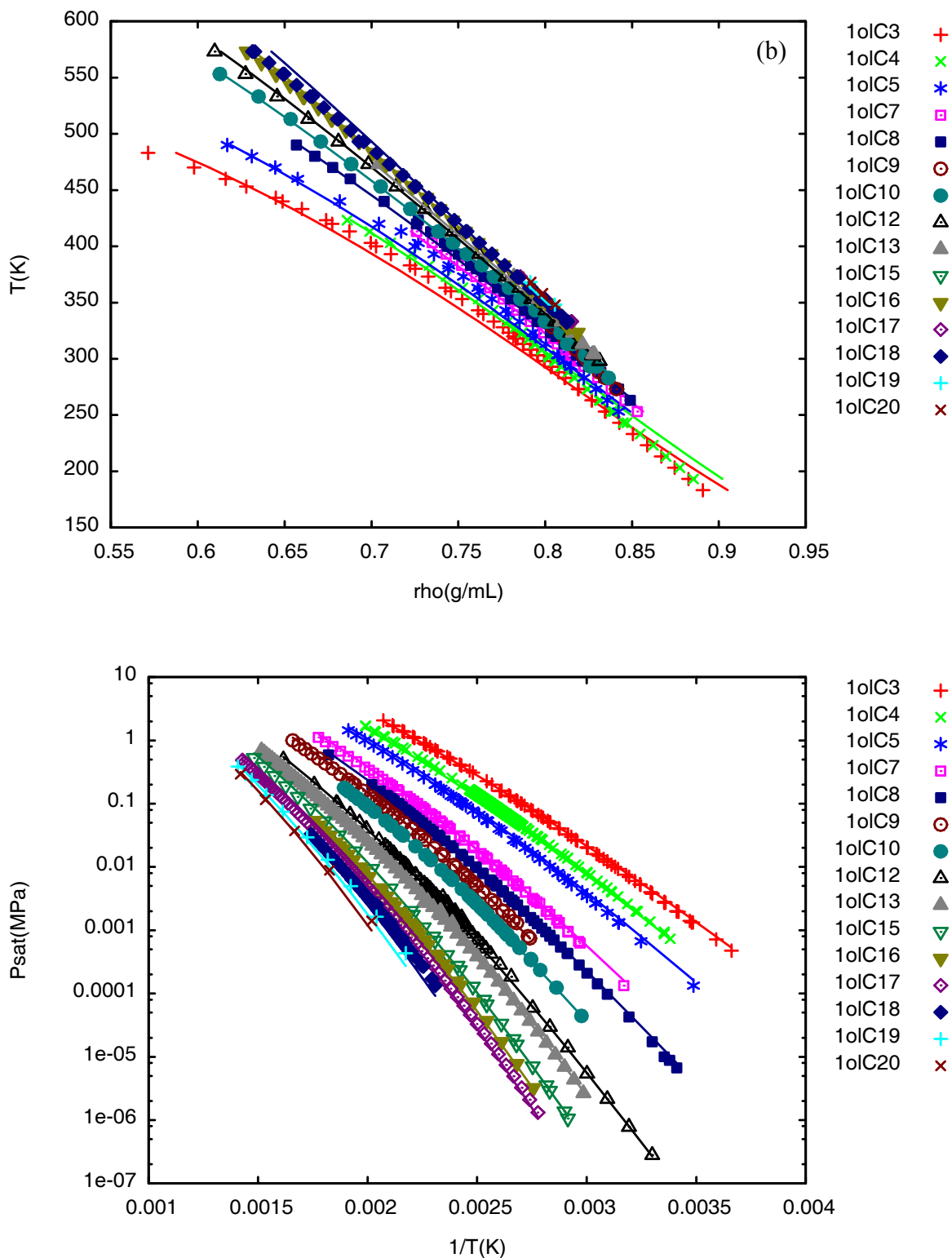


Figure A.4.5: Liquid densities (a) and vapor pressures (b) of primary alcohols. The symbol ‘1oICx’ denotes a primary alcohol with ‘x’ carbons in the backbone. For example, 1oIC8 in 1-octanol

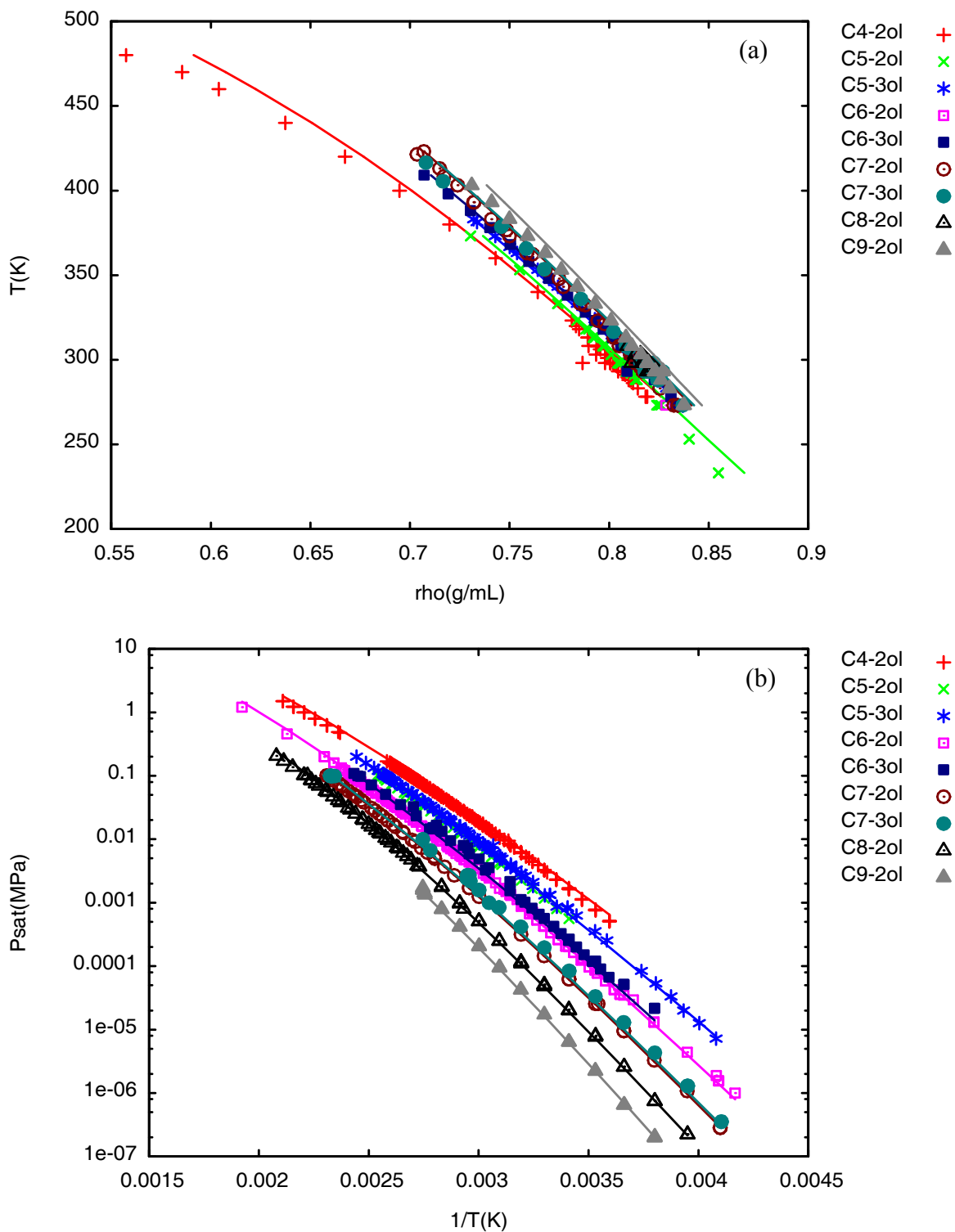


Figure A.4.6: Liquid densities (a) and vapor pressures (b) of secondary alcohols

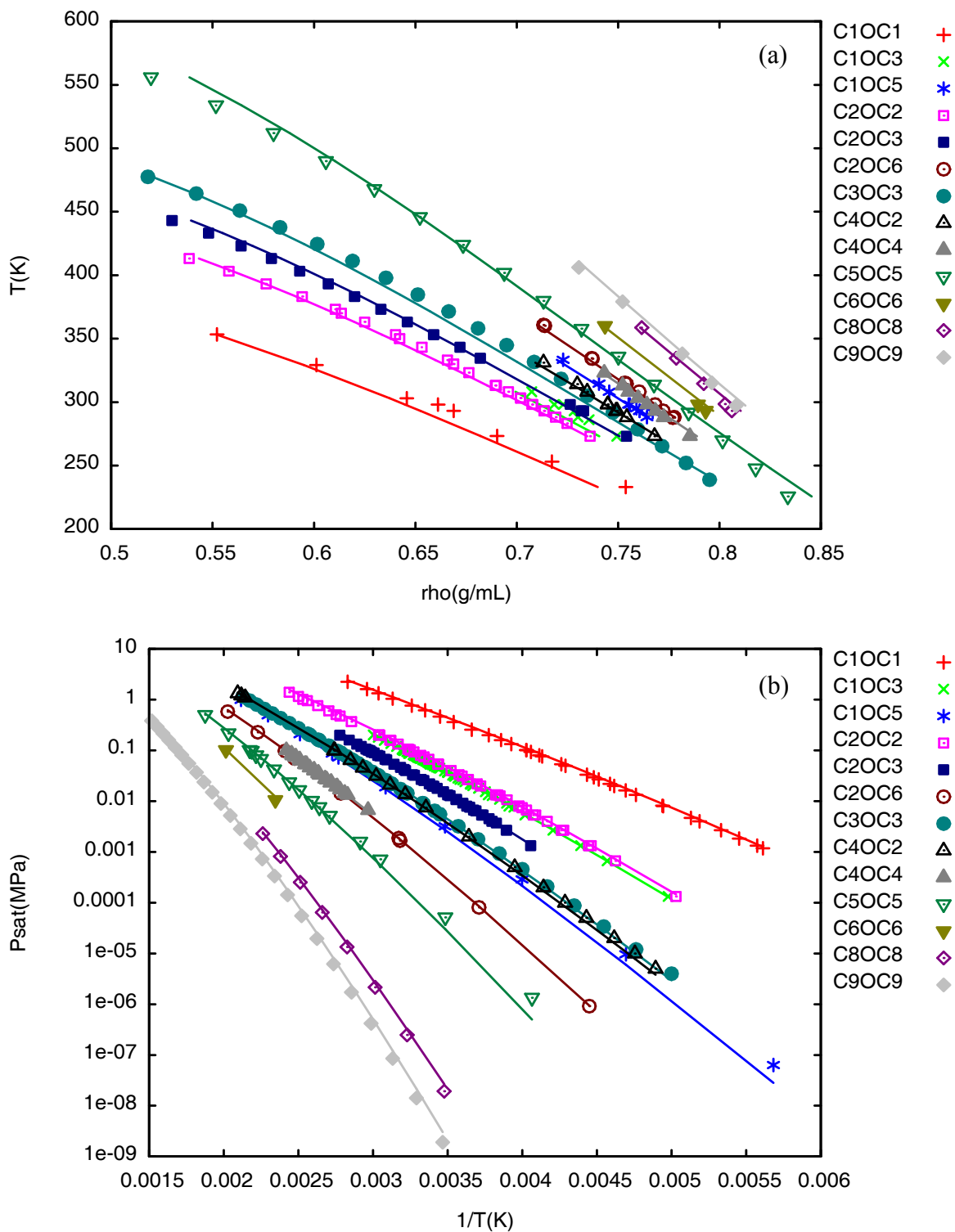


Figure A.4.7: Liquid densities (a) and vapor pressures (b) of ethers

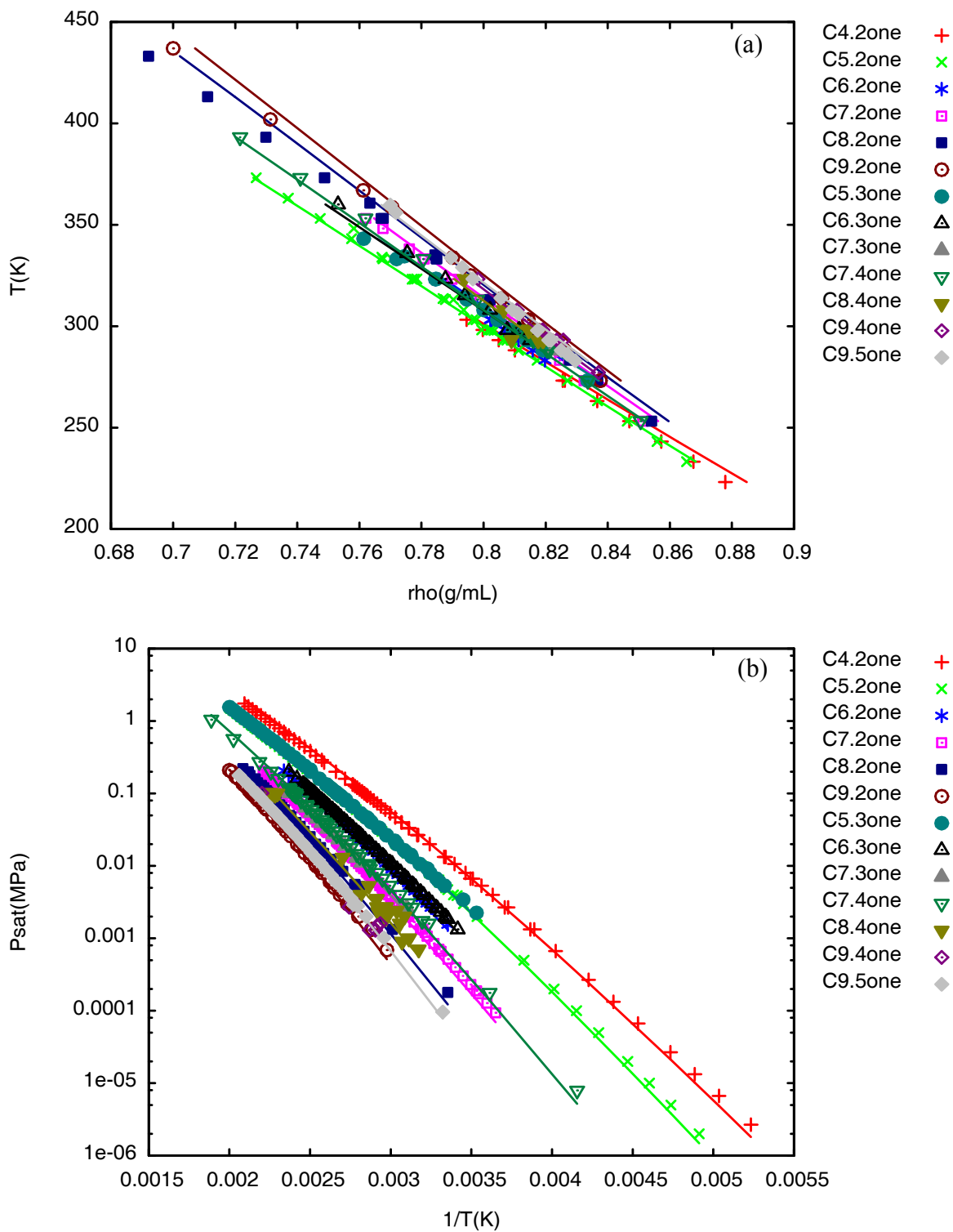


Figure A.4.8: Liquid densities (a) and vapor pressures (b) of ketones

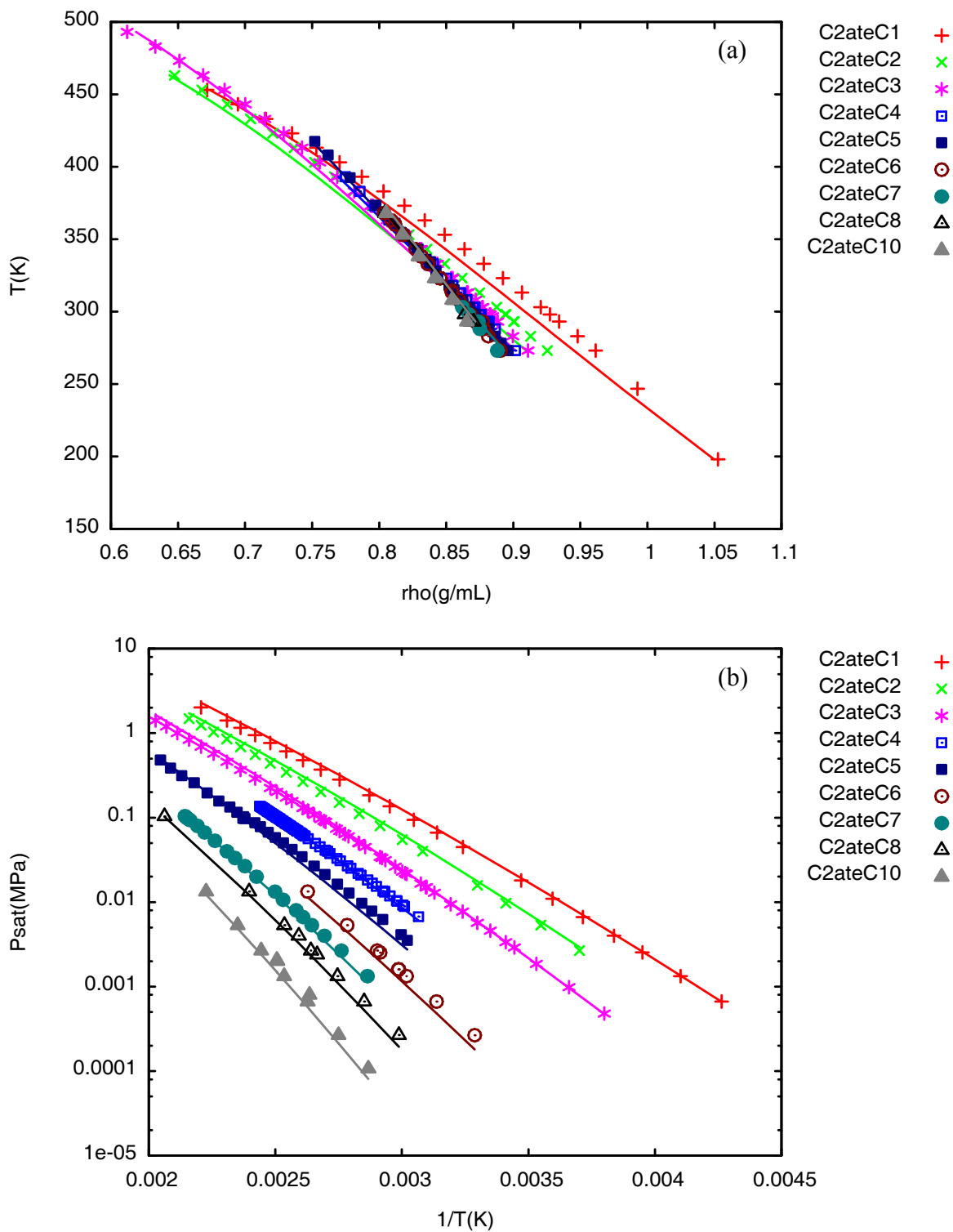


Figure A.4.9: Liquid densities (a) and vapor pressures (b) of acetates

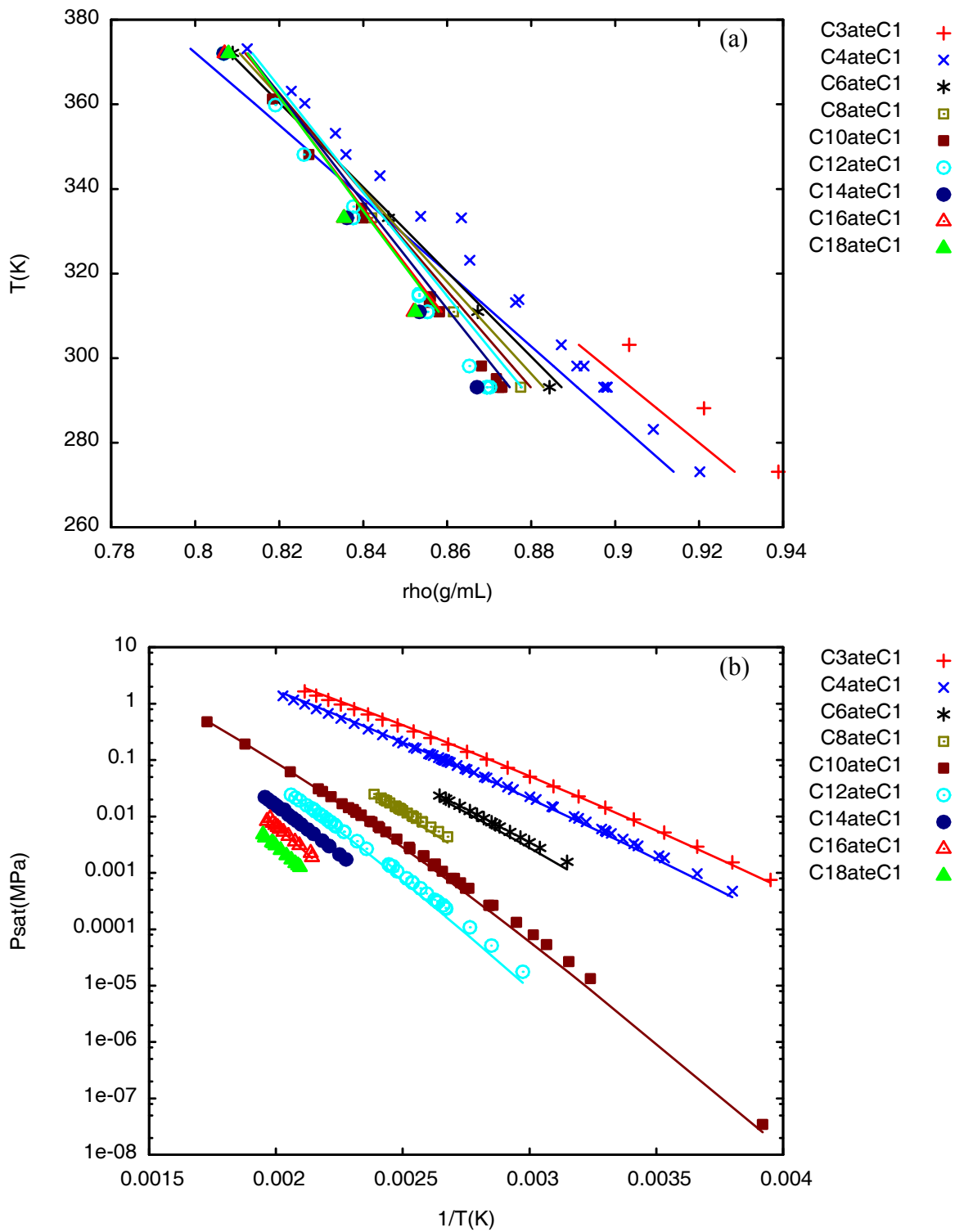


Figure A.4.10: Liquid densities (a) and vapor pressures (b) of methyl esters

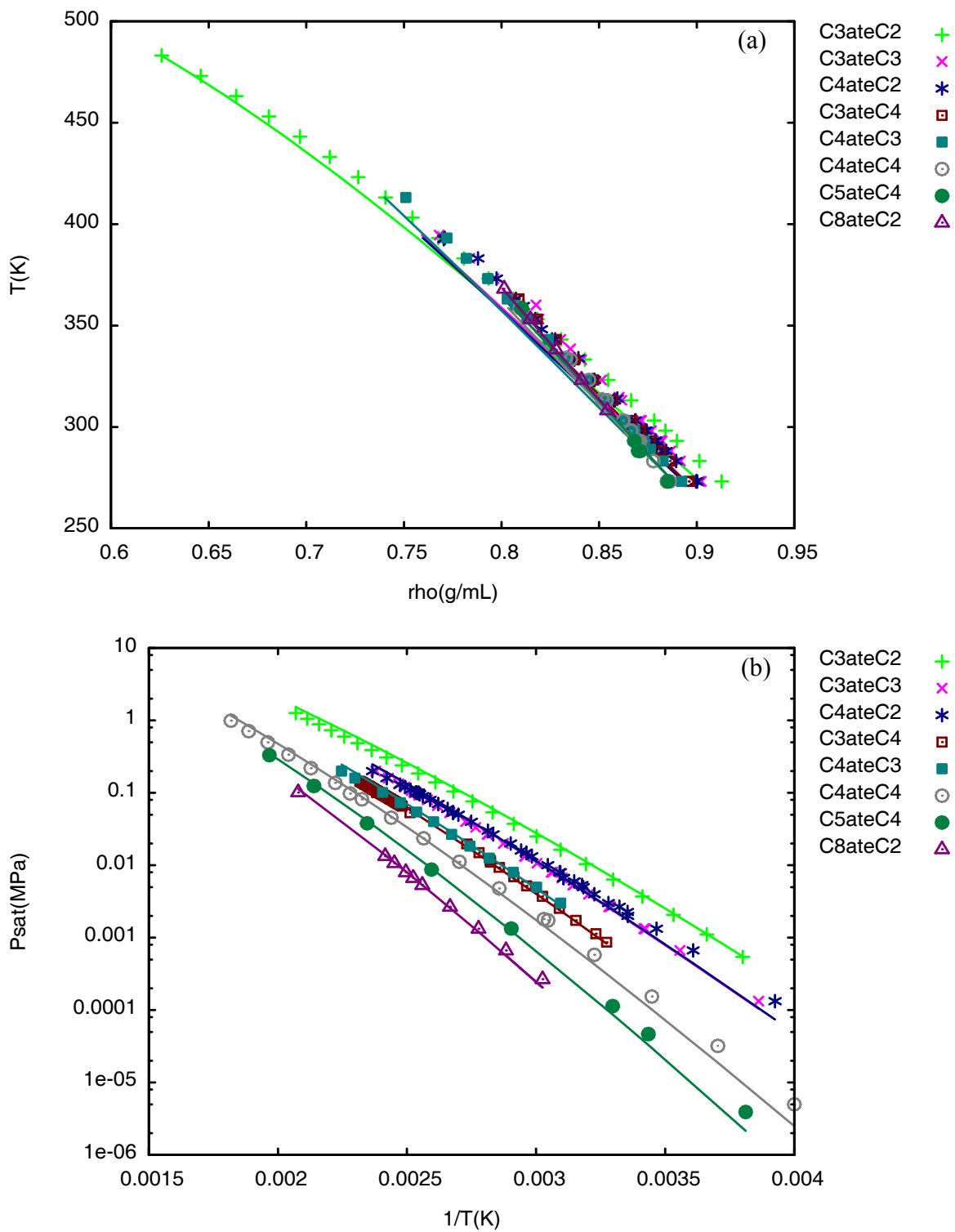


Figure A.4.11: Liquid densities (a) and vapor pressures (b) of esters higher than acetates

A.5. Tail corrections

The average potential energy due to particle i is given by (from the text “Understanding Molecular Simulation” by Frenkel and Smit):

$$\frac{E}{NkT} = \frac{\rho}{2kT} \int_0^{\infty} u(r)g(r)4\pi r^2 dr \quad (\text{A5.1})$$

where, ρ is the average number density of particles, $g(r)$ is the rdf at a distance r , $u(r)$ is the potential function and N is the total number of particles. For a L-J particle, the potential well extends to infinity, while the simulation box is limited. The general practice is to truncate the potential function at a cut-off distance (r_c), and add a tail correction to compensate for the truncation error, such that:

$$\frac{E}{NkT} = \frac{\rho}{2kT} \int_0^{r_c} u(r)g(r)4\pi r^2 dr + \frac{\rho}{2kT} \int_{r_c}^{\infty} u(r)g(r)4\pi r^2 dr \quad (\text{A5.2})$$

The second integral in equation A5.2 is the tail correction, which, on assuming $g(r) = 1$ beyond the cutoff separation, can be written as:

$$\frac{E^{tail}}{NkT} = \frac{\rho}{2kT} \int_{r_c}^{\infty} u(r)4\pi r^2 dr \quad (\text{A5.3})$$

Generally, r_c is chosen to be around 2.5σ , where the potential is about 1.6% of the minimum.

Though seemingly negligible, the tail correction due to the potential beyond r_c can be significant at liquid-like densities.

In SPEAD, Helmholtz energy is calculated using the configurational energy of the system, using a cut-off distance of 2.0σ . Tail corrections have not been accounted for in the previous SPEAD publications, and the results nevertheless, appear to be reasonably good, probably because the fourth well is an adjustable parameter, which in most cases is deeper than about 6% (as in a Lennard-Jones potential at 2.0σ) of the first well.

The integral for the tail correction is solved analytically, by using an approximation of the attractive potential beyond 2σ . Ignoring the repulsive contribution, the potential can be assumed to be of the form $-B/r^6$, and knowing that, at $r_c = 2\sigma$, the potential is ε_4 , B is found to be $64\varepsilon_4\sigma^6$, which would give:

$$\frac{E^{tail}}{NkT} = -\frac{\rho}{kT} \int_{r_c}^{\infty} 4\pi r^2 \frac{64\varepsilon_4\sigma^6}{r^6} dr \quad (\text{A5.4})$$

Since we are calculating the Helmholtz energy by summing over pair type, the factor 2 is dropped from the denominator. Integrating, we find for a particular pair type i :

$$\frac{E_i^{tail}}{NkT} = -\frac{32\rho_i\sigma_i^3\varepsilon_{4_i}}{3kT} \quad (\text{A5.5})$$

The Helmholtz energy term can be modified as follows to include the tail correction:

$$\frac{A - A^{ig}}{NkT} = \frac{A_0 - A^{ig}}{NkT} - \frac{\langle E + E^{tail} \rangle}{NkT} - \frac{\left(\langle (E + E^{tail})^2 \rangle - \langle E + E^{tail} \rangle^2 \right)}{2Nk^2T^2} \quad (\text{A5.6})$$

where, E is the potential energy due to the wells. Since:

$$E^{tail} = \sum_{pairs} E_i^{tail}$$

which is constant, it cancels out in the energy fluctuation term, and can simply be added to the energy term such that:

$$\frac{\langle E + E^{tail} \rangle}{NkT} = \frac{A_1 - \sum_{pairs} \frac{N_i \pi \sigma_i^3 \epsilon_{4i}}{3kV}}{T} \quad (A5.7)$$

Where, N_i is the number of pairs of types i and V is the volume of the simulation box.

A.6. Ratio of the number of intramolecular attractive pairs to total attractive pairs

This analysis is only for straight chain molecules. The derivation would be more tedious for branched compounds.

Consider the following system:

Total number of molecules = M

Number of sites in a molecule = N_s

Therefore, total intramolecular interactions in a molecule =

$$N_s C_2 = \frac{N_s!}{2(N_s - 2)!} = \frac{N_s(N_s - 1)}{2}$$

Similarly, the total number of attractive pairs in the simulation box can be given by:

$$\frac{MN_s(MN_s - 1)}{2}$$

Let the position where intramolecular attractions are counted from = x , which also denotes the minimum bond separation for the interaction to be counted. Therefore, number of intramolecular interaction to be ignored for attractions per molecule can be given by:

$$(N_s - 1) + (N_s - 2) + \dots + (N_s - (x - 1)) = \sum_{i=1}^{x-1} (N_s - i)$$

The first term denotes number of pair interactions separated by 1 bond, the second term, by 2 bonds and so on. The last term is for the interactions separated by $(x - 1)$ bonds, since the interaction separated by x bonds or more are included. So, the total intramolecular attractive pairs in the simulation box (N_I) can be given by:

$$N_I = M \left[\frac{N_s (N_s - 1)}{2} - \sum_{i=1}^{x-1} (N_s - i) \right]$$

Similarly, the total number of attractive pairs in the simulation box (N_T) can be given by:

$$N_T = M \left[\frac{N_s (MN_s - 1)}{2} - \sum_{i=1}^{x-1} (N_s - i) \right]$$

Therefore the ratio N_I/N_T can be given by:

$$\frac{N_I}{N_T} = \frac{\left[\frac{N_s (MN_s - 1)}{2} - \sum_{i=1}^{x-1} (N_s - i) \right]}{\left[\frac{N_s (MN_s - 1)}{2} - \sum_{i=1}^{x-1} (N_s - i) \right]}$$